INVESTIGATIONS OF ULTRASONIC ASSISTED FRICTION STIR WELDING PROCESS

A Thesis Submitted in Partial Fulfillment of the Requirements for the Award of the Degree of

DOCTOR OF PHILOSOPHY

IN

MECHANICAL ENGINEERING

BY

Shanti Lal Meena

(2K14/PhD/ME/02)

Under the supervision of

Dr. Qasim Murtaza
Professor,
Department of Mechanical Engineering, Delhi Technological University, Delhi

Dr. M.S. Nirajan
Associate Professor,
Department of Mechanical Engineering, Delhi Technological University, Delhi

Dr. R.S. Walia
Professor & Head, Production and Industrial Engineering, Punjab Engineering college, Chandigarh

DEPARTMENT OF MECHANICAL ENGINEERING

DELHI TECHNOLOGICAL UNIVERSITY

Bawana Road, Delhi-110042, INDIA

June 2022

DECLARATION

I hereby certify that the work which is being presented in this thesis entitled **"Investigations of Ultrasonic Assisted Friction Stir Welding Process"** submitted in partial fulfilment of the requirements for the award of the degree of Doctor of Philosophy in the Department of Mechanical Engineering, Delhi Technological University, Delhi. This is an authentic record of my own work carried out under the supervision of Dr. Qasim Murtaza, Dr. M. S. Niranjan and Dr. R. S. Walia. The matter presented in this thesis has not been submitted elsewhere for the award of a degree.

Place: Delhi **Shanti Lal Meena**

Date: 30/06/2022 **(2K14/PHD/ME/02)**

CERTIFICATE

On the basis of candidate's declaration, we hereby certify that the thesis entitled **"Investigations of Ultrasonic Assisted Friction Stir Welding Process"** submitted to the Department of Mechanical Engineering, Delhi Technological University, Delhi in partial fulfillment of the requirements for the award of degree of Doctor of Philosophy, is an original contribution with the existing knowledge and faithful record of the research work carried out by him under our guidance and supervision.

It is further certified that the work is based on original research and the matter embodied in this thesis has not been submitted to any other university/institute for award of any degree to the best of our knowledge and belief.

Dr. Qasim Murtaza
Professor,
Department of Mechanical Engineering, Delhi Technological University, Delhi

Dr. M.S. Nirajan
Associate Professor,
Department of Mechanical Engineering, Delhi Technological University, Delhi

Dr. R.S. Walia
Professor & Head, Production and Industrial Engineering,
Punjab Engineering college, Chandigarh

ACKNOWLEDGEMENTS

While bringing out this thesis to its final form, I came across a number of people whose contributions in various ways helped my field of research and they deserve special thanks. It is a pleasure to convey my gratitude to all of them.

First and foremost, I would like to express my deep sense of gratitude and indebtedness to my supervisors **Prof. Qasim Murtaza, Dr. M. S. Nirajan, and Prof. R.S. Walia** for their invaluable encouragement, suggestions and support from an early stage of this research work and providing me extraordinary experiences throughout the research work.

In addition to my supervisors, I would like to thank the other members of my research committee: Prof. S.K. Garg, Prof. R.C. Singh, Dr. Raminder Kaur, Prof. Akshay Dvivedi, and Dr. Jatinder Kumar for their insightful remarks and encouragement, as well as for the challenging question that motivated me to broaden my research from different angles.

I would like to extend my sincere gratitude to Central Research Facility-IIT Delhi and all my friends including Dr. Ravi Butola, Ankit Tyagi and Dr. Hemant Saxena and Dr. Yashwant Koli who helped me in every possible way to finish this research work.

I am grateful to my elder brother Mr. Prem Raj Meena for giving me the primrose path in my life. Last but not the least; I would like to thank my lovely wife, Veena Meena and my adorable children, Jianshi and Dhurvit for supporting me and encouraging me to pursue this degree.

Date: ___/___/___

Shanti Lal Meena

(2K14/PHD/ME/02)

PREFACE

This thesis describes a hybrid form of the Friction Stir Welding Process, which is a new emerging, green, and energy-efficient thermo-mechanical process for improving the material's properties through localized plastic deformation, resulting in a microstructure with ultra-fine, equidistant grains. By integrating ultrasonic vibrations into the conventional Friction Stir Welding Process, researchers would be able to obtain better mechanical properties. The contents of the thesis are as follows:

Chapter 1 In this chapter, the Friction stir welding process and its various classifications have been described. It has been determined how the Friction Stir Welding Process removes material from the processed parts. Later in this chapter, various hybrid FSW forms and their benefits are discussed.

Chapter 2 With regard to conventional Friction Stir Welding and its hybrid forms, a thorough literature review has been conducted. In addition, studies pertaining to the variable parameters affecting mechanical properties, material removal, surface finish, surface roughness scatter, residual stress, wear, and tool wear rate were reviewed. In the final section, hybrid types of Friction Stir Welding are discussed, followed by research gaps, research objectives, and research methodology.

Chapter 3 This chapter covers the selection of work materials, UAFSW tool materials, and experimentation specifics. The components and configurations utilized in this hybrid procedure are described in detail. This chapter also covers the welding technique of Ultrasonic Assisted Friction Stir Processing. .FEA has also been discussed for modifying workpiece surface and tool temperature process parameters. Later in this chapter, the detailed mechanical, microstructure, residual stress, and wear testing procedures are presented

Chapter 4 This chapter includes optimization using Taguchi analysis along with ANOVA (Analysis of variance). Optimization was performed for output parameters such as microhardness, ultimate tensile strength and residual stress.Data analysis procedure, estimation of optimum responses and confirmation of test have also been discussed in this chapter.

Chapter 5 This chapter discusses the details for effect of process parameters on microhardness, tensile test and residual stress. Results of thermal analysis have been discussed. In addition, this chapter examines microstructure, SEM/EDS XRD, and wears analysis.

Chapter 6 This chapter summarizes present research investigation. Important conclusions of the experimental investigation regarding optimum process parameters have been presented. Significant findings for microstructural changes, XRD and wear have been drawn from performed experimentation. This chapter also introduces scope for further research in this field.

TABLE OF CONTENTS

DECLARATION i

CERTIFICATE ii

ACKNOWLEDGEMENTS iii

PREFACE iv

TABLE OF CONTENTS vi

TABLE OF FIGURES xi

LIST OF TABLES xv

NOMENCLATURE xvi

ABSTRACT xvii

CHAPTER - 1 INTRODUCTION 1

1.1 Historical Perspective 1

1.2 Need OF FSW Process Choice 3

1.3 Applications 4

1.3.1 Aerospace sector 4

1.3.2 Shipbuilding 4

1.3.3 Automotive industries 5

1.3.4 Railway industry 5

1.4 Work Material 6

1.5 Research Motivation 6

1.6 Summary 7

CHAPTER - 2 LITERATURE REVIEW 8

2.1 General Perspective on FSW 8

2.2 Effects on mechanical properties and microstructure by varying FSW parameters 9

2.3 Research Gaps 15

2.4 Research Objectives 16

2.5 Research Methodology 17

2.6 SUMMARY 18

CHAPTER - 3 EXPERIMENTAL METHODS 19

3.1 Friction Stir WeldingMachine and Its Specifications 19

3.2 Friction Stir Welding Tool 20

3.3 Selection of Workpiece Material 21

3.4 Experimental Setup of the Hybrid Friction Stir Welding 23

3.4.1 Components of UAFSW 23

3.5 process parameters for UAFSW 26

3.6 Finite Element Modelling 27

3.6.1 Tool geometry of FSW 27

3.6.2 Boundary Conditions 28

3.7 Planning of Experiments 29

3.8 Experimental Procedure 30

3.9 Mechanical Properties of UAFSW joints 30

3.9.1 Measurement of Hardness 30

3.9.2 Tensile Test 32

3.9.3 Residual Stress 33

3.10 Wear Behaviour of UAFSW Joints 36

300 37

3.11 Metallurgical Characterization of UAFSW welded Joints 38

3.11.1 Microstructural characterization 38
3.11.2 X-Ray diffraction 40
3.12 Summary 41
CHAPTER - 4 OPTIMIZATION OF UAFSW PARAMETERS BY TAGUCHI METHOD 42
4.1 Taguchi Experimental Design and Analysis 42
4.1.1 Taguchi methodDOE 42
4.1.2 Experimental design strategy 42
4.1.3 Loss function 43
4.1.4 Singal to Noise ratio (S/N Ratio) 44
4.2 Data Analysis. 45
4.2.1 Selection of OA 46
4.2.2 Assignment of parameters and interaction to the OA: 46
4.2.3 Selection of outer array 47
4.2.4 Experimentation and data collection: 48
4.3 Parameters Design Strategy 48
4.3.1 Parameter classification and selection of optimal levels: 48
4.3.2 Determination of confidence interval: 48
4.3.3 Estimation of optimum response characteristics 49
4.3.4 Confirmation test 50
4.4 Summary 53
CHAPTER - 5 RESULTS AND DISCUSSION 54
5.1 Effects on Mechanical Properties of UAFSW 54
5.1.1 Microhardness 54
5.1.2 Optimization of various Parameters for MH 56
5.1.3 Effects of vibrations on MH 57

5.1.4 Effects of tilt angle on MH 58
5.1.5 Effects of rotational speed on MH 59
5.1.6 Effects of travel speed on MH 60
5.1.7 Effects of amplitude on MH 60
5.1.8 ANOVA for MH 61
5.2 Ultimate tensile strength 64
5.3 optimization of various Parameters for UTS 64
5.3.1 Effects of vibrations on UTS 64
5.3.2 Effects of tilt angle on UTS 66
5.3.3 Effects of travel speed on UTS 67
5.3.4 Effects of rotational speed on UTS 67
5.3.5 Effects of amplitude of vibration on UTS 68
5.3.6 Selection of optimal levels for UTS 70
5.4 Residual Stress 72
5.4.1 Effects of vibrations on residual stress 79
5.4.2 Effects of tilt angle on residual stress 80
5.4.3 Effects of travel speed on residual stress 80
5.4.4 Effects of rotational speed on residual stress 82
5.4.5 Effects of amplitude of vibration on residual stress 82
5.4.6 Selection of optimal levels for residual stress 83
5.5 Estimation of Optimum Responses 85
5.6 Confirmation Test 86
5.7 Thermal Analysis and Solution Controls 86
5.7.1 Heat distribution of UAFSW 87
5.8 Metallurgical Characterization of UAFSW 88

5.8.1 Microstructural characterization 88

5.8.2 XRD analysis 91

5.9 Wear Behavior of UAFSW Joints 93

CHAPTER - 6 CONCLUSIONS AND FUTURE SCOPE 98

6.1 Conclusions 98

6.2 Future Scope 100

References 101

LIST OF PUBLICATIONS 113

TABLE OF FIGURES

Figure 1.1 Principle of the FSW process (a*)* Schematic representation of the friction stir welding process (b) Process diagram for FSW [4] 2

Figure 2.1 Different zones in FSW process 8

Figure 2.2 Schematic diagram of the various FSW tool geometries [4] 10

Figure 2.3 Schematic of the laser assisted friction stir-spot welding [71] 13

Figure 2.4 Setup of ultrasonic assisted FSW 14

Figure 2.5 Experimental setup for ultrasonic wire-EDM [78] 14

Figure 2.6 Flow diagram for research methodology 17

Figure 3.1 FSW machine 19

Figure 3.2 Geometry of FSW tool (a) Experimental tool (b) Designed tool 21

Figure 3.3 EDS of AA 7075-T6 21

Figure 3.4Aluminium sheet of AA7075-T6 with dimensions of 250 x 40 x 3 in mm 22

Figure 3.5 (a) Generator box (b) Transducer with ultrasonic horn 24

Figure 3.6 Component of UAFSW 25

Figure 3.7Complete setup of UAFSW 25

Figure 3.8Assembly of geometry in the FEM 28

Figure 3.9 Tool and workpiece positions of FSW and UAFSW 29

Figure 3.10 Samples for microhardness 31

Figure 3.11 Fischer scope HM2000S 31

Figure 3.12 Rectangular sub size specimen 32

Figure 3.13 Specimen for tensile test before and after 32

Figure 3.14 Portable XRD - residual stress analyzer 33

Figure 3.15 Systematic diagram of residual stress of UAFSW joint 35

Figure 3.16 Experimental set up for wear test 37

Figure 3.17Olympus GX41 microscope 39

Figure 3.18 Experimental Set up of SEM and FESEM (IIT Delhi, Delhi) 40

Figure 4.1Step to be followed in Taguchi DOE 43

Figure 5.1Average values of microhardness of UAFSW Joints 55

Figure 5.2S/N ratio and main effect of vibration type on MH 58

Figure 5.3S/N ratio and main effect of tilt angle on MH 59

Figure 5.4S/N ratio and main effect of tool rotational speed on MH 60

Figure 5.5S/N ratio and main effect of travel speed on MH 61

Figure 5.6S/N ratio and main effect of Amplitude of vibration on MH 61

Figure 5.7UTS values of welded joints 64

Figure 5.8S/N ratio and main effect of vibrations on UTS 66

Figure 5.9S/N ratio and main effect of tilt angle on UTS 67

Figure 5.10S/N ratio and main effect of travel speed on UTS 68

Figure 5.11 S/N ratio and main effect of rotational speed of tool on UTS 69

Figure 5.12 S/N ratio and main effect of amplitude of vibration on UTS 69

Figure 5.13Average residual stress of UAFSW joints 72

Figure 5.14Full 2D and 3D Debye ring and its distribution of residual stresses for (a) BM, (b) continuous vibration and (c) Discontinues vibrations 74

Figure 5.15 Debye ring and half value for (a) BM (b) continuous vibration and (c) Discontinues vibrations 76

Figure 5.16 Residual stress graphs for (a) continuous vibration (b) discontinuous vibration 77

Figure 5.17 Residual stress graphs for base metal 78

Figure 5.18S/N ratio and main effect of type of vibration on residual stress 80

Figure 5.19S/N ratio and main effect of tilt angle on residual stress 81

Figure 5.20 S/N ratio and main effect of travel speed on residual stress 81

Figure 5.21S/N ratio and main effect of rotational speed on residual stress 82

Figure 5.22 S/N ratio and main effect of amplitude of vibration on residual stress 83

Figure 5.23Distribution of heat during welding 86

Figure 5.24Heat distribution of UAFSW in the weld zone 87

Figure 5.25UAFSW stir zone temperature (a) at 1000 RPM continuous vibrations (b) at 800 RPM with continuous vibrations (c) at 1000 RPM with discontinues vibrations d) 800 RPM with discontinuous vibrations 88

Figure 5.26 Microstructure image of BM at 20X 89

Figure 5.27 Microstructure at 20X (a) with continuous vibrations (b) Discontinuous vibrations at 800rpm 90

Figure 5.28Microstructures at 20X a) with continuous vibrations b) Discontinuous vibrations at 1000rpm 90

Figure 5.29 (a) SEM image of base metal (b) EDS of Base metal(c) SEM image of with vibrations welded joint (d) EDS of welded Joint 91

Figure 5.30 XRD analysis of base metal AA 7075-T6 92

Figure 5.31 XRD analysis of UAFSW joint with continuous vibrations 92

Figure 5.32 XRD analysis of UAFSW joint with discontinuous vibrations 93

Figure 5.33 COF Vs Sliding distance graph 94

Figure 5.34 Wear Vs Sliding distance graph 94

Figure 5.35(a) COF (b) Wear Vs Sliding distance graph of UAFSW joints 95

Figure 5.36 FESEM image of worm out surface of UAFSW 96

Figure 5.37 EDS analysis of worn-out surfaces of UAFSW 97

LIST OF TABLES

Table 3.1Specification of FSW Machine 19

Table 3.2Chemical Composition & Mechanical Properties of AA7075-T6 22

Table 3.3 Parameters & Justification for selecting the parameters 26

Table 3.4 Parameter used for wear test 37

Table 4.1The parameters used for experiments 51

Table 4.2L18 orthogonal array of parameters 52

Table 5.1Average values of MH and S/N ratios (Larger-the-Better) for MH 56

Table 5.2ANOVA of the Raw data for MH 62

Table 5.3ANOVA of the S/N Ratio for MH 63

Table 5.4Average values of UTS and S/N ratios (Larger-the-Better) for UTS 65

Table 5.5 ANOVA of the S/N Ratio for UTS 70

Table 5.6 ANOVA of the Raw data for UTS 71

Table 5.7 Average values of UTS and S/N ratios (Lower-the-Better) for residual stress 78

Table 5.8 ANOVA of the raw data for Residual stress 83

Table 5.9 ANOVA of the S/N Ratio for Residual stress 84

Table 5.10Predicted optimal value, confidence intervals and results of confirmation 85

NOMENCLATURE

ANOVA	Analysis of variance
AS	Advancing Side
ASTM	American Society for Testing Materials
BM	Base Metal
DOE	Design of Experiments
EDS	Energy Dispersive Spectrometer
FEA	Finite Element Analysis
FESEM	Field Emission Scanning Electron Microscope
FSW	Friction Stir Welding
HAZ	Heat Affected Zone
MH	Micro Hardness
OA	Orthogonal Array
RS	Retreating Side
S/N Ratio	Signal to Noise Ratio
SEM	Scanning Electron Microscope
TMAZ	Thermo-Mechanically Affected Zone
TWI	The Welding Institute
UAFSW	Ultrasonic Assisted Friction Stir Welding
UTS	Ultimate Tensile Strength
XRD	X-Ray Diffraction

ABSTRACT

The work has been done on hybrid technology, which coordinates with ultrasonic energy to friction stir welding. This experimental study intends toto build up an ultrasonic assisted friction stir welding (UAFSW) process that may improve weld quality and productivity. Experiments have been carried out on the AA7075-T6 sheets of the dimension of250mm x 40mm x 3mm with UAFSW setup using the process parameters such as rotational speed, traverse speed, tilt angle, types of vibration, and amplitude of the vibration. Total of Eighteen experiments were performed using L_{18} orthogonal array (OA) with three levels and five factors. Process parameters were optimized for the response such as microhardness, tensile strength and residual stress of the welded region via Taguchi design of experiments (DOE) optimization technique. Maximum tensile strength is achieved at higher tool rotational speed, traverse speed, and minimum at vibration amplitude, according to the analysis. Maximum microhardness values were observed in the centre of the welded region. It has also been observed with scanning electron micrograph (SEM) that cavity defects and improper mixing of the materials were found at low tool rotational speed and without ultrasonic assisted FSW. ANSYS simulation software has been used for thermal analysis of the welding process. Maximum temperature has been observed to be achieved at high tool rotational speed and low travel speed. During in the traverse phase, the weld line temperature rises, but does not surpass the melting point of the workpiece material. A solid continuous joint appears between the two sheets as the temperature drops.

This experimental investigation focuses into the UAFSW process to explore the possibility of enhancing the usefulness of the conventional FSW process by applying continuous and discontinuous vibrations. This research suggests that developed UAFSW process is one of the most significant processes in the field of joining processes with

enhanced mechanical properties. The experimental results indicate that mechanical properties such as MH, UTS, residual stress, and wear are most affected and improved. FSW aided by ultrasonic energy produces the maximum microhardness of 201.32 HV in the welded region at rotational speed of 1000 rpm, traverse speed of 60 mm/min, amplitude of vibration of zero microns, tilt angle of 1.5 degree, and continuous vibrations, respectively. In this investigation, it was discovered that the maximum microhardness value of a UAFSW-welded joint is more than double that of its base metal at optimal parameters. It is also determined that the microhardness value in the centre of the welded region is greater than that of the HAZ. The experimental results show the minimum value of microhardness is 106.13 HV at continuous vibrations. It was also observed that the amplitude of vibration is having least effect on MH.

The percentage contribution of L18 OA, the optimal level contribution, has been determined to be 24.73 percent for maximum travel speed. The percentage contribution for other parameters is 24.14 percent for vibration type, 4.66 percent for tilt angle, 9.7 percent for rotational speed, and 3.27 percent for amplitude type. It was revealed that the type of vibrations had the greatest impact on tensile strength, 58.97 percent. Maximum tensile strength was achieved at a rotational speed of 600 rpm and a translational speed of 40 mm/min. During this investigation, it was also discovered that increasing the ultrasonic vibration continuously generates higher heat input, which facilitates material flow around the tool and increases the joint's tensile strength. Additionally, it was determined that the amplitude of vibration (0.23 percent) is the least significant contributor and was not significantly affected.

The experimental results show that the residual stress of welded region varies from -54.66 MPa to – 11 MPa as compared to base metal’s residual stress of -176 MPa. The negative sign shows residual stresses are compressive in nature. The optimal level

contribution for maximum rotational speed has been determined to be 39.23 percent. Other parameters have a 12.24 percent contribution for vibration type, 17.64 percent for tilt angle, 5.6 percent for travel speed, and 16.19 percent for amplitude type. The structural-thermal options of SOLID226 and CONTA174 are used to conduct a nonlinear transient analysis. FSW simulation incorporates nonlinearity, contact, friction, large plastic deformation, structural-thermal coupling, and varying loads for every load step and validated using thermal imaging. With continuous and discontinuous vibrations, the UAFSW exhibits a uniform distribution of grains devoid of voids. Because of this, mechanical properties are improved.

Coefficient of friction and wear are found lower at 150N load and have significant effects with the rotational speed, traverse speed, tilt angle, minimum amplitude, and the type of vibrations. The tribological test showed a 72.88% decrease in COF and 71% reduction in the wear at test conditions of 1 m/s sliding velocities, 350^{o}C temperature, and 150N load with UAFSW. The variation of COF with sliding distance shows the maximum values for base metal whereas, it decreases with the applications of vibration in FSW. The COF is lowest for UAFSW with discontinuous vibrations. The variation of wear with sliding distance is greatest for base metal, whereas it decreases when vibration is applied to FSW. UAFSW has the lowest COF with discontinuous vibrations.

***Keywords*-** UAFSW, DOE, orthogonal array, SEM, XRD, wear test.

CHAPTER - 1

INTRODUCTION

This chapter provides an overview of historical perspective of FSW process along with why there is a need of UAFSW process. In addition, work material, applications, advantages and limitations of FSW process were also discussed along with research motivation.

1.1 HISTORICAL PERSPECTIVE

In the early days of human civilization, the industrial revolution was a major turning point that propelled the development of new techniques, processes, and materials, and the twentieth century is evidence of the remarkable growth of industrial development and engineering design. In response to customer demand for highly engineered, high-quality, and high-performance products, the emphasis has shifted to mechanical joints such as riveting joints, bolt and screw joints, adhesive joints using glues and epoxy resins, welding, soldering, and brazing joints. Welding plays an important role in the fabrication of various materials. Welding is a fabrication manufacturing process used to join metal to metal and thermoplastics through sourcing of fusion, which aids in the creation of complex parts in the manufacturing industries[1]–[3]. In the case of complex parts, individual components are manufactured separately and then joined using a specific welding technique based on the material. Furthermore, welding techniques are not the only way to manufacture the product; they are an alternative method. A fabrication process is the act of combining two or more components into a single component. The various processes of fabrication can be categorized as follows: (i) mechanical joining with bolts, screws, and rivets; (ii) adhesive bonding with synthetic glues like epoxy resins; and (iii) welding, brazing, and soldering. Due to the permanent nature of the joint and its strength being equal to or in some cases greater than that of the base metal, welding is one of the most frequently employed fabrication techniques.

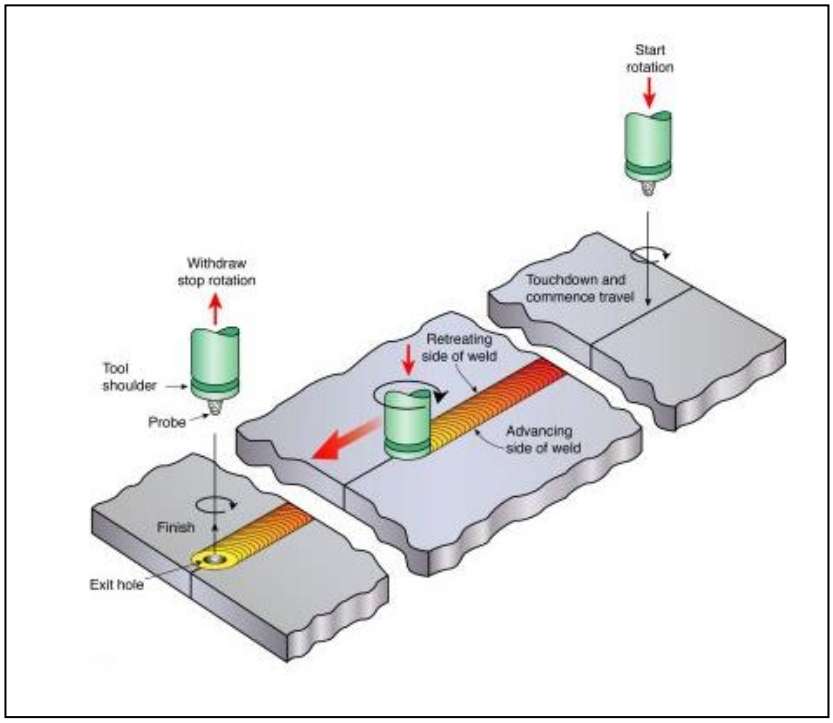

(a)

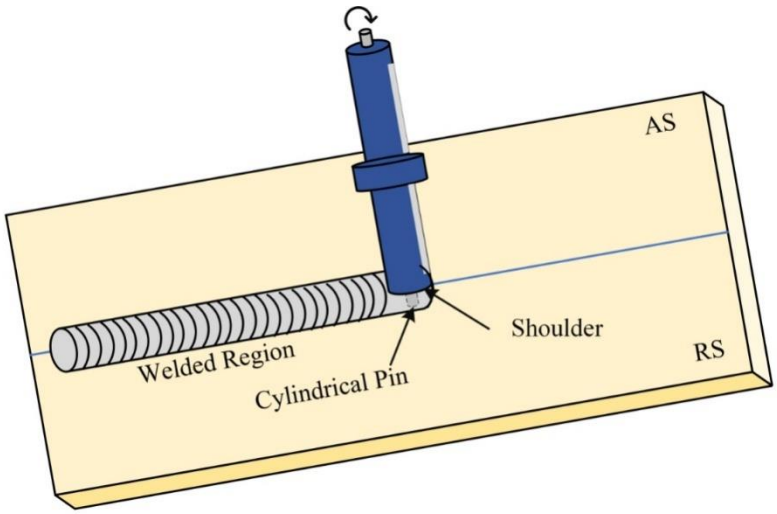

(b)

Figure 1.1 Principle of the FSW process (a*)* Schematic representation of the friction stir welding process (b) Process diagram for FSW [4]

Friction stir welding (FSW) was developed as a solid-state joining technique by The Welding Institute (TWI) of the United Kingdom in 1991[4], [5] and initially applied to aluminium alloys (AA). The fundamental concept of FSW is astonishingly simple. A non-consumable

rotating tool with a uniquely designed pin and shoulder is inserted into the adjacent edges of the sheets or plates to be joined and moved along the joint line (Figure 1.1). [6]–[8]

The primary functions of the tool are (a) heating the workpiece and (b) material movement to create the joint. The heating is caused by friction between the tool and the workpiece and plastic deformation of the workpiece. Localized heating softens the material surrounding the pin, and the rotation and translation of the tool cause material to move from the front to the back of the pin. As a result of this procedure, a strong joint is produced. Due to the tool's diverse geometrical characteristics, material motion around the pin can be quite intricate[9]–[12]. During the FSW process, the material undergoes intense plastic deformation at a high temperature, resulting in the formation of fine, equiaxed recrystallized grains. The superior mechanical properties of friction stir welds are a result of their fine microstructure[5], [13]–[15].

1.2 NEED OF FSW PROCESS CHOICE

FSW is the most noteworthy advancement in the welding area in the last 15 years and a "green" technology owing to its energy effectiveness, environmental friendliness, and adaptability. The absence of cover gas and flux makes the process environmentally friendly[16]–[18]. Due to its low energy consumption, absence of gas emissions, and lack of consumable materials such as filler rod and electrodes,, In 2002, the American Welding Society conducted a survey that revealed $34.4 billion is spent annually in the United States on arc welding, including consumables, repair, and energy consumption[19]. 10 percent of joining processes have reportedly been replaced by FSW. The rate of adoption of FSW has increased rapidly [20].

FSW has many advantages over conventional welding techniques, including:

i. It produces results while consuming relatively less energy

ii. Does not require any cover gases or flux.

iii. Does not require filler metals, thereby demonstrating the ability to join any type of aluminium alloy without regard to compositional compatibility.

iv. Allows simple joining of various aluminium alloys

v. Does not require consumables like electrodes

vi. Does not release any gases.

1.3 APPLICATIONS

There are numerous applications of FSW for joining purposes. The Major FSW process applications are as follows:

1.3.1 Aerospace sector

FSW has been broadly adopted and utilised in the production of rocket-fuel tanks. The typical tank's production time has been drastically reduced, resulting in significant cost savings. Utilizing FSW in the production of aerospace parts is primarily motivated by weight reductions, which directly translate into cost reductions. Several applications in the commercial and military aircraft industries, including carrier beams, floors, and complete fuselages and wings, are being evaluated [5], [13], [21]–[23].

1.3.2 Shipbuilding

Imagine a large catamaran that, like a toy boat, can be assembled from building blocks. Each component would fit together perfectly., ensuring of dimension accuracy and making necessary adjustments easier. FSW is the precursor to this type of shipbuilding construction methodology[24]–[26]. The typical alloys used in shipbuilding are from the 5xxx or 6xxx series due to their corrosion resistance and strength, respectively. Other applications include deck, side, bulkhead, and floor panels, as well as marine and transportation structures.

1.3.3 Automotive industries

With its large manufacturing batches, six sigma requirements, and challenging material combinations, the automotive industry is an ideal field for FSW applications. In theory, all aluminium components of a vehicle, including pistons, crash boxes, rear spoilers air rear axles, drive shafts, water coolers, engine blocks, intake manifolds, cylinder heads, dashboards, suspension systems, , alloy wheels, bumper beams, and stiffening frames, can be friction stir welded[27], [28].

1.3.4 Railway industry

The publication of the commercial production of high-speed trains made from aluminium extrusions that can be welded using friction stir welding has occurred:

• High-speed trains

• Rolling stock of railways, underground carriages, trams

• Railway tankers and freight wagons Container bodies etc[25], [29].

Numerous studies have been done on the use of ultrasonic energy to plastic deformation of metals. There are claims that ultrasonic oscillations in the tooling decrease static deformation forces, increase processing speeds, and enhance product quality [30].These effects have been demonstrated by a variety of industrial processes, including machining, drilling, and welding. Ultrasonic machining and drilling techniques[31]–[33] have been demonstrated to be effective in machining difficult-to-cut alloys such as titanium. Absorption of ultrasound energy occurs in regions of the metal that are capable of carrying the mechanism of plastic deformation, i.e., dislocations and grain boundaries, and this makes it easier for dislocations to overcome energy obstacles.

1.4 WORK MATERIAL

Aluminum is the second most frequently welded metal due to its unique combination of light weight and relatively high strength. Aerospace structures that require high-strength, fatigue- and fracture-resistant welds from AA of the 7XXX series is extremely difficult to weld[34], [35]. Due to their poor solidification microstructure and porosity in the fusion zone, these AA are generally categorised as non-weldable. Due to these factors, it is difficult and unattractive to weld these alloys using conventional techniques. In fact, all of these issues can be resolved by employing an innovative welding technique known as FSW[36], [37]. FSW is used to join metal sheets such as a variety of AA, titanium alloys, Mg alloys, Cu, stainless steels, and Ni alloys with no use of filler metal or shielding gas. Material with a thickness between 0.5 and 65 mm can be welded from one side with full penetration and no porosity or inner voids. The FSW process occurs in the solid phase at temperatures below the melting point of the material, thereby avoiding resolidification-related issues such as porosity and cracking[38]. SMAW (Shielded metal arc welding)[39], SAW (Submerged arc welding), FCAW (Flux-cored arc welding), and ESW (Electro slag welding)[40] are inapplicable for AA7XXX. Even previously thought to be non-weldable aluminium alloys have been welded without flaws and with excellent mechanical properties[41].

1.5 RESEARCH MOTIVATION

Due to their superior mechanical properties, Al alloys are rapidly replacing their conventional counterparts in nearly all advanced engineering applications. Hybrid FSW processes are incorporated into the Al alloys to achieve improved mechanical properties. Porosity defects, solidification defects, and cracks are not an issue with FSW/UAFSW, which are the primary benefits. FSW provides a low convergence of defects and is exceptionally tolerant of process parameter and material variations[42]–[44].

In this experimental investigation, we introduce a hybrid technology that combines ultrasonic vibrations and FSW. Incorporating ultrasonic vibrations into the FSW process is anticipated to provide numerous advantages in terms of mechanical properties like UTS, hardness, residual stress and wear resistance.

1.6 SUMMARY

With the industry shifting towards a green and sustainable joining technique, FSW is one of the most versatile choices available. Joining of Aluminum is one of the predominant challenges in the industry owing to their poor solidification microstructure and porosity. In this work a hybrid FSW process has been investigated for joining of Aluminium. The process parameters, joint performance and the microstructural evolution have been studied in detail as explained in the coming chapters.

CHAPTER - 2

LITERATURE REVIEW

This chapter provides a review of the literature on welding of AA and other materials using various solid-state techniques. In addition, numerous hybrid techniques for welding for advancement of AA by friction stir welding are discussed. It also covered the research gap analysis, the objective of the research work, and the research work's methodology. Numerous research papers on AA have been published in so many journals. The following literature reviews attempt to shed light on the previously mentioned topic.

2.1 GENERAL PERSPECTIVE ON FSW

Friction stir welding (FSW) was developed as a solid-state joining technique by The Welding Institute (TWI) of the United Kingdom in 1991[4], [5] and initially applied to AA. Typically, in FSW, the joint material can be divided into four distinct Microstructural zones based on how they are affected. These zones are identified as depicted in Figure 2.1.

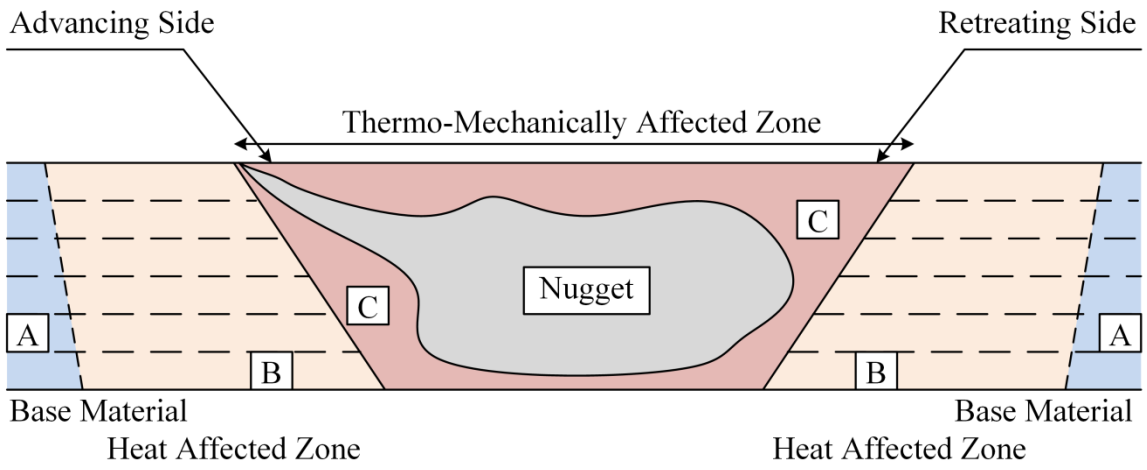

Figure 2.1 Different zones in FSW process

In unaffected material, the zone is unaffected by the welding procedure's heat, and the microstructure and mechanical properties of the base material are unaltered. In the heat

affected zone (HAZ), the microstructures and properties of the base material are affected by the heat generated during the welding process, but there is no plastic deformation. This zone has the same grain structure as the underlying material. In the thermomechanical Affected zone (TMAZ)[45], [46], the base material has undergone plastic deformation around the FSW tool, but recrystallization does not occur due to inadequate heat or deformation strain, and there is a distinct boundary between this zone and the recrystallize zone or stir zone. In the nugget zone, intense plastic deformation of the material caused by frictional heat results in the formation of re-crystallized fine grain microstructure in the vicinity of the stir zone. It is additionally known as the dynamically recrystallized zone (DXZ). It was observed that the temperature distribution in the nugget zone is higher than that of the other zones. For the welding of aluminium alloys or other dissimilar alloys, various welding variables such as tool rotation, transverse speed, tool tilt, plunge depth, and tool design have been examined[47].FSW tests were conducted on Al 6061 alloy using a vertical milling machine in hybrid mode. The optimized process parameters that control the quality of the weld are a) axial force, b) rotation speed (rpm), c) traverse speed (mm/min), and d) tool tilt angle. The findings demonstrated that each weld zone's grain size varied and was influenced by the joint's particular material composition and FSW process parameters. The heat affect zone (HAZ), the thermos-mechanically affected zone (TMAZ), and the nugget zone were found to have the coarsest grain sizes.[48].

2.2 EFFECTS ON MECHANICAL PROPERTIES AND MICROSTRUCTURE BY VARYING FSW PARAMETERS

The influence of shoulder geometry on the mechanical and microstructural properties of friction stir-welded joints was investigated. The effects of three shoulder geometries have been studied: a) scroll and fillet, b) cavity and fillet, and c) fillet alone. Visual inspection,

macrograph, micro hardness, bending and tensile tests were used to determine the effect of the three shoulder geometries. Optical microscopy was typically used to examine the resulting microstructure, removing the influence of shoulder geometry on nugget grain size. The investigation revealed that the optimal joint for thin sheets is a shoulder with a fillet and

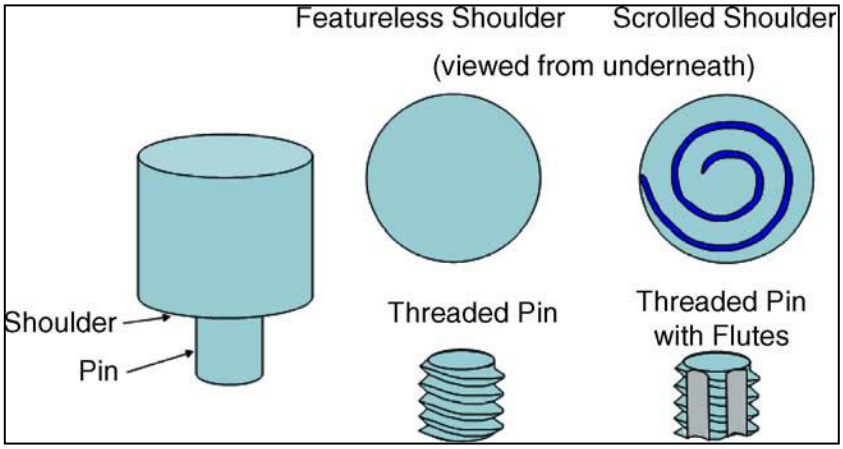

Figure 2.2 Schematic diagram of the various FSW tool geometries [4]

a cavity. The most influential aspect of process development is tool geometry. The tool geometry plays an essential role in material flow, which in turn determines the traverse rate at which FSW can be performed[36], [49]. A FSW instrument consists of a shoulder and a pin, as depicted in Figure 2.2.

Compared to other tool pin profiles, square pin profiles produce welds that are both mechanically and metallurgical sound[37], [50], [51]. Among all other pin profiles, the joint fabricated with a square pin profiled tool has the highest hardness value, 105 HV, while the joint fabricated with a straight cylindrical pin profiled tool has the lowest hardness value, 85 HV[52].

The welds fabricated with the conical shoulder exhibited a larger nugget grain size with fewer hardening in substances than the welds fabricated with the scrolled shoulder, which exhibited a small nugget grain size with an abundance of hardening substances. Effects of various

parameters like, tool rotation rate and tool traverse speed, and the gap width investigated in the welding process; particularly, the plunge force [53]–[56].

Tool geometry is the most influential aspect of process development. The tool geometry plays a critical role in material flow and in turn governs the traverse rate at which FSW can be conducted[57], [58].

On AA6063-T6 aluminium alloy, the effects of process variables such as axial force, tool travel, and rotational speed were studied. With a tool feed rate of 40.2 mm/min, tool rotational speeds between 1200 and 1400 rpm, and an axial force of 10 kN, improved mechanical properties can be achieved during friction stir processing. Various combinations of the process variables resulted in a maximum increase of 46.5% in ultimate tensile strength, 133% in ductility, and 33.4% in micro hardness in comparison to the parent material[59].The AA6082-T6 alloy exhibits strong flow softening during tensile loading at high temperatures and demonstrates excellent FSW weldability. Under the same welding conditions, the AA5083-H111 alloy exhibits poor weldability due to its infinitely slowly steady flow behaviour at increasing temperatures[53]. The best weld quality is achieved with a tapered pin at low welding speed and high rotation speed, as the shear strength decreases significantly at high rotation speed and the tool forces are lower at low welding speed[60].With the circular pin, the tensile strength and breaking loads increased as the tool's rotational speed increased, but they decreased once the tool reached its maximum speed. Deflections of friction stir welded specimens and base materials were compared, and they exhibited nearly identical trends under various load conditions, with deflections increasing with increasing load for all specimens [61].

Frictional surface deposition was utilized to successfully deposit AA 6082 on AA 2024. The interface was devoid of porosity, and no evidence of intermetallic formation was discovered.

High travel speeds reduce the oxidative layer of UAFSW thickness, width, and bonding width. Cross sections that are concave will result from excessive forces. Bonding at UAFSW welded region degrades as travel speeds increase. Reduced rotational speeds were advantageous for joining[62]. The results of tensile tests revealed adequate joint efficiencies and surprisingly high yield stresses. In bending fatigue tests, all joint types exhibited comparable levels of fatigue resistance. Similar joints had fatigue strength orders of AA5083-AA5083 and AA6082-AA6082, while dissimilar joints had fatigue strength orders of AA5083-AA6082[63].On the advancing side, the micro hardness values of the TMAZ were relatively high in the upper and lower portions of the FSW joint. The grain structure of the HAZ is identical to that of the base material[46].Researchers examined the wear characteristics of Al-7075 alloys. Utilizing a pin-on-disc test at room temperature and dry conditions, the wear behaviour under a constant load of 40 N is studied[64].

2.3. Hybrid Processing

Numerous researchers have created hybrid processes. In conventional processing, ultrasonic energy or some other source of energy was used to achieve exceptionally good results in terms of mechanical properties [65]–[68].

In an effort to reduce weld root defects in AA6082-T6 alloy, a concept of FSW aided by electrical current was presented, tested, and validated. The concept relies on forcing an electrical current through the weld root in order to raise the local temperature and improve the viscoplasticity of the material. Due to the Joule effect, the generated heat enhances the material's viscoplasticity in this region, thereby minimizing the root defects. Electrical current appears to improve the mechanical performance of FSW butt joints by increasing the viscoplastic material flow without affecting the metallurgical properties of FSW[69], [70].On

AA6061 aluminium alloy material, welding was performed successfully by using ultrasonic assisted friction stir spot-welding (FSSW).

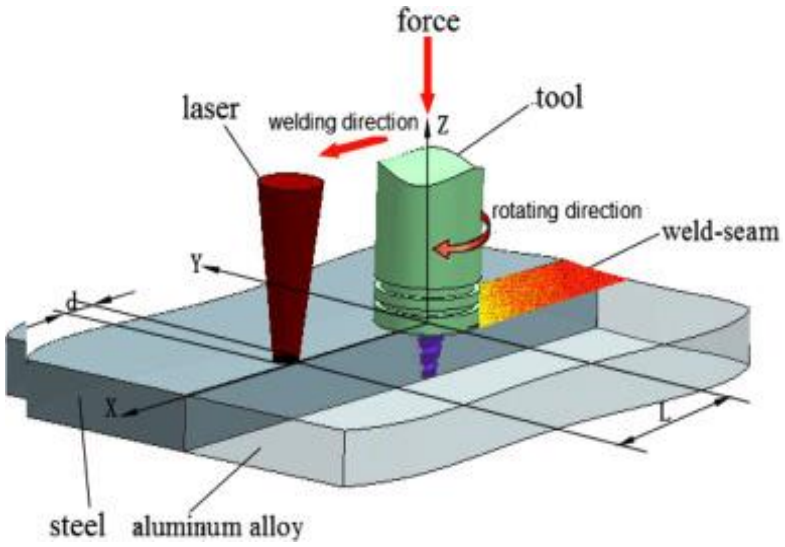

Figure 2.3 Schematic of the laser assisted friction stir-spot welding [71]

To increase the weld strength of a friction stir-spot welding joint with the aid of laser beam and systematic analyses of all significant process factors. Maximum hardness values were obtained by laser assisted friction stir-spot welding as shown in fig. 2.3[71].

By employing ultrasonic vibration during friction stir welding tunnel flaws from the tool are abruptly eliminated[72]. To join the dissimilar metals 6061-T6 aluminium alloys and Q235 steel, a laser assisted friction stir welding. From the HAZ to the WNZ, the size of crystalline grain particles decreased. In TMAZ, the crystalline grain particles were small enough to be stirred with a pin tool[73], [74].It has been observed that ultrasonic energy decreases axial load during welding and enhances material flow along the joint line. As the mechanical properties of the material improved, internal flaws were eliminated[64].

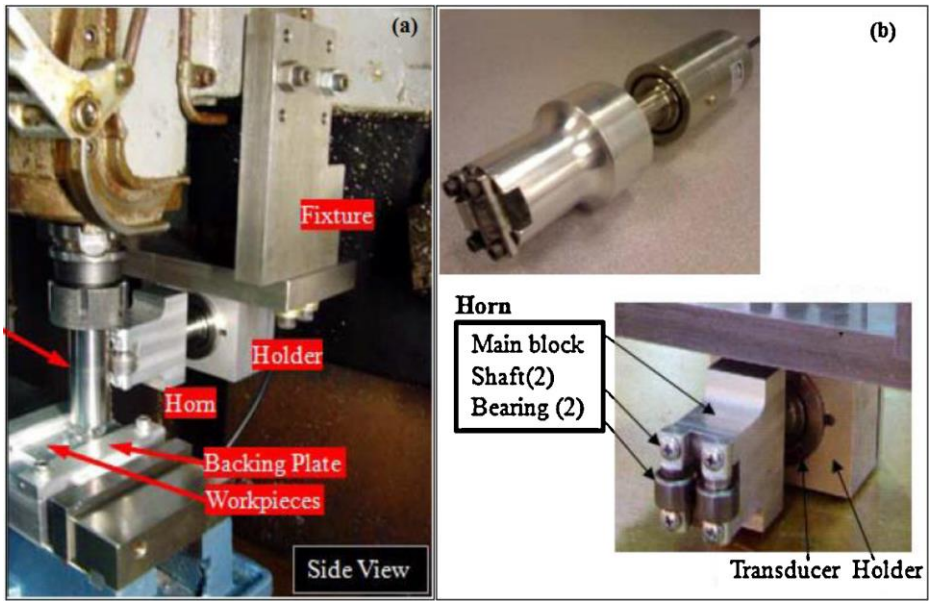

Figure 2.4 Setup of ultrasonic assisted FSW

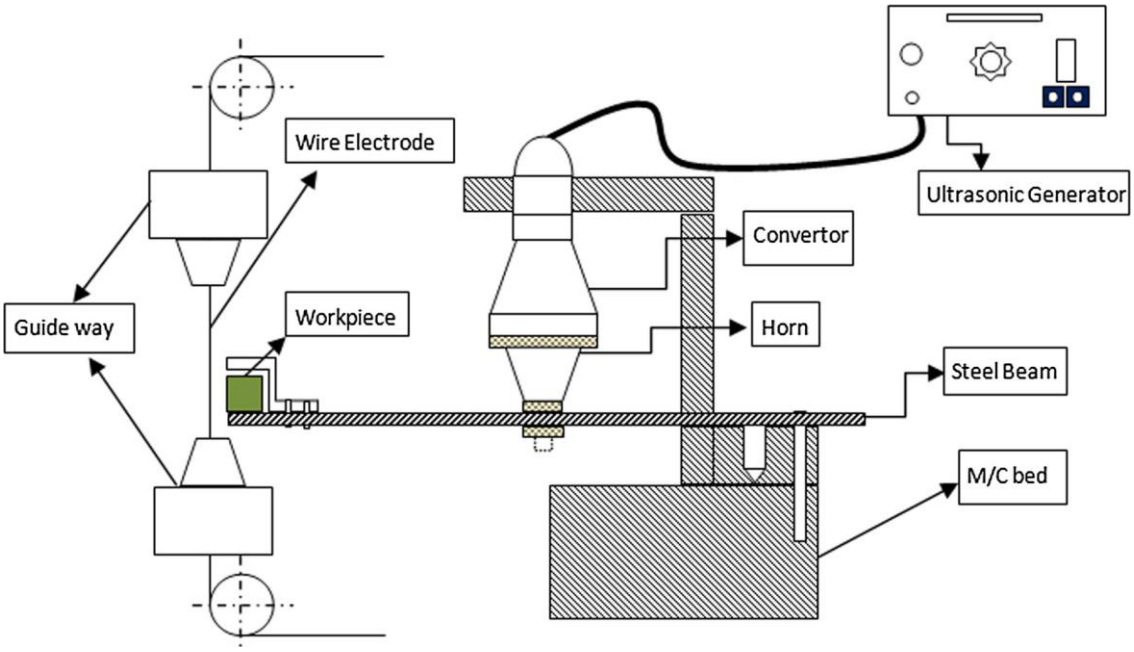

Figure 2.5 Experimental setup for ultrasonic wire-EDM [78]

Hybrid approaches offer heating and cooling in the form of friction stir welding. Various preheating techniques involving the application of an inert gas burn in front of the stirring tool have been utilized. It has been established Water significantly increased the tensile strength of FSW that had been cooled. Maximum tensile strength of 158 MPa was achieved,

along with an increase in the material's hardness[75]. A novel ultrasonic assembly (as shown in figure 2.4) is designed and constructed so that ultrasonic vibrations can be inducted into the weldment along the welding direction by means of the welding tool. At optimal parameters, a reduction in tool torque and input power is perceived[76], [77].

Ultrasonic vibration is combined with conventional Wire-EDM (as shown in figure 2.5) in a novel Hybrid Wire EDM process. It was observed that discontinuous vibration enhances the erosion rate and diminishes the resultant stresses. High Peak current and duty cycle degrade the surface texture, causing high tensile residual stresses as a result of debris and microstructures [78], [79]. Using the hole drilling method, the residual stresses induced in FSW aluminium alloys were studied. Vibrations with a frequency of 200 Hz and a power of 200 W can reduce the maximum residual tensile stress by approximately 45% and significantly increase tensile strength. Due to the peening effect, ultrasonic vibrations also prevent defects such as voids and tunnels in the weld zone during ultrasonic assisted friction stir welding[80]–[82].

2.3 RESEARCH GAPS

The following research gaps have been identified in the thorough literature survey on friction stir welding.

1. The majority of researchers have examined the impact of a limited number of process parameters on friction stir welding of AA.
2. Review of the relevant literatures reveal that researchers have conducted the majority of their studies by varying a single parameter at a time, without taking into account the interaction effect of two or more parameters.

3. Effect of process parameters such as tool rotational speed and welding travel speed. Types of vibrations, the amplitude of vibrations, and the tilt angle are yet to be investigated on bead geometry in UAFSW of AA 7075- T6.
4. Very few research works have been carried out on residual stresses, wear behavior and temperature distribution in weld bead using ultrasonic assisted FSW of AA 7075-T6.

Thus, considering the above research gaps, following research objectives have been drawn.

2.4 RESEARCH OBJECTIVES

The objective of this study is to develop a UAFSW technique that can enhance mechanical properties and weld quality. Since the ultrasonic assisted FSW process proposed is a new solid-state welding process, design and control guidelines are provided. In pursuit of a fundamental understanding of the ultrasonic assisted FSW process and a systematic approach to addressing the underlying scientific and technical challenges, the following objectives have been identified:

1. Design and Development of ultrasonic assisted friction stir welding (UAFSW) experimental setup.
2. Study of various process parameters such as tool rotational speed, welding travel speed, types of vibrations, amplitude of vibrations and tilt angle using design of experiment on the response joint strength, microhardness, and residual stress.
3. Thermal analysis of heat affected zone in UAFSW using soft computing.
4. Post process analysis of weld using Scanning electron microscope, Electron dispersive spectroscopy (EDS), X-Ray diffraction (XRD) technique.

2.5 RESEARCH METHODOLOGY

To achieve the proposed research objectives, the following methodology has been adopted. In the first phase of the research, experiment setup and tool design have been investigated. In the second phase of research work, the study of various process parameters using the design of the experiment to optimize joint strength and microhardness will be carried out.

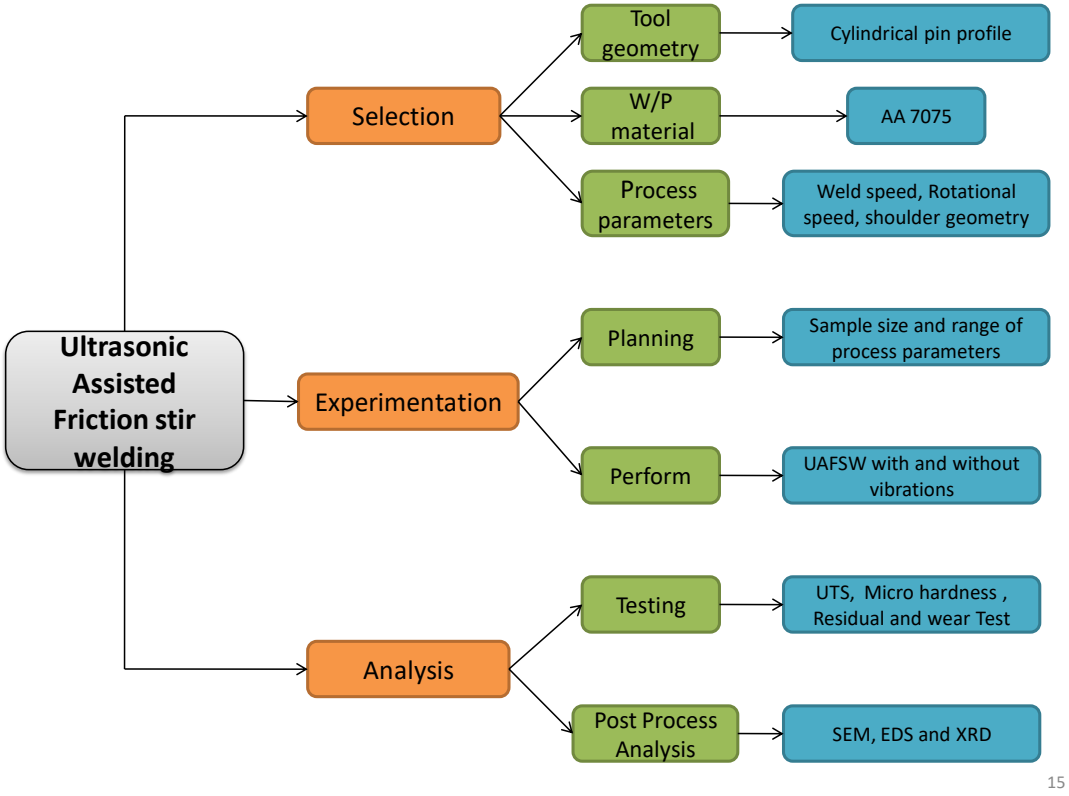

Figure 2.6 Flow diagram for research methodology

In the next stage, thermal analysis of heat affect zone will be done using soft computing. Finally, post processes analysis has been carried out using XRD, EDS, and SEM. For achieving the same, the methodology has been given in the form of a flowchart inFigure 2.6.

2.6 SUMMARY

This chapter outlined the different major literatures available on FSW of different materials and the influence of process parameters on the joint. Even though investigations have been carried out on FSW of different materials but very few too little works is available on the studies of process parameters on the joint properties in case of hybrid FSW, specifically Ultrasonic assisted FSW. The objectives for the present work have been formulated in a manner to address these research gaps and the methodology for achieving the same. has been given in the form of a flowchart.

CHAPTER - 3

EXPERIMENTAL METHODS

3.1 FRICTION STIR WELDINGMACHINE AND ITS SPECIFICATIONS

In the United Kingdom in 1991, "The Welding Institute" invented a highly innovative process for low melting temperature alloys called "Friction Stir Welding"[4]. This FSW machine is used for laboratory experiments and is depicted in Figure 3.1.

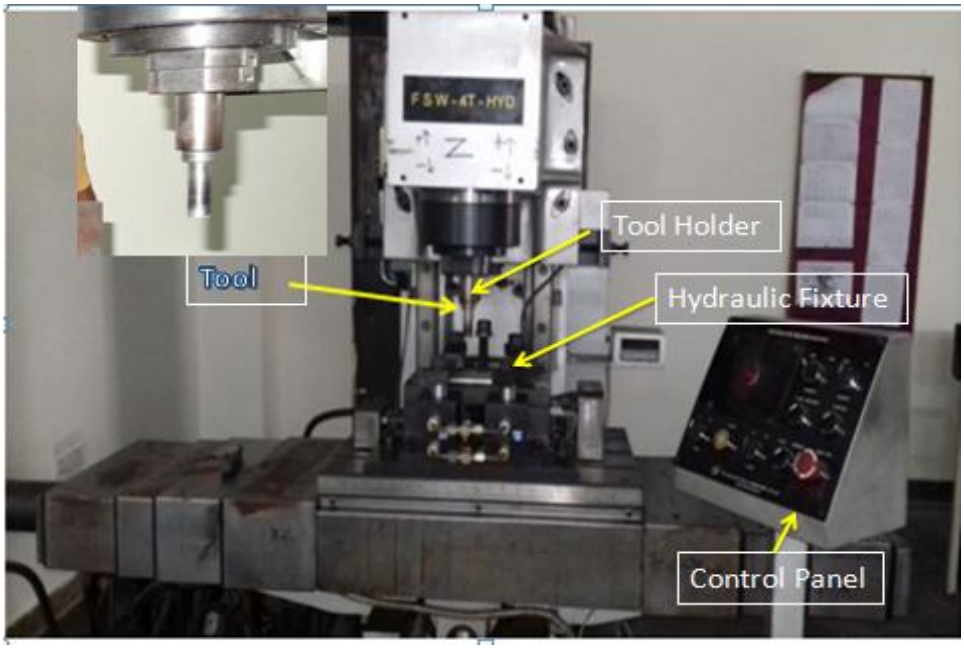

Figure 3.1 FSW machine

On this machine, plates as thick as 6 millimeters can be welded from mild steel and aluminium alloy. This machine can be manually or automatically operated. With the aid of this machine, welding can only be performed in a straight line. The machine's specifications are listed in Table 3.1.

Table 3.1Specification of FSW Machine

Machine Capacity	Machine Size(mm): 1300x1650x2000
Welding Material	Mild Steel, aluminium

Machine weight	Two ton
Job Size	6 mm Maximum thickness
Welding Geometry	Straight
Travel	Xaxis-600mm, Yaxis-200mm, Zaxis-300mm
Axis Trust Force	Xaxis-2500Kgf, Zaxis-4000Kgf
Spindle speed	1400 RPM (Max.)
Spindle drive	3-phase AC drive,
Spindle housing Tilting	Angle -5º to +5º
Tool Holder	ISO 40 taper single lock holder
Spindle move to table	300 mm
Fixture	Hydraulic clamping, T-slot table
Hydraulic power pack motor	2.2 Kw/1440 rpm, 440V
Tank Capacity	80 lt.
Lubrication pump	Manual centralized lubrication
Controller	The PC-based control system
Total connected Load	415,50 Hz/17KVA, AC 3 phase
Oil-to-oil intensifier	1 No pressure booster

3.2 FRICTION STIR WELDING TOOL

The geometry of the FSW tool is depicted in Figure 3.2.The choice of tool and tool material is crucial to any fabrication procedure. For experimental purposes, H13 tool steel was used to in the UAFSW process for joining the two sheets.

As it has a high hardness value (55-65 HRC) and strength even at high temperatures, as well as good hardenability, it can withstand high temperatures. The FSW tool has a cylindrical pin with a cylindrical shoulder. The design of the tool has a significant impact on the quality of the weld.

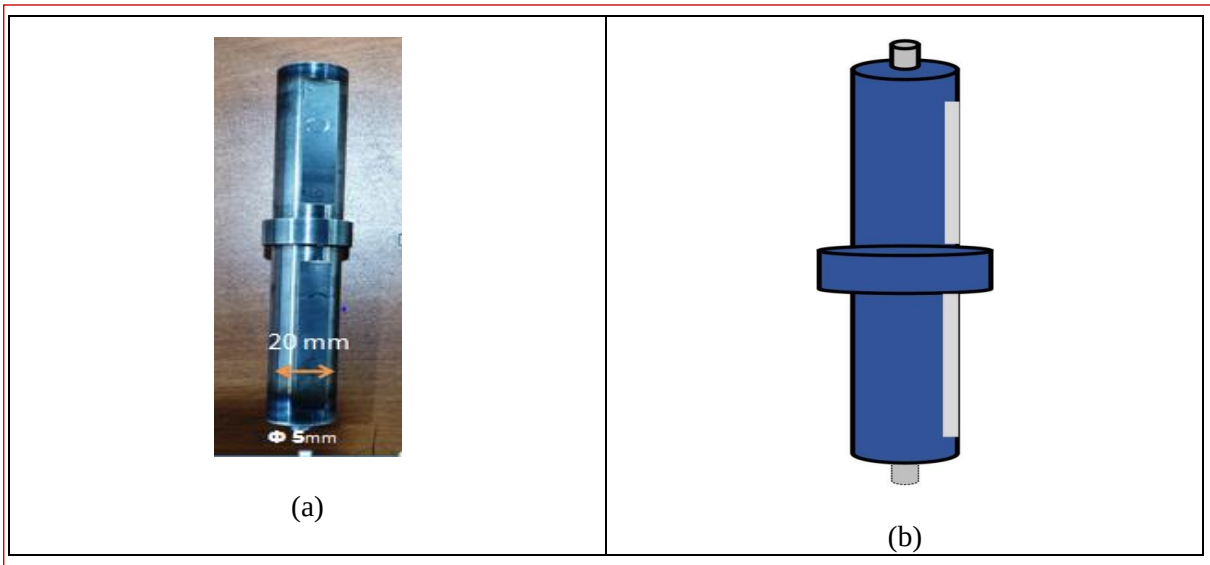

Figure 3.2 Geometry of FSW tool (a) Experimental tool (b) Designed tool

3.3 SELECTION OF WORKPIECE MATERIAL

The selection of work material is an important factor of any fabrication procedure. In this experimental investigation, AA7075-T6 work material has been utilised. Among the series of aluminium alloys, AA7075 has exceptional corrosion resistance and high strength, and is therefore widely used in the marine and aerospace industries.

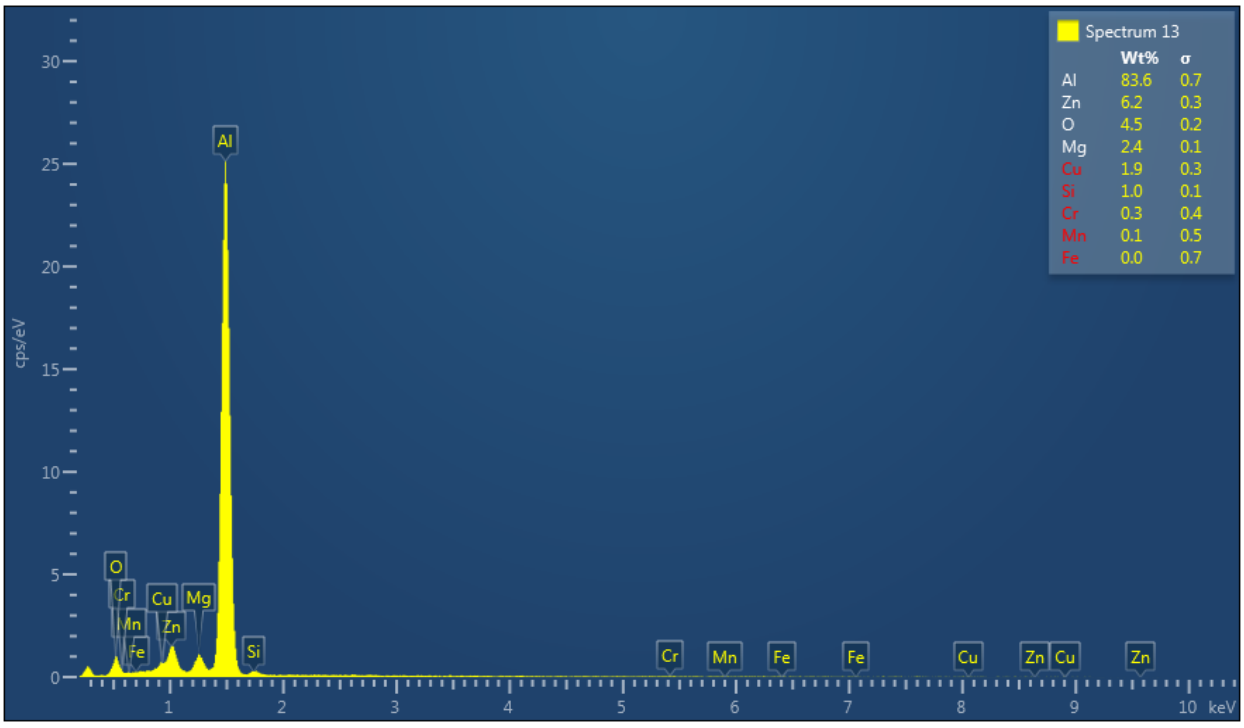

Figure 3.3 EDS of AA 7075-T6

Aluminium's mechanical properties (tensile strength, hardness, ductility, lightweight material, low density, and ease of fabrication) can be improved and adjusted through alloying and processing[83]–[85]. AA 7075-T6 combines zinc, copper, magnesium, and other machinable and precipitation solidifiable substances. Aluminum, magnesium, silicon (these substances are heat treatable and generally utilised for extrusion, sheets, and plates- all are weld capable but can be defects sensitive). The workpiece's dimensions are 250 mm in length, 80 mm in width, and 3 mm in thickness and shown in Figure 3.4. Table 3.2 displays the chemical composition and mechanical properties.

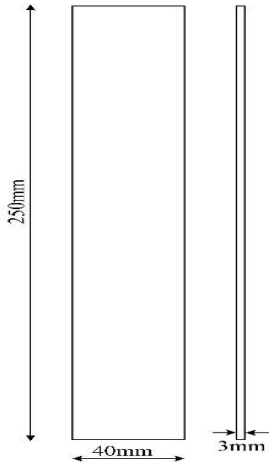

Figure 3.4Aluminium sheet of AA7075-T6 with dimensions of 250 x 40 x 3 in mm

Table 3.2Chemical Composition & Mechanical Properties of AA7075-T6

Chemical Composition of AA7075-T6										
Element	Si	Fe	Cu	Mn	Mg	Cr	Zn	Ti	Others	Al
Wt %	0.4	0.5	1.2-2.0	0.3	2.1-2.9	0.18-0.28	5.5-6.1	0.20	0.05	Rest

Mechanical Properties of AA7075-T6					
International alloy Designation	Young Modulus (GPa)	Percentage Elongation	Tensile strength (MPa)	Vicker hardness (Kgf/mm^2)	Yield Strength (MPa)
AA 7075	71.77	11	572	103	503

3.4 EXPERIMENTAL SETUP OF THE HYBRID FRICTION STIR WELDING

Ultrasonic vibration enhanced friction stir welding (UVeFSW) was created in order to utilise the acoustic softening effect[74].where the ultrasonic vibration is transmitted directly into a workpiece close to the rotating tool. Previous research has demonstrated that UVeFSW not only improves the microstructure and mechanical properties of the joints, but also reduces the welding loads and expands the process parameter window in order to produce defect-free weld joints[76], [86].

The proposed ultrasonic system consists of an ultrasonic generator box, transducer, and horn and operates at 20 kHz.

3.4.1 Components of UAFSW

There are three main components which are attached in a conventional FSW to make a hybrid FSW that is called UAFSW. These components are the following:

i. Ultrasonic Generator box
ii. Transducer, and
iii. Ultrasonic Horn

These components are specially designed to achieve the ultrasonic vibrations desired. The efficient transfer of ultrasonic power is of the utmost importance and depends on the intricate and thorough design of ultrasonic components. The ultrasonic generator box generates 20 kHz ultrasonic energy and transmits it to the ultrasonic horn. The diagram depicts the anatomy of the generator box in Figure 3.5 (a). The ultrasonic generator transmits pulses of electrical energy to the transducer, which converts the energy into mechanical vibrations. It was an ultrasonic generator with an internal system that automatically adjusted the output frequency to match the horn's resonant frequency. The selection of the automatic ultrasonic generator was motivated by its safety features, such as automatic shutoff in the event of a

malfunction or failure of the horn. With two metres (upper and lower metres) and an amplitude controller, this generator has been designed specifically for this experiment. The upper metre indicates ultrasonic power, while the lower metre indicates horn match. The amplitude controller modifies the frequency's amplitude. The amplitude range is 33-99 μm A booster is used to increase the vibration's amplitude.

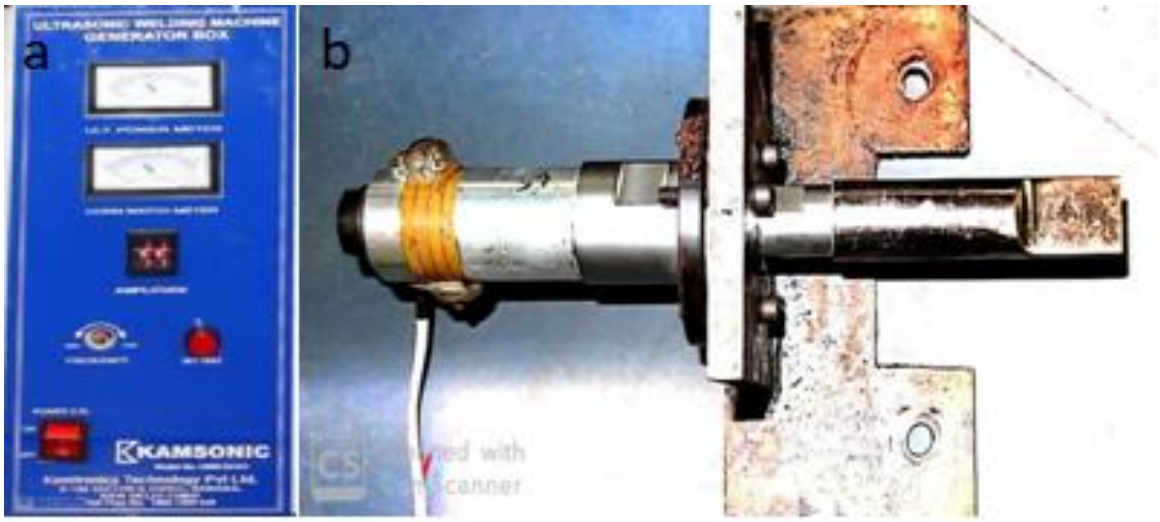

Figure 3.5 (a) Generator box (b) Transducer with ultrasonic horn

The function of the ultrasonic transducer is to convert one form of energy into another. These devices employ similar operating principles to radar and sonar systems. The converter converts the electrical energy received from the power supply into mechanical vibrations, hence its name. In the present investigation, the transducer was designed to achieve longitudinal vibration. It produces a 20 kHz frequency when supplied with 220VAC.A systematic view of various components of UAFSW are shown in Figure 3.6

The horn's design is crucial because even a slight shift in instrument length can result in a variation in resonance frequency and, consequently, amplitude. The ultrasonic horn has a rectangular cross-section measuring 30 mm by 5 mm in size. The rectangular horn is designed to transmit maximum ultrasonic energy to the welded region in order to improve the

mechanical properties of HAZ and TMAZ[87]. The uniquely designed fixture holds the horn horizontally against the workpiece. Figure 3.7 illustrates complete set up of UAFSW.

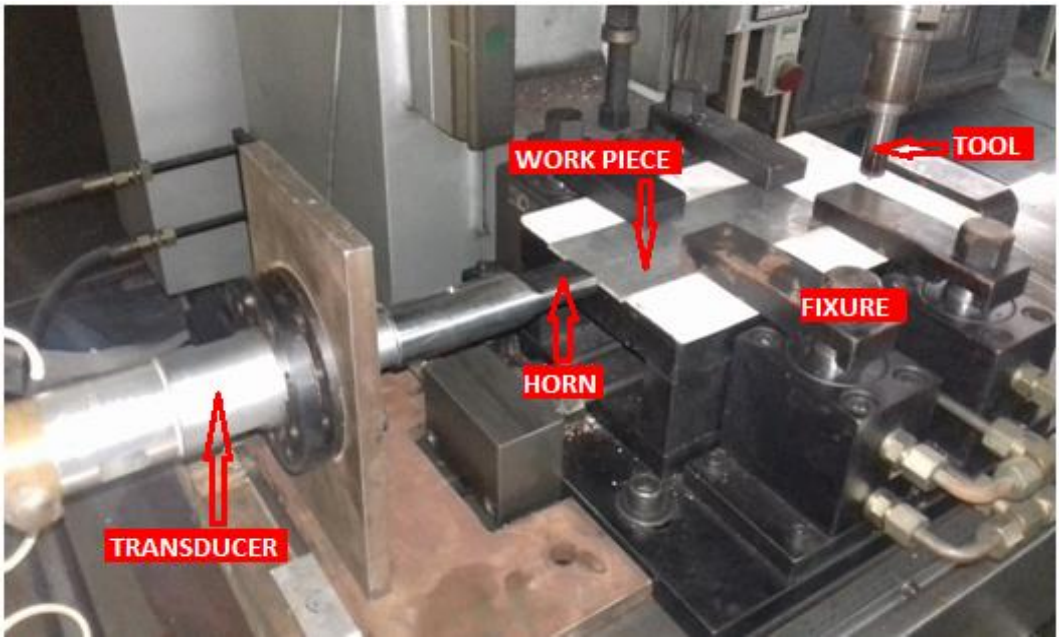

Figure 3.6 Component of UAFSW

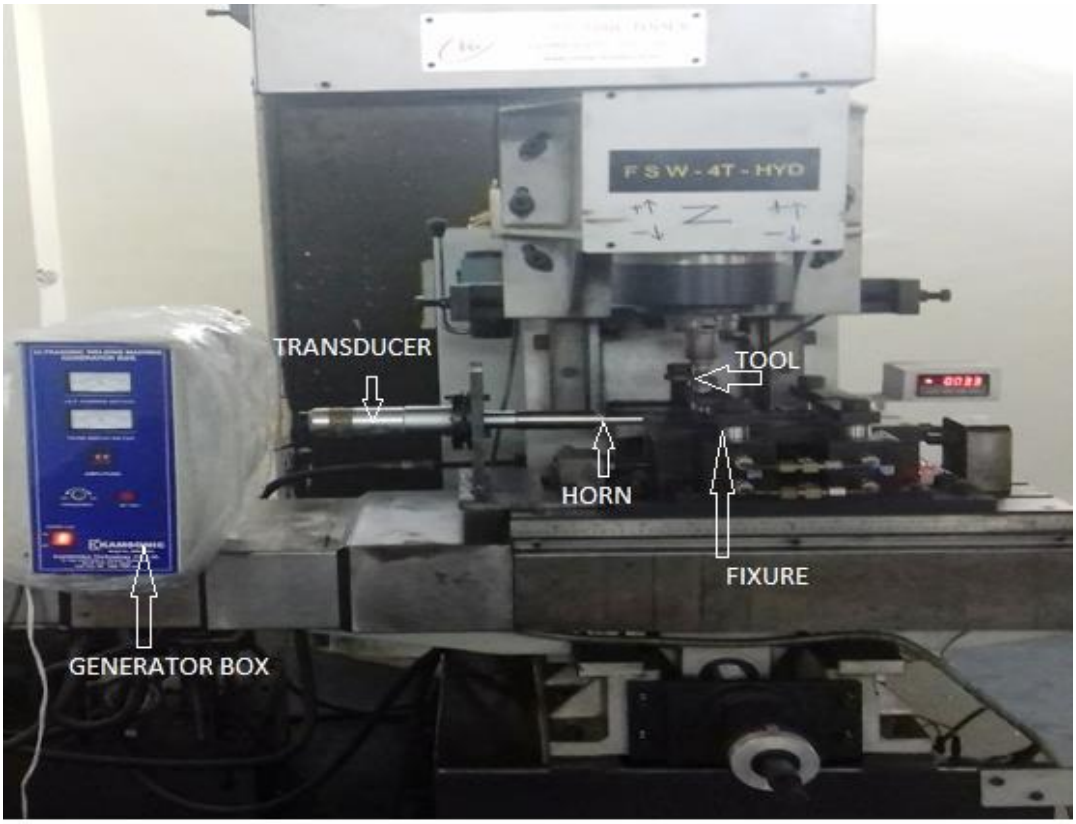

Figure 3.7Complete setup of UAFSW

3.5 PROCESS PARAMETERS FOR UAFSW

FSW entails both complex material growth and plastic deformation. During the welding procedure, the material flow pattern, joint quality, and temperature distribution are dependent on the process parameters, tool geometry, and hybrid approaches. Numerous parameters of FSW, such as rotational speed, tool geometry, travel speed, tilt angle, and axial force, have a significant impact on the mechanical properties of the aluminium alloy, as determined by a review of the relevant literature and trial experiments. For this experimental investigation, the most significant parameters are chosen. The selected welding process parameters and the rationale for their selection are outlined in table 3.3 and table 3.4.

Table 3.3 Parameters & Justification for selecting the parameters

Parameters	**Justification for selecting the parameters**
Tool Rotational Speed of the tool (RPM)	The speed of rotation aids in stirring and mixing the material surrounding the tool[52], [88]
Traverse speed (mm/min.)	The traverse speed aided the forward and backward movement of the stirred material and completed the welding process[52], [88]
Amplitude in (μm)	Amplitude facilitates the increase or decrease of ultrasonic energy[89]
Types of Vibration (KHz)	To study the effects of both continuous and discontinuous vibrations[89]
Tilt Angle (Degree)	To study the impact of material flow during the welding[90], [91]

Table 3.4 welding process parameters and their values at different levels

Factor Number	**Factor Name (Units)**	**Values taken at different levels**		
1	Type of vibration (KHz)	Continuous	Discontinuous	-
2	Tilt angle (Degree)	0	1.5	3
3	Travel Speed(mm/min.)	40	50	60
4	Rotational speed (RPM)	600	800	1000
5	Amplitude (μm)	0	44	88

3.6 FINITE ELEMENT MODELLING

In structural mechanics, finite element discretization is the dominant method for separating a complex model into disjoint components of small geometries. In addition, Finite Element Methods can capture a significant portion of the process's complexity, allowing the differential equation governing the process to be determined[92], [93].

3.6.1 Tool geometry of FSW

The process is assembled as depicted in Figure 3.6. For the tool's dimensions, the pin's height is assumed to be 1.6 mm, its diameter is assumed to be 5 mm, the shoulder's diameter is assumed to be 20 mm, and the shoulder's height is assumed to be 50 mm. For the dimensions of the workpiece consisting of two identical sheets, the length of each sheet is assumed to be 250 mm, its width is assumed to be 40 mm, and its thickness is assumed to be 3 mm.

The width of the sheet was determined to be 40 mm due to insignificant effects observed at a distance equal to three times the shoulder radius of the tool. The workpiece is modelled as a lagrangian bilinear-isotropic body, while the tool is modelled as a lagrangian linear-elastic body. In structural-thermal analysis mode, SOLID226 (coupled-field solid) elements are

utilised. Using CONTA174 and TARGE170, the contact pairs between the two sheets and between the tool and each of the workpieces are defined as standard surface-to-surface contact pairs. A hexahedral mesh is employed, with a finer mesh near the weld line. With =0.3, Coulomb's law of friction describes the contact between tool and workpiece[93].

3.6.2 Boundary Conditions

As shown in Figure 3.6, the ends of the sheets (20 percent) are constrained in all three directions to prevent displacement due to force exerted by the tool and spreading, thus simulating the action of backing sheets. The bottom of the workpiece is constrained in a

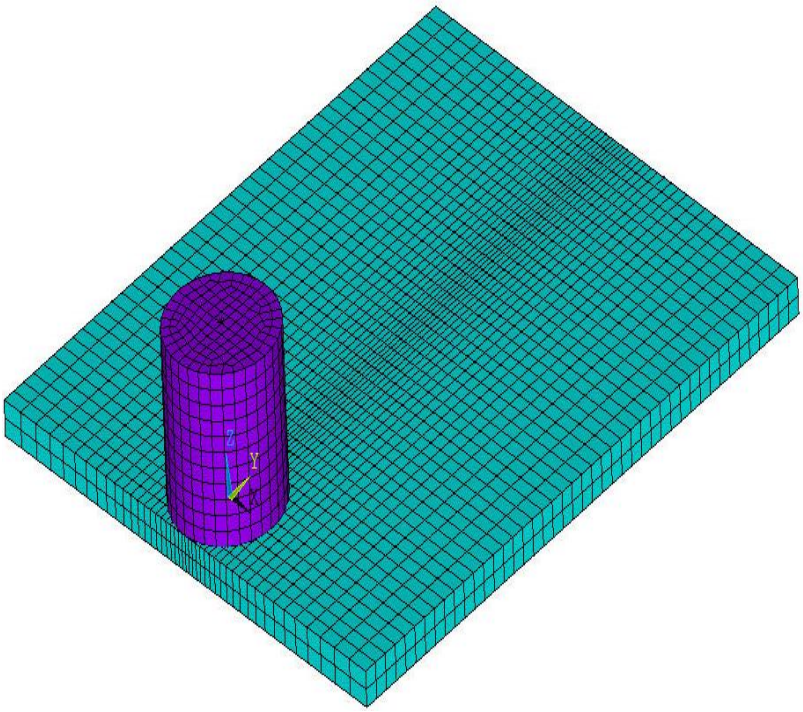

Figure 3.8Assembly of geometry in the FEM

direction parallel to the tool's rotation axis (z-axis). Both the initial and reference temperatures are set to 298K. Convection heat loss occurs from the bottom of the workpiece with a heat transfer coefficient of $300\mathrm{W/m^2K}$, and from all other surfaces of the workpiece and the tool with a heat transfer coefficient of $30\mathrm{W/m^2K}$. Due to the small proportion of heat

lost due to radiation, radiation heat losses are disregarded. To achieve continuous bonding and simulate perfect thermal contact between sheets, a thermal contact conductance of 2e06W/m^2K is specified between sheet-to-sheet contact pairs. To model friction-induced heat generation, two real constants are specified. The real constant is set to 1 so that all frictional dissipated energy is converted into heat. Next, the factor for heat distribution between the contact and target surfaces is specified, and the actual constant is set to 0.95, so that 95 percent of the frictional generated heat flows into the workpiece and only 5 percent flows into the tool. The tool-to-workpiece contact pair is specified with a low TCC value of 10W/m2K because the majority of the heat generated is transferred to the workpiece. According to the pilot node, a rigid surface constraint is defined for the tool to make it behave as a single entity.

3.7 PLANNING OF EXPERIMENTS

For creating models based on experimental data, it is essential to plan experiments methodically. Design of experiment (DOE) refers to the series of experiments or data collection in which variation is present, regardless of whether the process is under control. A

(a) (b)

Figure 3.9 Tool and workpiece positions of FSW and UAFSW

properly organised and implemented experiments essential for drawing obvious and correct conclusions from the experimental findings. DOE is an extremely valuable method for accomplishing these tasks. Sir Roland Fisher established the fundamental rule of experimental design and the combined data analysis technique known as Analysis of Variance (ANOVA) in 1920 as part of his efforts to increase crop yields. Various types of matrices are utilised for systematic experiment planning and analysis of multiple response variable choices. Taguchi's Method, for example, makes extensive use of orthogonal arrays (OA)[94], [95].

3.8 EXPERIMENTAL PROCEDURE

Various levels of consideration for these variables have been applied to the experiments. The experimental tests were conducted with UAFSW apparatus. Aluminum alloy AA 7075-T6 sheet with dimensions of 250 mm in length, 40 mm in width, and 3 mm in thickness was used for the joining process of two sheets. A total of eighteen samples were welded using UAFSW and process parameters were varied according to the design matrix using Taguchi L18 orthogonal array and UAFSW. Tool position and tool geometry remained unchanged throughout all experiments. Tool and work piece positions during wxperimets are shown in Figure 3.9.

3.9 MECHANICAL PROPERTIES OF UAFSW JOINTS

3.9.1 Measurement of Hardness

A material's hardness is its resistance to plastic deformation, typically by penetration. Additionally, hardness can denote resistance to bending, scratching, abrasion, and cutting.

Samples with a rectangular-square cross section were specifically prepared for microhardness and microstructure evaluating as shown in fig. 3.10. These samples were cut parallel to the centre processing line of the welded sheets.

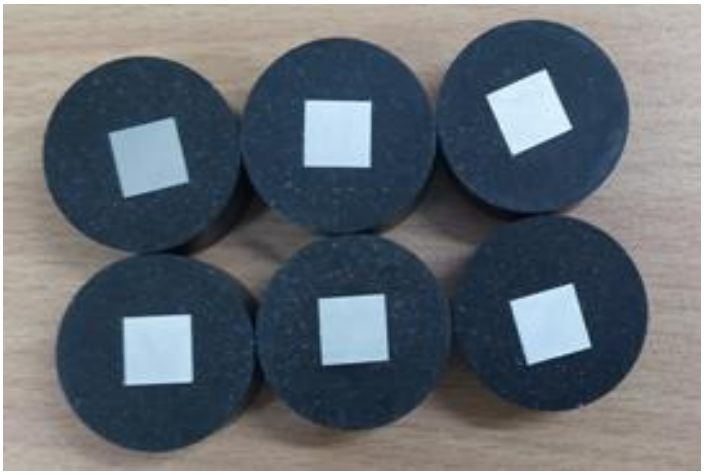

Figure 3.10 Samples for microhardness

Figure 3.11 Fischer scope HM2000S

Using the Fischer scope HM2000S Microhardness tester as shown in fig. 3.11, which measures Vickers hardness, the cross-section of the weld zone along the weld line is evaluated for three points of average hardness. The required sizes of 18 hardness specimens were cut perpendicular to the weld zone line. The Vickers hardness test is an optical method for measuring the indentation size. To ensure the precision of the experiment, the average of three readings was taken for each sample. The microhardness test was initiated with a load of 0.300 N and a dwell time of 20 seconds.

3.9.2 Tensile Test

According to the design matrix, 18 welding joints were fabricated. Typical tensile test samples were extracted perpendicular to the weld zone line using a wire EDM machine in accordance with American Society for Testing Materials (ASTM) E8M-11 standards as depictedin Figure 3.12[96].

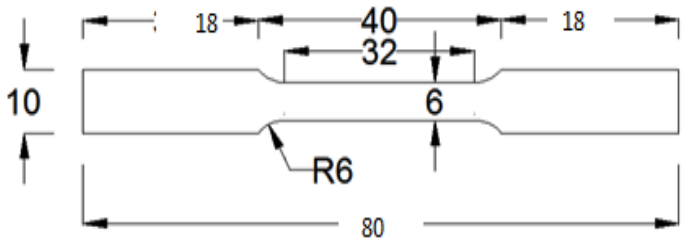

Figure 3.12 Rectangular sub size specimen

The tensile tests were carried out with a universal testing machine (AI-UTM-40T). A tensile specimen whose dimensions are known is subjected to a longitudinal or axial load at a specific extension rate until failure. During the test, the applied tensile load and extension are recorded in order to calculate stress and strain. Professional societies such as the American Society for Testing and Materials (ASTM) provide a variety of universal testing standards, which are selected based on the need. Each standard contains a number of test standards suited to varying materials, dimensions, and fabrication histories.Specimen for tensile test before and after shown in Figure 3.13.

(a) (b)

Figure 3.13 Specimen for tensile test before and after

3.9.3 Residual Stress

There are a number of unfavourable effects on components caused by joining process by various methods, one of the major of which is residual stress on the weld surface. Numerous factors, including heating, cooling, re-solidification, melting, and phase transformations with volume change, contribute to residual stress. This residual stress induces a decrease in the product's reliability and an uncertain failure rate for the manufactured goods. Therefore, it was necessary to investigate residual stress so that these stresses could be reduced and product dependability improved. Techniques for measuring residual stress can be categorised as destructive testing, semi-destructive testing, and non-destructive testing (NDT)[97], [98].

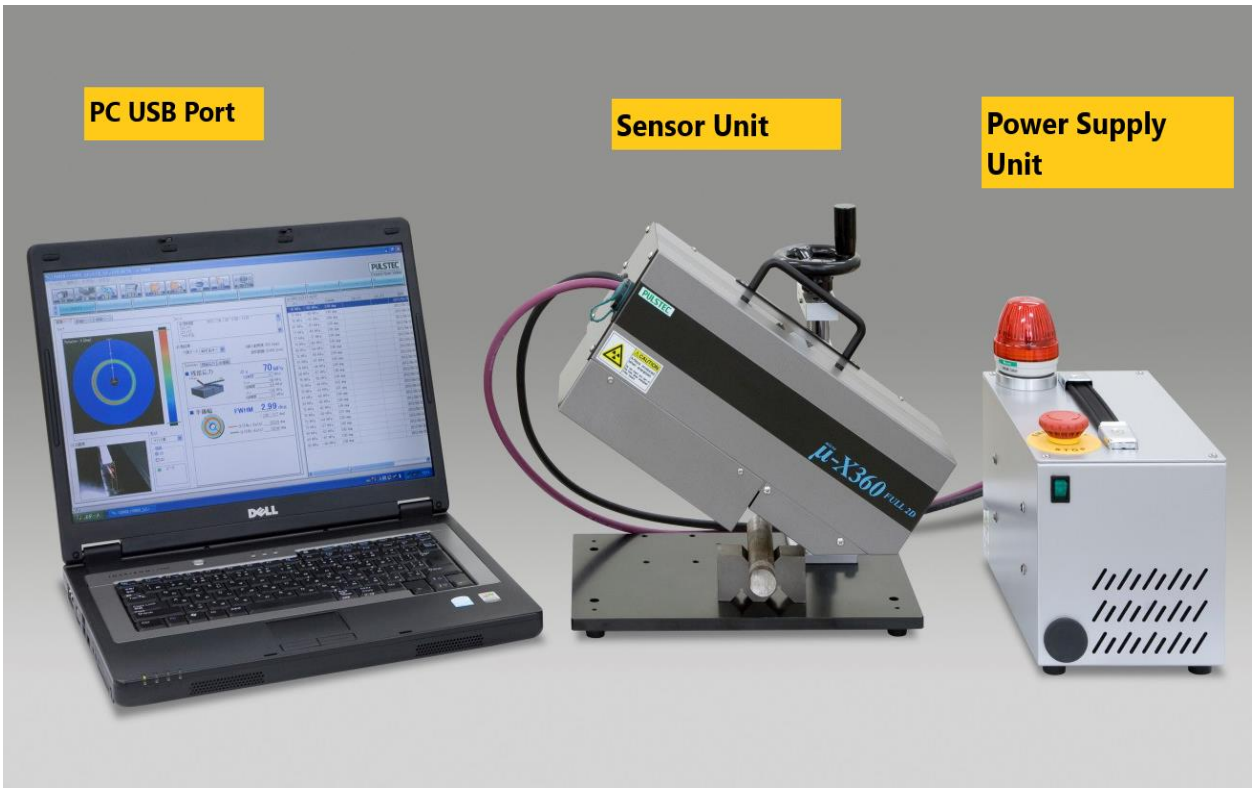

Figure 3.14 Portable XRD - residual stress analyzer

NDT is superior to destructive and semi-destructive testing in several ways. NDT is applicable to a wide range of materials, and measurement precision is high. There are

numerous NDT techniques for measuring residual stress, including X-ray diffraction, Berkhausen noise, neutron diffraction, and ultrasonic testing.

Because X-ray diffraction technique can be used to measure residual stress in a wide variety of materials, the X-ray diffraction method has several advantages over other techniques. Other advantages of the X-ray diffraction technique include the ability to analyse micro and macro residual stress, as well as the technique's portability, which enables readings to be taken in any orientation.

During UAFSW, residual stresses are generated due to the plastic deformation of metal. Consequently, the fatigue life of the produced composites may be increased or decreased. Therefore, it is essential to examine and regulate it. Depending on the processing of the materials, residual stress can be either positive or negative [53].

Portable X-ray residual analyzer (Figure 3.14) (PULSTEC-X360n) (based on cos method), a non-destructive X-ray analyzer from PULSTEC Industrial Corporation Limited, was used in this research study to measure residual stress in UAFSW with the following specifications: X-ray beam (wavelength = 2.29, energy = 0.15, current (1 mA), tube voltage (30 kV), and source (Cr Ka/Ni Kb filter). Using a single incidence X-ray angle to detect the entire Debye ring data and removing the impact of the non-goniometer stage on the measurement output, this analyzer could accurately measure stress. The X-ray signals and Debye ring distortion are automatically collected and stored on the computer. The X-ray exposure diameter was 1mm, the exposure time was 30s, and the incidence angle of the X-rays was 35.0 degrees.

The varied orientations of grain crystals that satisfy Bragg's law cause X-ray diffraction.As a result of the variance in crystal orientation, diffracted X-rays form a cone around the incident x-ray axis.

$$n\lambda = 2dsin\theta \tag{3.1}$$

Where n is the "order" of reflection, λ is the wavelength of the incident X-rays, d is the interplanar spacing of the crystal, and θ is the incidence angle equal to the scattering angle.

Residual stresses on welded samples result from a biaxially applied load and thermal stresses on the body, and can be calculated using the following equations:

$$\sigma = \sigma_{thermal} + \sigma_n \tag{3.2}$$

Where,

$$\sigma_n = \frac{1}{2}\{(\sigma_x + \sigma_y) + (\sigma_x - \sigma_y)cos2\theta\} + \tau_{xy}sin2\theta \tag{3.3}$$

$$\sigma_{thermal} = \{\frac{\alpha TL - \lambda}{L}\}E \tag{3.4}$$

hence, The cumulative residual stress on a material will be:

$$\sigma_x = -\frac{E}{1+\nu}\cdot\frac{1}{\sin 2\eta}\cdot\frac{1}{\sin 2\psi_o}\cdot\left(\frac{\partial\varepsilon\alpha_1}{\partial\cos\alpha}\right) \tag{3.5}$$

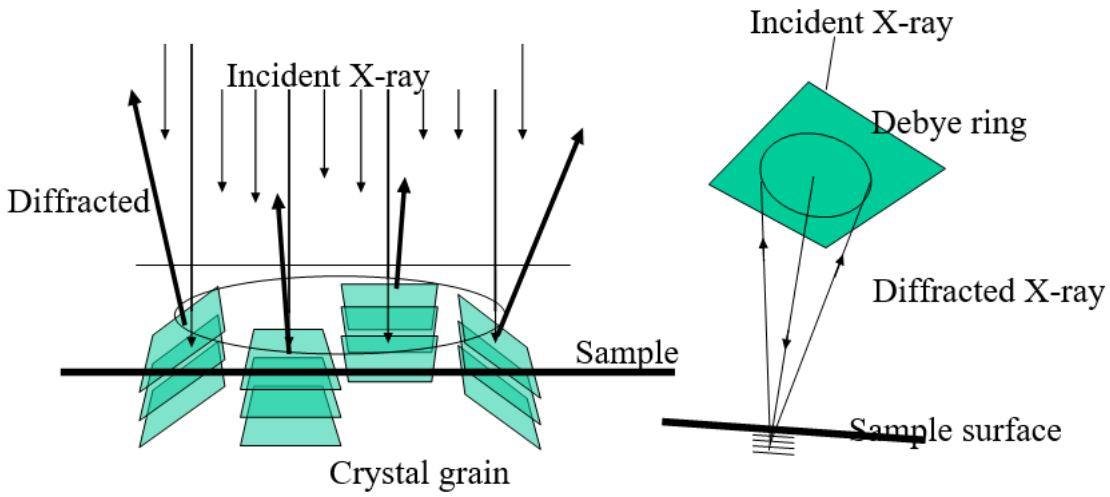

Figure 3.15 Systematic diagram of residual stress of UAFSW joint

Where on the surface is residual stress developed, v is the poisson ratio, is the diffraction lattice angle, is the X-rays incident angle, and is the Azimuth angle of the Debye ring.

The body was subjected to a biaxial load and thermal stresses, resulting in residual stresses in the welded samples. The residual stress concentration in the substrate material is represented by the Debye ring produced by a single exposure of incident X-ray for a brief duration. The exact location of Debye rings was measured to calculate residual stress. Their locations directly reflect the amount of stress they are experiencing. Various colour combinations are used to represent the concentrations of residual stress, such as red for the highest concentration and blue for the lowest. Figure 3.15 depicts the systematic diagram of the residual stress analyzer.

3.10 WEAR BEHAVIOUR OF UAFSW JOINTS

The wear behaviour of UAFSW welded joints was investigated using a pin on disc tribometer (Make: DUCOM, Atlas; TR-20L-PHM 800-DHM850) and tests were conducted in accordance with the ASTM G99-04 Standard. The Pin on Disk wear test conditions are detailed in Table 3.4. The pin-on-disc machine setup and pin-on-disc machine setup schematic are displayed in Figure 3.16. The 6 mm diameter pin specimens for the wear test were cut from the welded joints, and the 55-60 HRC-hardened EN-24 steel counter disc was used. The surface roughness (Ra) of the counter disc was measured using a surface roughness tester (Make: TAYLOR HOBSON). Prior to the sliding wear test, the disc's surface was ground on a 1200-grit emery paper to maintain an initial surface roughness (Ra) of 0.2m. The test specimens and disc were cleaned with acetone prior to the wear test. Before measuring the weight loss, the worn surfaces were cleaned with acetone and dried following the wear test.

Table 3.4 Parameter used for wear test

Sr. No.	Test condition	Parameters used
1	Sliding distance(m)	1500
2	Pin diameter, Height(mm)	8
3	Track diameter(mm)	40-50
4	Disc diameter(mm)	100
5	Disc surface roughness(Ra)	0.25
6	RPM	300
7	Temperature(ºC)	100ºC
8	Load (N)	100

Figure 3.16 Experimental set up for wear test

Before and after the test, the wear test specimens were weighed to an accuracy of 0.01mg using an electronic weighing balance (Make: SHIMADZU).

3.11 METALLURGICAL CHARACTERIZATION OF UAFSW WELDED JOINTS

3.11.1 Microstructural characterization

In recent years, friction stir welding of metals and their compounds has been investigated. The mechanical and physical properties of processed materials and joints are influenced by the microstructure of metals and their alloys; therefore, it is essential to examine the microstructure evolution during FSW. Recent research indicates that dynamic restoration phenomena can occur as a result of the coexistence of strain and heat during FSW. The type of restoration phenomenon is dependent on material properties and processes, the management of which can influence the microstructure of joints or processed metals, and thus their mechanical properties. The microstructure is crucial because the grain structure refinement that results from friction stir processing is one of its most significant effects. The composite material is endowed with superior mechanical properties as a result. SEM was utilised to investigate the microstructural behaviour of the material in the weld zone for each sample by employing conventional metallurgical planning and image techniques. The heat-treatable aluminium alloys (2xxx, 6xxx, and 7xxx) are strengthened by second-stage particles and are well-known for compound precipitation solidification. Copper (2xxx), magnesium and silicon (6xxx), and magnesium and zinc (7xxx) are, in order, the essential alloying elements for the three compound classes.

Figure 3.17Olympus GX41 microscope

In the vast majority of instances, a single precipitation event is primarily responsible for the strengthening effect. However, it may be due to a small number of precipitate phases in the microstructure. Due to the heat contribution of FSW in these alloys, non-tempering metallurgical development, such as ageing, precipitation development, or disintegration, may occur in different regions of the joints.

The samples were ground in a mounting press and mounted with Bakelite powder for sample preparation. The samples were then polished with 320, 400, 600, 800, 1000, 1200, 1500, and 2000 grit emery paper, followed by alumina suspension and velvet cloth. Figure 3.17 depict a machine an Olympus GX41 microscope. Microstructural characterization was conducted to determine surface shape and grain structures of welded samples. Machine for SEM and FeSEM analysis are shown in Figure 3.18.

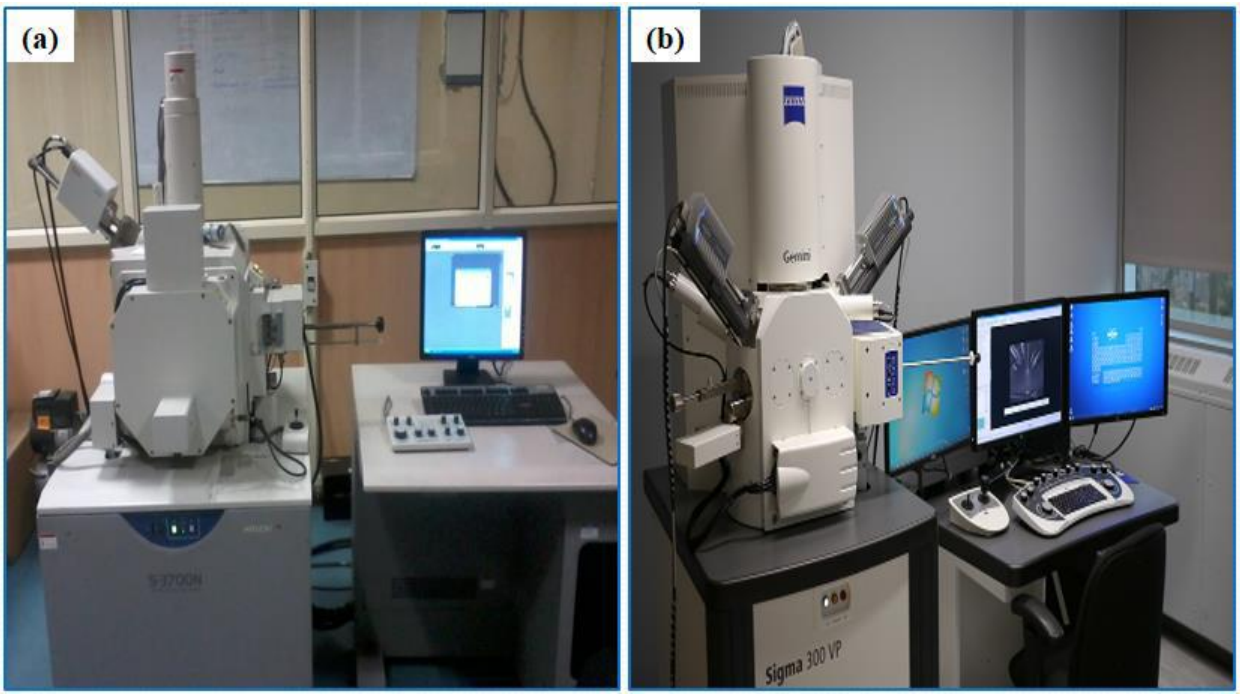

Figure 3.18 Experimental Set up of SEM and FESEM (IIT Delhi, Delhi)

3.11.2 X-Ray diffraction

Crystallographic structure, chemical composition, and physical properties of materials can be determined using X-ray scattering techniques. Observing the scattered intensity of an X-ray beam striking a sample as a function of incident and scattered angle, polarisation, wavelength, or energy is necessary for these techniques. A cathode ray tube (CRT) produces X-rays, which are then filtered to produce monochromatic radiation, collimated to concentrate, and directed at the sample. When the conditions of Bragg's law are met, the interaction of incident rays with the sample produces constructive interference and a diffracted ray. The relationship between the wavelength of electromagnetic radiation, the diffraction angle, and the lattice spacing of a crystal is described by this law.

In the present study, using X-ray diffraction (XRD) analysis, the presence of a crystalline phase in the material was determined[15], [80]. X-ray diffraction (BRUKAR D8 ADVANCE) was used to determine the different phases. At room temperature, XRD diffractometer with Cu-K X-ray radiation (= 1.54056). Each sample's X-ray diffraction

pattern was recorded ranging from 10 to 80 degrees. The graph was used to identify the position of the peak and record the corresponding value. The phases were identified by matching the Bragg's angle values and interplanar spacing (d) with the standard values of X-ray diffraction files.

3.12 SUMMARY

The details regarding the machine to be used, the set up that has been developed for the UAFSW, the material used and the process parameters that have been investigated for the present work has been highlighted in this chapter in complete details. The caveats of the FEM analysis done on the UAFSW have also been detailed in this chapter. Finally, the experimental details regarding the joint strength, wear behaviour and Microstructural features have been explained and also the machines to be used for their analysis i.e., Optical microscope, SEM, XRD etc has been discussed.

CHAPTER - 4

OPTIMIZATION OF UAFSW PARAMETERS BY TAGUCHI METHOD

This chapter deals with Taguchi's recommended standard procedure for data analysis. From experimental data, each parameter at different levels is discussed for the mean values and S/N ratio response characteristics.

4.1 TAGUCHI EXPERIMENTAL DESIGN AND ANALYSIS

The Taguchi technique involves reducing process variation via the design of experiments. The technique's primary objective is to generate quality for the organisation. Taguchi devised a method for designing an experiment to determine how various process parameters influence the mean and variance of process execution, which reveals the characteristics of the process, i.e. how well the process is functioning. Taguchi's DOE entails the use of OA (Orthogonal Arrays) to frame the parameters affecting the process from its target value and the acceptable levels of deviation. Instead of testing every possible factorial design combination, the Taguchi strategy tests sets of combinations. This method considers the accumulation of basic data to determine which factors have the greatest impact on the quality of a product with the least amount of experimentation, saving time and resources[99].

4.1.1 Taguchi methodDOE

Step to be followed in Taguchi DOE are as follows and is shown in Figure 4.1.

4.1.2 Experimental design strategy

Taguchi Suggests Orthogonal array experiments are conducted in a systematic order. First, choose the optimal OA for the experiment and assign the essential parameters. Taguchi suggests using linear graphs and triangular tables to make parameter allocation straightforward. The Taguchi method aims to achieve the following:

i. To determine the optimal conditions or settings for a process or product.

ii. To calculate the effect of single parameters and their interaction on the process's performance.

iii. evaluates the response below the optimal level.

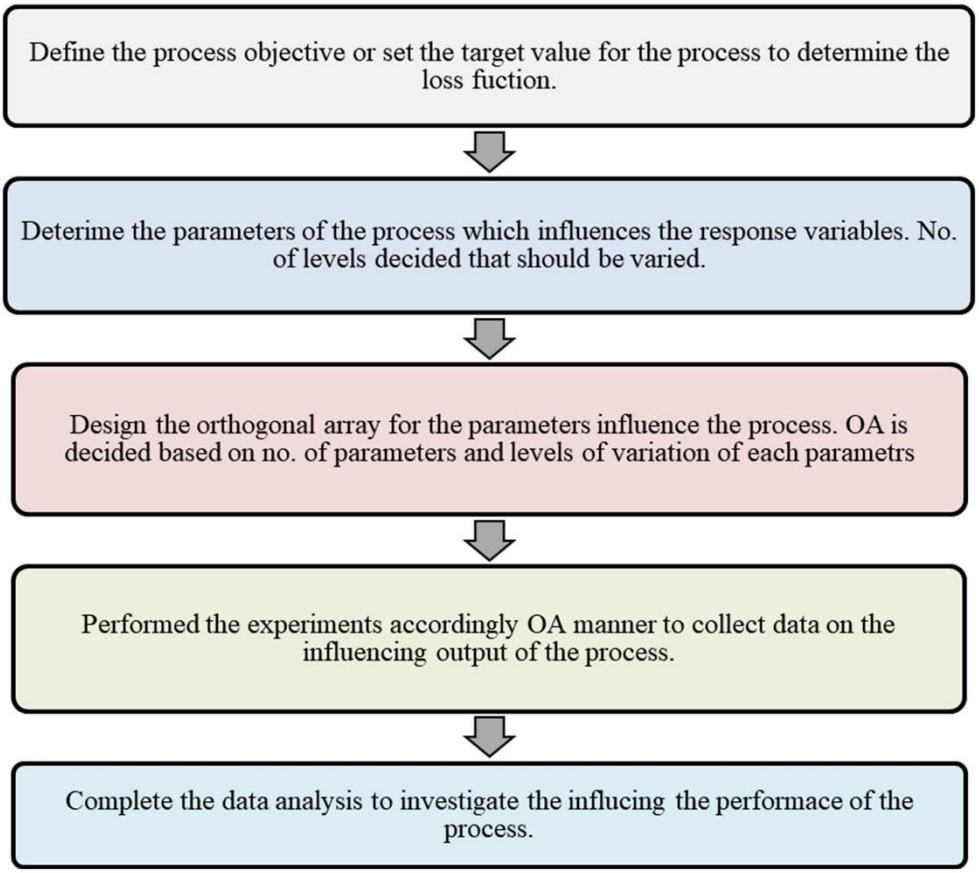

Figure 4.1Step to be followed in Taguchi DOE

Taguchi suggested two distinct approaches for conducting an exhaustive investigation of tests. The first is the conventional method, in which the effects of a single run or the average of repeated runs are analysed using fundamental impact and ANOVA[100]. Taguchi describes Signal-To-Noise (S/N) ratio for similar steps in the investigation as the second approach for comparing multiple runs.

4.1.3 Loss function

Taguchi defines the quality by 'quality loss' or 'Loss-function'. The quadratic relationship suggested by Taylor series expansion.

$$L(y) = k(y - m)^2 \quad (4.1)$$

In mass production, average loss/ unit is

$$L(y) = \{k(y_1 - m)^2 + k(y_2 - m)^2 + \cdots\cdots\cdots + k(y_n - m)^2\} \quad (4.2)$$

Final equation to be written as,

$$L(y)=k(MSD) \quad (4.3)$$

In calculating the loss function main two observations are to be noticed:

i. When the observed value of a product deviates from its target value, the greater of the two values represents the loss. When the observed value precisely matches the target value, there is no loss.
ii. The loss is a continues function

4.1.4 Singal to Noise ratio (S/N Ratio)

Taguchi transformed the quality loss function into the signal-to-noise (S/N) ratio, a circumstantial measurement that combines the mean level of the quality characteristics and the standard deviation around this mean into a single metric. The S/N ratio combines multiple redundancies (a minimum of two information foci are required) into a single value.A higher S/N ratio indicates a higher quality standard with less deviation from the target value[99]. The following three types of S/N ratio are utilized:

i. Higher the better

$$(S/N)_{HB} = -10 \log (MSD_{HB}) \quad (4.4)$$

Where $MSD_{HB} = \frac{1}{2}\sum_{J=1}^{R}(\frac{12}{yj})$ (4.5)

ii. Lower the better

$$(S/N)_{LB} = -10 \log (MSD_{LB}) \quad (4.6)$$

Where $MSD_{LB} = \frac{1}{R}\sum_{J=1}^{R}(y21)$ (4.7)

iii. Nominal the best

$(S/N)_{NB}$= -10 log (MSD_{NB}) (4.8)

Where $MSD_{NB} = \frac{1}{R}\sum_{J=1}^{R}(y - y\circ)^2$ (4.9)

R= No. of repetitions

Thus, in all three expressions, the MSD with the smallest magnitude is sought. The constant value 10 has been selected to increase the S/N number for each examination, and the minus sign is used to set the S/N proportion of larger is better in comparison to the square deviation of smaller is better. The S/N ratio is a concurrent statistic, as previously mentioned. A concurrent statistic can examine and combine two characteristics of a distribution into a single number or merit figure. The S/N ratio combines the mean level of a quality characteristic and its standard deviation into a single metric [101].

4.2 DATA ANALYSIS.

Taguchi proposed a variety of data analysis techniques, such as the observation method, the ranking method, the column effect method, ANOVA, S/N ANOVA, the plot of average response curves, and interaction graphs, among others [102]. In this investigation, however, the plot of average response curves was employed. Normal reactions at each level of a parameter are plotted to illustrate the pattern. It is a visual representation of the influence of the parameter on the objective function. Inferable from these bends is the correlation between the modification of the response characteristic and the modification of a parameter's value. ANOVA for OAs is typically conducted in the same manner as other randomised controlled trials [102]. As a result of the analysis, the S/N ratio is regarded as a measure of the diversity within a sample when noise factors are present. On the basis of the S/N ratio, one can conduct a standard ANOVA to identify the significant parameters (mean and variation). Utilizing interaction graphs to determine the optimal combination of intuitive parameter values [103].

4.2.1 Selection of OA

The selection of OA requires two steps. The first is the selection and interaction of process parameters, while the second is determining the level counts for the selected parameters.

Taguchi recommends utilising a variety of techniques to investigate the parameters that relate to the product or process performance characteristics[102].

- Brainstorming
- Flowcharts
- Cause and effect diagram

The total degree of freedom (DOF) of an experiment is directly proportional to the total number of trials.

Taguchi represents an OA as:$L_N(S^k)$

Where, S= Numbers of levels for every factor

k= Max. no. of factors whose effect can be estimated without any interaction

N= Total no. of trials during experiments

4.2.2 Assignment of parameters and interaction to the OA:

The OAs have a few sections available for parameter tasks, and a few segments can assess the impact of these parameters' communications in this manner. Taguchi has provided two tools to assist with cluster parameters and communications[99], [102].

Each OA is accompanied by a unique arrangement of direct charts and a triangular table. The straight charts depict various sections to which parameters may be allocated, and the

segments along these lines evaluate the transmission of these parameters. The triangular tables contain all conceivable parameter associations (sections).

4.2.3 Selection of outer array

Taguchi classifies factors as either controllable or uncontrollable (noise factors). Easily manipulable factors are referred to as controllable factors. In contrast, noise factors are nuisance variables that are challenging, impossible, or expensive to control. Noise factors account for variations in the performance of a process. Taguchi proposes an outer array for noise factors and an inner array for controllable factors. Utilizing an outer array injects noise variability into the experiment. However, repeated experiments against the trial conditions of the inner array (the OA used for the controllable factors) are permitted, and the noise variation is not forced into the experiment in this instance. Using the outer array will result in the same assignment considerations. However, the outer array should not be as complex as the inner array, as the outer array consists solely of controlled noise [102]. Taguchi divides factors (parameters) into two fundamental categories: controllable elements and uncontrollable elements (noise factors). Controllable factors are those that are susceptible to manipulation. However, disturbance factors are aggravating elements that are difficult, absurd, or costly to manage. The noise factors determine the variability in the execution of a procedure. Taguchi recommends using an external display for noise factors and an internal cluster for controllable elements. Using an external cluster restricts the investigation's noise spectrum. However, tests against the initial conditions of the internal cluster (the OA used for the controllable elements) can be repeated, and the noise variety is not compelled into the examination in this instance. If implemented, the external display will have the same task-related considerations. However, the external display should not be as erratic as the internal cluster, as the external display is merely commotion, which is solely governed by the test (Ross, 1996)

4.2.4 Experimentation and data collection:

Each of the inner array's initial states are investigated individually. Essentially, each preliminary investigation is repeated (if external array is not used) or according to the external array (if utilized). To reduce test predisposition, randomization should be communicated. The data (raw data) is recorded for each preliminary condition, and the S/N ratios of the reprocessed data foci are calculated and recorded for each preliminary condition.

4.3 PARAMETERS DESIGN STRATEGY

4.3.1 Parameter classification and selection of optimal levels:

When the ANOVA on the raw data (which identifies control parameters that affect the mean) and the S/N data (which identifies control parameters that affect the variance) are complete, the control parameters can be classified into four groups [99].

Group I: Parameters which affect both average and variation

Group II: Parameters which affect variation only

Group III: Parameters which affect average only

Group IV: Parameters which affect nothing.

The design strategy for parameters involves selecting the appropriate levels of group I and group II parameters to reduce variation, and group III parameters to achieve the desired mean. Since nothing is altered, the parameters for group IV can be set to their most economical levels.

4.3.2 Determination of confidence interval:

The calculation of the mean is merely an approximation based on the typical trial results. There is a 50 percent statistical chance that the actual mean is greater than. Estimates of a measurable parameter are typically expressed as a range within which the parameter is likely

to fall, with a specified degree of confidence. It is known as the confidence interval (CI). The confidence interval is, ultimately, the range between which the true mean should fall at a specified level of confidence. Taguchi suggests the following two types of confidence interval based on the evaluated mean of the optimal experimental condition:

i. In the vicinity of the evaluated norm for a treatment condition expected from the trial.
ii. Approximately the evaluated norm of a treatment condition used in an affirmation trial to measure expectations.

CIPOP applies to the entire population, i.e., all parts created under the predetermined conditions at any given time, whereas CICE applies only to a sample group created under the predetermined conditions. CICE should be somewhat more comprehensive due to the smaller sample size (in affirmation tests) relative to the total population.

4.3.3 Estimation of optimum response characteristics

Predicted in this section are the optimal values for the response characteristics and their respective confidence intervals. The results of acceptance experiments indicate that optimal results have been achieved. From the preferred response characteristics, the optimal levels of the process parameters have been determined. Only the impact of significant parameters is taken into account when estimating the optimal value of every response characteristic. The mean value of response characteristics derived from affirmation experiments must meet the CICE confidence level of 95%. However, the average value of the quality characteristic obtained from the confirmation experiments may fall within the confidence interval of 95 percent (CIPOP). The optimal values for both raw data and S/N ratio are determined via analysis. The optimal settings for the confirmation experiments have been determined on the basis of the raw data. Depending on the optimal setting selection of the process, the optimal response parameters have been evaluated with confidence intervals.

4.3.4 Confirmation test

The affirmation experiment is the last step in validating the findings of previous experiments. A number of tests are conducted under the optimal conditions for the significant parameters, while the insignificant parameters are set to economical levels. The confirmation experiment results are compared to the expected average based on the tested parameters and levels. To confirm the experimental conclusion, it is strongly advised to conduct the confirmation experiment.

Using ANOVA, the effect of UAFSW parameters and contribution of each parameter to output responses such as microhardness ultimate strength and residual stress have been investigated. Taguchi proposes two distinct approaches for conducting the overall research to optimize any parameter. First, there is the conventional method, in which the results of a single run or the mean of multiple runs are calculated using the basic impact and ANOVA tests (Raw data investigation). Taguchi unequivocally recommends utilising signal-to-noise ratio (S/N) for similar steps in the examination when analysing multiple runs. The signal-to-noise ratio is a concurrent quality metric related to the variation within a work sample [101]. By increasing the S/N ratio, unexpected variation can be contained. The S/N ratio determines the most efficient arrangement of working conditions from the variety of outcomes.

The S/N ratio is considered an exam response (change in raw data). Taguchi suggests using external OA to intentionally introduce a variety of noise into the examination, i.e., the noise is introduced on purpose. However, forms are typically subject to a number of noise considerations that combine to have a substantial impact on the variety of responses. During experimentation, it is typically unnecessary to identify specific disturbance factors and consciously control them for a highly "noisy" system. It suffices to generate iterations at each

exploratory state of the controllable parameters and then dissect them using an appropriate S/N ratio.

The effects of the selected UAFSW process parameters on the chosen quality attributes were analysed by plotting the principal impacts based on the raw data. Through the analysis of S/N ration and the analysis of raw data, the optimal condition for each of the quality attributes has been determined. Instead of utilizing an external array, tests were repeated three times for each experimental condition.

The design of experiments (DOE) is a plan or model for gathering data on the presence of deviation and the process's degree of control. DOE is utilised to examine how the various process parameters influence the output or performance of the process. Taguchi's DOE entails the use of Orthogonal Arrays to frame the parameters affecting the process from its target value and the acceptable levels of deviation. The purpose of the test was to examine the effect of certain UAFSW parameters on the response characteristics of the UAFSW process. The tests were conducted using the appropriate orthogonal array (OA).

Table 4.1The parameters used for experiments

Factor Number	**Factor Name (Units)**	**Level**		
		L1	**L2**	**L3**
1	Type of vibration (KHz)	Continuous	Discontinuous	-
2	Tilt angle (Degree)	0	1.5	3
3	Travel Speed (mm/min.)	40	50	60
4	Rotational speed (RPM)	600	800	1000
5	Amplitude (μm)	0	44	88

Table 4.1 lists the various parameters utilised during the experiments. Type of vibration, tilt angle, tool travel speed, tool rotation speed, and amplitude are the selected response characteristics to be verified.

For this experimental investigation, an L18 orthogonal array was constructed using the design of experiments to reduce the number of experiments required to analyze the effects of all of the selected parameters. The array containing the parameter values is shown in Table 4.2. In total, eighteen experiments were conducted.

Table 4.2L18 orthogonal array of parameters

Experiment	**Factor 1 (Vibration)**	**Factor 2 (Tilt angle)**	**Factor 3 (Travel Speed)**	**Factor 4 (RPM)**	**Factor 5 (Amplitude)**
1	1	1	1	1	1
2	1	1	2	2	2
3	1	1	3	3	3
4	1	2	1	1	2
5	1	2	2	2	3
6	1	2	3	3	1
7	1	3	1	2	1
8	1	3	2	3	2
9	1	3	3	1	3
10	2	1	1	3	3
11	2	1	2	1	1
12	2	1	3	2	2
13	2	2	1	2	3
14	2	2	2	3	1

15	2	2	3	1	2
16	2	3	1	3	2
17	2	3	2	1	3
18	2	3	3	2	1

According to the L18 OA orthogonal array depicted in Table 3.4, the process parameters have been arranged. For instance, to conduct experiments, one must conduct an examination to determine the influence of five distinct free factors, each with three values. A L18 orthogonal array may be the best option at that time. The L18 orthogonal display is implied for comprehending the influence of five independent factors, each of which has a 3-factor level value. This array assumes that no interaction exists between any factors. Despite the fact that, in general, no interaction model assumption is valid, there are a few instances where interaction is supported by reasonable evidence. For these experimental investigations, an L18 orthogonal array is employed.

4.4 SUMMARY

This chapter includes optimization of various response parameters using Taguchi L18 OA analysis along with ANOVA (Analysis of variance). Optimization will be performed for output parameters such as microhardness, ultimate tensile strength and residual stress at different level in the next chapter. Data analysis procedure, estimation of optimum responses and confirmation test have also been discussed in this chapter.

CHAPTER - 5

RESULTS AND DISCUSSION

This chapter analyses and discusses the outcomes of experiments conducted utilising UAFSW. This study aimed to investigate the effects of continuous and discontinuous ultrasonic vibrations on the FSW process. Various applications of ultrasonic vibrations in various types of machining and fabrication processes have been reported[71], [104]. By incorporating ultrasonic vibrations into the FSW process, numerous advantages are anticipated in terms of weld quality, improvement of mechanical and wear properties. AA 7075-T6 sheets (3 mm) were welded using an UAFSW that integrated ultrasonic vibrations. The optimal combination of process-enhancing parameters is identified by ANOVA. Further, using a SEM/FESEM, the sample's surface topography has been analysed to determine its microstructure. Also, X-ray diffraction was used to analyse the surface phase transformations caused by ultrasonic vibrations. At last, wear behaviour of UAFSW welded joints has been analysed.

5.1 EFFECTS ON MECHANICAL PROPERTIES OF UAFSW

5.1.1 Microhardness

Resistance to surface indentation is defined as hardness. Conflicting variables used for determining micro-hardness of welded pieces. When the size of the grains is refined, it increases microhardness, while the increase in temperature results in annealing. Annealing overpowers the effect caused by refinement of grains resulting in decreased hardness [42], [105]. Therefore, the increase in hardness caused by the combined effort of refinement of grains as well as homogenous reinforcement particles dispersion dictated by FSW [106]**.** The detailed microhardness values of the UAFSW samples and BM are shown in Figure 5.1. The welded samples are having higher hardness when compared to BM sample.

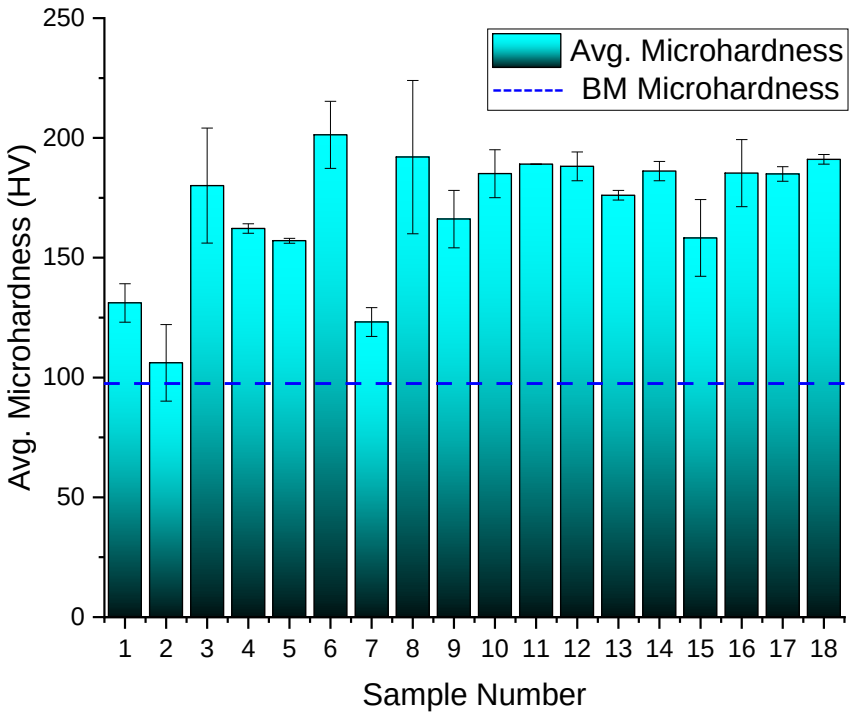

Figure 5.1Average values of microhardness of UAFSW Joints

The maximum hardness value of the Hybrid FSW joints has been found at 1000 rpm and 60 mm/min welding speed with the cylindrical tool pin profile, its value is more than double that of the BM. It is also has been observed that from the base material to the HAZ, the hardness value declined, and the boundary area between the TMAZ and the HAZ appeared to have the lowest hardness value. However, the nugget zone's hardness values were higher than those of TMAZ and HAZ.

From Figure 5.2 - 5.6, shown that a continuously increasing the rotational speed and the discontinuous vibrations applied to the workpiece causes to improve the microhardness of the weld joint is relatively increased. By varying the rotational speed in conjunction with ultrasonic vibration, it is possible to increase the hardness of the welded joint, as compared to welding without ultrasonic vibration. Effect of hardening is due to intense stirring in the

processed zone. Ultrasonic vibration increases the heat input and metal flow to the processing zone, resulting in uniform grain refinements and an increase in microhardness. The effect of varying traverse speed causes a continuous decrease in hardness.

5.1.2 Optimization of various Parameters for MH

The average values of MH of UAFSW welded samples with respect to varying process parameters, as well as the calculation of S/N ratios for a "larger is better" type of quality characteristic, are provided in the Table5.1.In addition, the effect of independent process parameters for UAFSW, such as vibration type, tilt angle, travel speed, rotational speed and amplitude of vibration, on the response characteristics has been discussed. The average response characteristics and S/N ratio for each parameter at all three levels have been determined.

Table 5.1Average values of MH and S/N ratios (Larger-the-Better) for MH

Experiment No.	Average value of MH	Variance	Sum of Squares	S/N Ratio (Larger-the-Better)
1	131.1167	16.04083333	51606.82	42.34501971
2	106.1133	64.03853333	33908.2	40.46560112
3	180.0967	144.0280333	97592.48	45.07134606
4	162.1833	1.100833333	78912.5	44.19975947
5	157.07	0.2647	74013.48	43.92177153
6	201.32	49.3072	121687.8	46.06709621

7	123.1433	9.061633333	45510.96	41.8030017
8	192.01	256.0003	111115.5	45.60587171
9	166.13	36.0507	82869.63	44.39757023
10	185.07	25.0147	102802.7	45.34036419
11	189.0267	0.002133333	107193.2	45.530461
12	188.14	9.0588	106208.1	45.48739294
13	176.0767	1.017633333	93011.01	44.91375056
14	186.16	4.0768	103974.8	45.39670211
15	158.2533	64.19253333	75260.74	43.96461358
16	185.3233	49.31363333	103132.8	45.34603219
17	184.9867	3.080533333	102666.4	45.34202086
18	191.0667	1.013333333	109521.4	45.62345711

5.1.3 Effects of vibrations on MH

As shown in Figure 5.2, the MH was higher for discontinuous vibrations than for continuous vibrations. Moreover, the S/N ratio increased during discontinuous vibration.

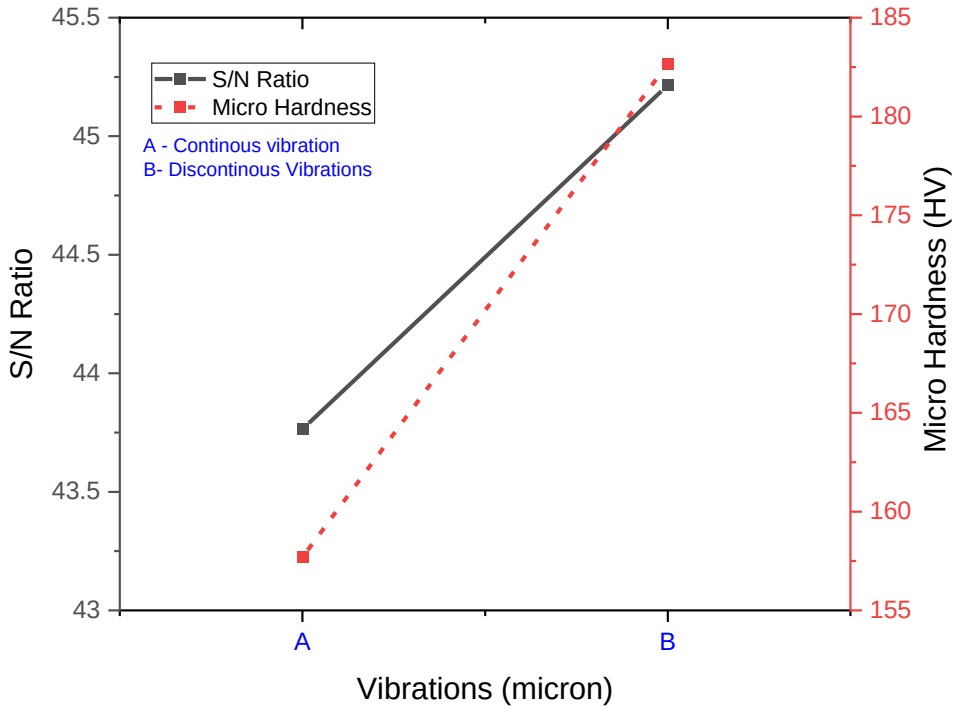

Figure 5.2S/N ratio and main effect of vibration type on MH

Multiple discharge points with sufficient time intervals were the most significant effect of horizontal discontinuous vibration. In the interim, the additional inertial forces introduced into the workpiece aided in the removal of debris.

5.1.4 Effects of tilt angle on MH

As shown in Figure 5.3, the MH first decreases from 0 to 1.5º and it is also called the tilt angle, after which the value of MH increases from 1.5º to 3° angle. The similar trend is observed for S/N ratio. The values first decrease then increases as tilt angle varies from zero degree to 3°. The maximum value of MH and S/N ration is observed at 3º angle.

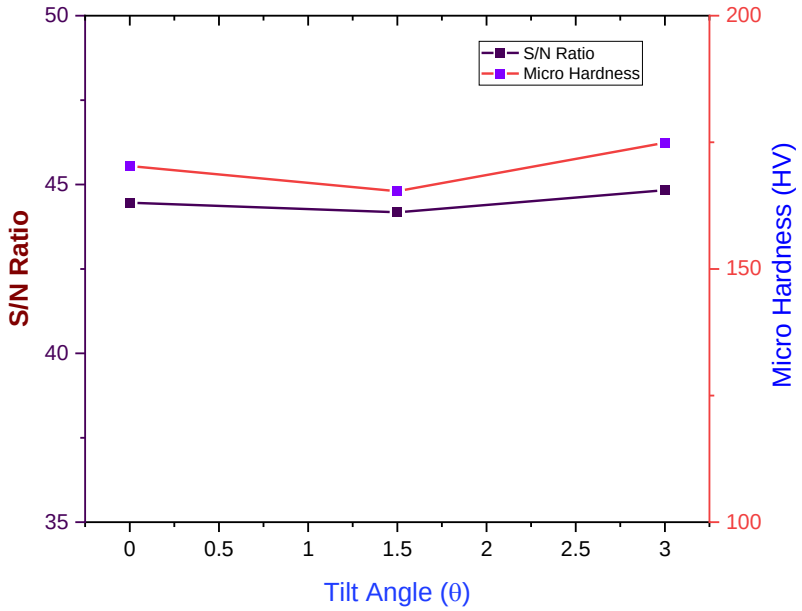

Figure 5.3S/N ratio and main effect of tilt angle on MH

5.1.5 Effects of rotational speed on MH

The Figure 5.4 indicates that the MH first increases from 600 to 800 RPM, and then there is a slight decrease in MH at 1000 RPM. The similar trend is observed for S/N ratio but the values first increases and then drastically decreases as the rotational speed varies from 600 to 1000 RPM. The maximum value of MH and S/N ration is observed at 600 RPM.

The higher tool rotation speeds are more desirable for dispersal and suspension of congregations of particles inside the welded zone. The microhardness value increases as the rotational speed of the tool increases, and then decreases as the rotational speed exceeds 1000 rpm, which causes tool wear at high rotational speeds. Similar results have been reported by [107]: an increase in tool rotational speed causes more grain growth during dynamic recrystallization and there is a decrease in microhardness.

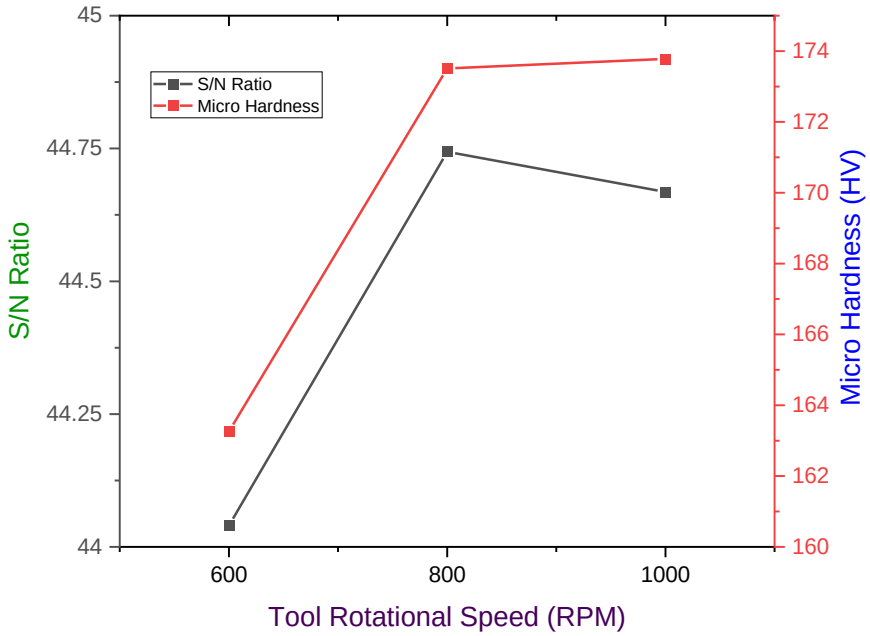

Figure 5.4S/N ratio and main effect of tool rotational speed on MH

5.1.6 Effects of travel speed on MH

As depicted in Figure 5.5, the MH increases from 40 to 60 mm/min travel speed. The similar trend is observed for S/N ratio. The values increase as the travel speed varies from 40 to 60 mm/min. The maximum value of MH and S/N ration is observed at 60 mm/min[108].

5.1.7 Effects of amplitude on MH

At last Figure 5.6 reflects that the S/N ratio decreases from 0 to 44 microns amplitude and then slightly increases at 88 microns amplitude. On the other end the MH decreases from 0 to 88 microns and the maximum value of MH and S/N ration is observed at zero microns. This was due to the increased amplitude of vibration disturbance in the welded region that led to the decrease in the weld quality [89], [109].

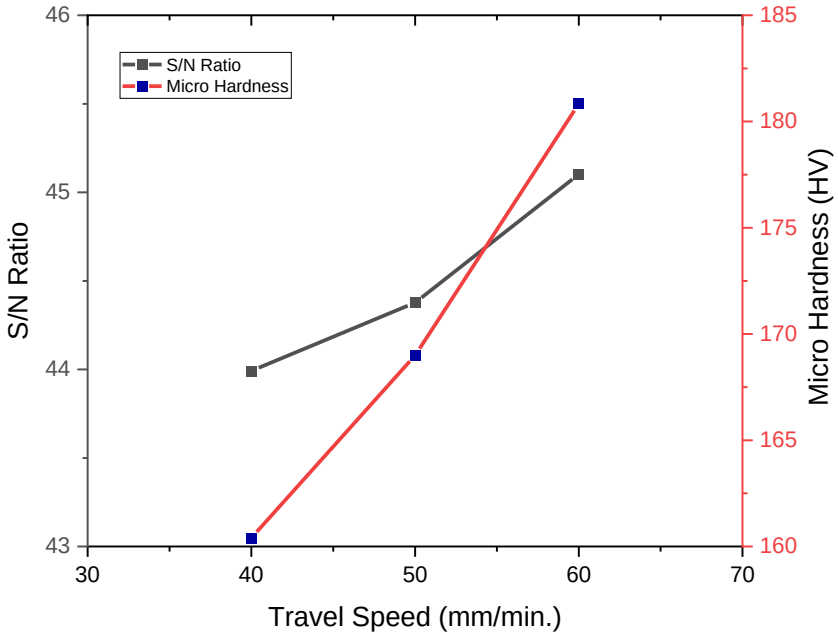

Figure 5.5S/N ratio and main effect of travel speed on MH

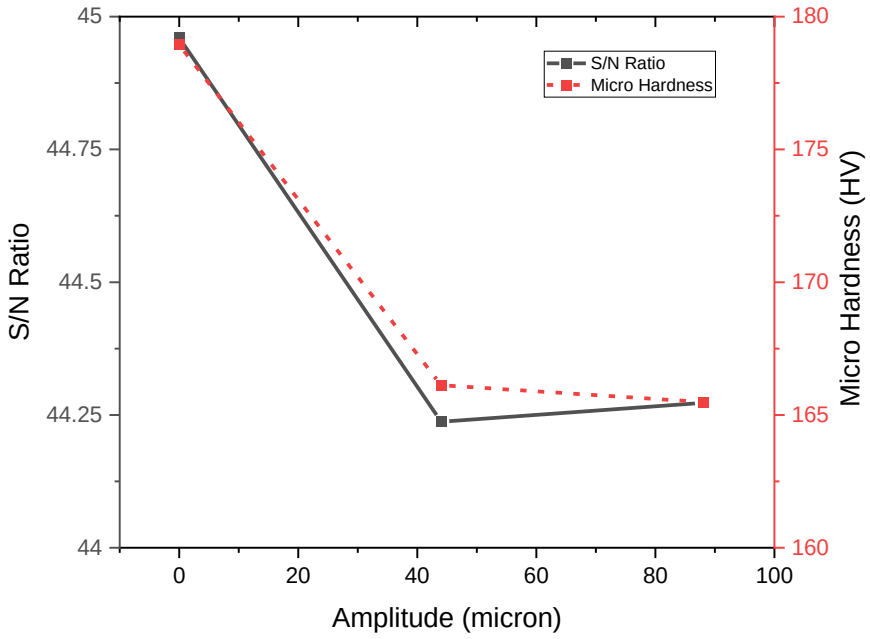

Figure 5.6S/N ratio and main effect of Amplitude of vibration on MH

5.1.8 ANOVA for MH

ANOVA was performed to determine which factors significantly affect the response characteristics. The main effect of microhardness at various levels on S/N data and raw data

is presented in Tables 5.2 and 5.3, respectively. The results indicate that all of the factors had a significant impact on the MH for UAFSW process, both in terms of the raw data and the S/N ratio. The column “P” represents the percentage contribution of the exacting factor to the response characteristic.

Table 5.2ANOVA of the Raw data for MH

Source	**SS**	**DOF**	**V**	**P**	**F-ratio**	**Significant**
Type of vibration	8431.501	1	8431.501	22.7666	32.83301	Yes
Tilt Angle	1294.331	2	647.1657	3.494933	2.520121	Yes
Rotational speed	3751.311	2	1875.655	10.12923	32.83301	Yes
Travel Speed	9519.035	2	4759.518	25.70314	18.53398	Yes
Amplitude	1177.654	2	588.8272	3.179883	2.292945	Yes
E	10785.58	42	256.7995	34.7271	*	
Total (T)	37034.52	51		100		
Significant at 95% confidence level, F critical =3.2236 (Tabulated Value) SS-Sum of Squares, DOF-Degree of Freedom, V-Variance, P- % contribution						

According to the S/N Table, UAFSW's travel speed is the most significant factor in MH. Table 5.3 indicates that amplitude of vibration (3.17 percent) is a contributor to raw data, but S/N ratio was not significantly affected.

Table 5.3ANOVA of the S/N Ratio for MH

Source	**SS**	**DOF**	**V**	**P**	**F-ratio**	**Significant**
Type of vibration	9.487015	1	9.487015	24.12504	5.08804	Yes
Tilt Angle	1.833036	2	0.916518	4.661326	0.491544	Yes
Rotational speed	3.815223	2	1.907611	9.701934	1.023083	Yes
Travel Speed	9.722396	2	4.861198	24.7236	2.60714	Yes
Amplitude	1.28658	2	0.64329	3.271713	0.345007	No
E	11.18743	6	1.864571	33.5191	*	
Total (T)	39.32435	15	*	100		
Significant at 95% confidence level, F critical =5.143 (Tabulated Value) SS-Sum of Squares, DOF-Degree of Freedom, V-Variance, P- % contribution						

The parameter of vibration amplitude is insignificant. Based on the analysis of raw data, it is also the least significant parameter influencing the MH. The small observed effect of this interaction can be explained by the fact that the amplitude of vibrations only plays a role in the MH when vibrations are present. The unpooled ANOVA table was used to identify insignificant parameters, and their effect on MH is disregarded. The pooled ANOVA table is created, and the results are listed alongside it.

5.2 ULTIMATE TENSILE STRENGTH

Utilizing the Universal Testing Machine, the tensile test was conducted (UTM). In accordance with ASTM E8M-11 subsize requirements, tensile specimens were fabricated. The transverse direction, which is perpendicular to the welding direction, was used to prepare tensile specimens. The specimens were cut using wire EDM, and the test was conducted on all 18 specimens. Figure 5.7 depicts a specimen for a tensile test and a fractured sample.

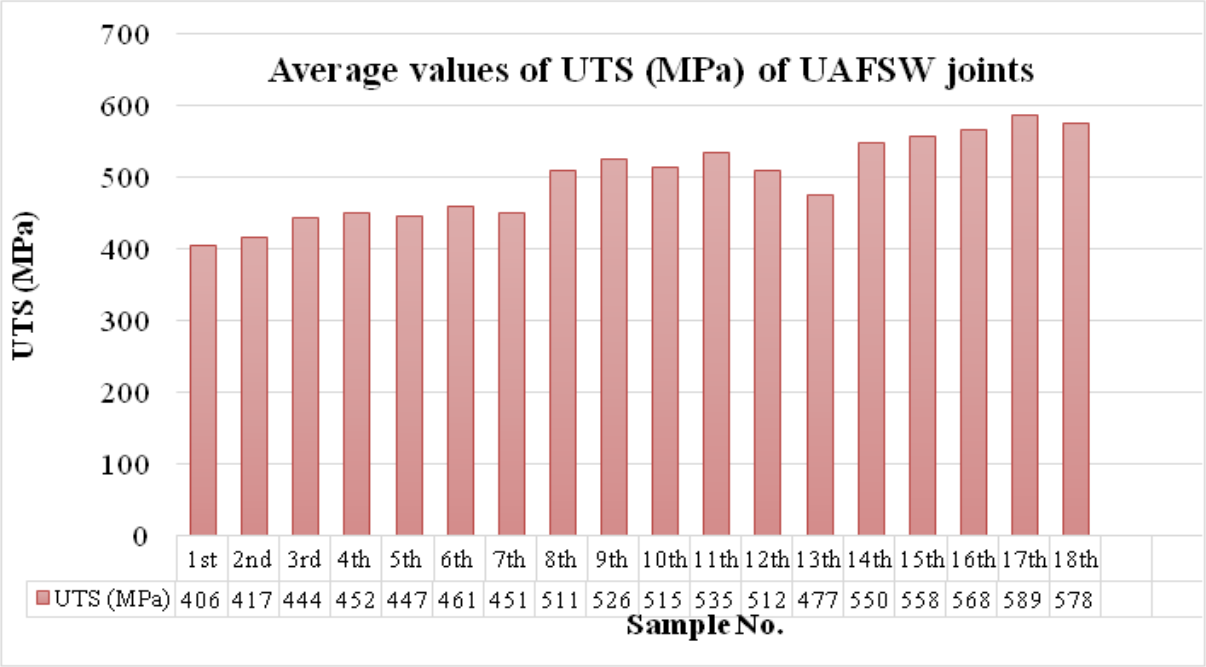

Figure 5.7UTS values of welded joints

5.3 OPTIMIZATION OF VARIOUS PARAMETERS FOR UTS

The average value of weld joint tensile strength and S/N ratio for each UAFSW welded sample are calculated and displayed in Table 5.4.

5.3.1 Effects of vibrations on UTS

The effect of vibrations on UTS has been perceived and shown in Figure 5.8. Discontinuous vibrations cause a greater increase in UTS than continuous vibrations. The highest value of MH is obtained at discontinuous vibrations.

Table 5.4Average values of UTS and S/N ratios (Larger-the-Better) for UTS

Experiment No.	**Average value of UTS**	**Variance**	**Sum of Squares**	**S/N Ratio (Larger-the-Better)**
1	406.6667	1.333333333	496136	52.18470164
2	414.3333	6.333333333	515029	52.34667754
3	444.6667	17.33333333	593220	52.95992593
4	452	4	612920	53.10259864
5	447.6667	2.333333333	601221	53.01899388
6	461	13	637589	53.27348929
7	451.3333	17.33333333	611140	53.08921297
8	511.3333	49.33333333	784484	54.17243878
9	526.6667	16.33333333	832166	54.43020214
10	515	7	795689	54.23591457
11	535	1	858677	54.56704529
12	512.6667	25.33333333	788532	54.19586649
13	477.6667	2.333333333	684501	53.58240977
14	550	1	907502	54.80722508
15	558	4	934100	54.93257239

16	568.3333	9.333333333	969027	55.09181102
17	589.3333	44.33333333	1042030	55.4061207
18	578.6667	58.33333333	1004682	55.24706433

The cause of higher UTS at discontinuous vibration is that there are multiple discharge points with sufficient time intervals. Meanwhile, the additional inertial forces introduced into the workpiece assisted in debris removal.

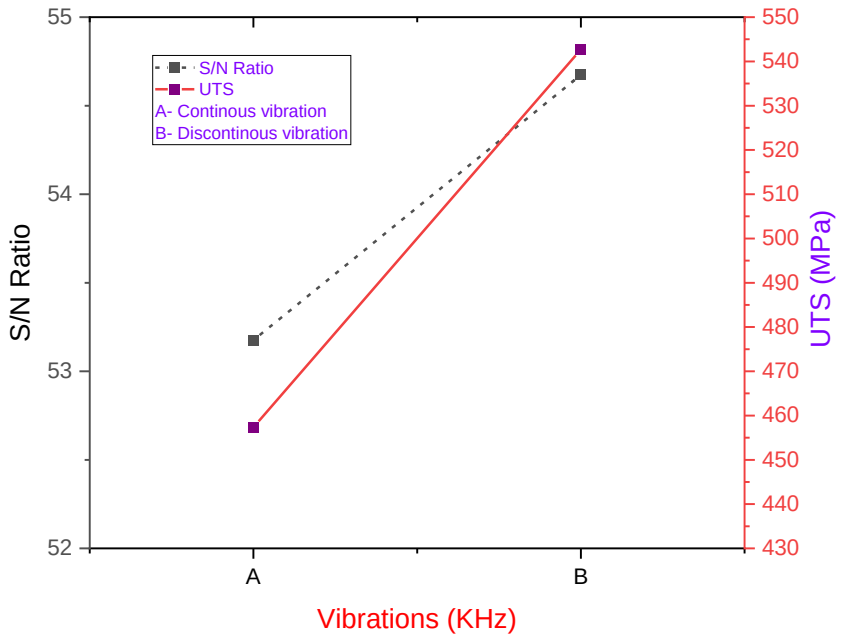

Figure 5.8S/N ratio and main effect of vibrations on UTS

5.3.2 Effects of tilt angle on UTS

The effect of tilt angle on UTS is shown in Figure 5.9.The UTS increases from 0 to 3° angle. The similar trend is observed for S/N ratio. The values increase as the tilt angle varies from 0 to 3°. The maximum value of UTS and S/N ration is observed at 3°.

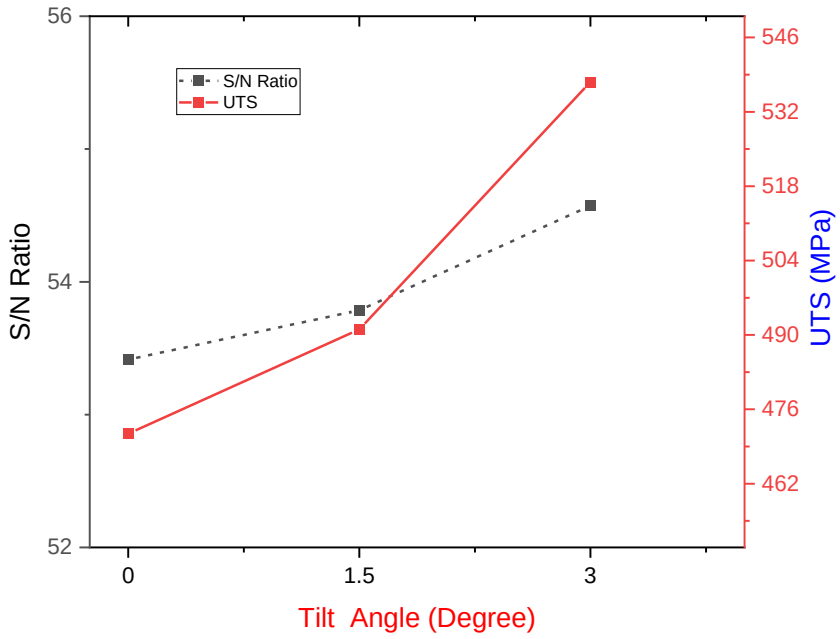

Figure 5.9S/N ratio and main effect of tilt angle on UTS

5.3.3 Effects of travel speed on UTS

The Figure 5.10 indicates that the UTS first increases rapidly 40 to 50 mm/min travel speed and then there are slight increase in UTS at 60 mm/min. The same trend holds true for the S/N ratio.

5.3.4 Effects of rotational speed on UTS

The Figure 5.11 depicts the UTS increases as the rotational speed of the tool increases, and then decreases as the rotational speed exceeds 1000 rpm, which causes tool wear at high rotational speeds. S/N ratio also demonstrates a similar trend.Similar results have been reported byAzizieh et al.[107]: an increase in tool rotational speed causes more grain growth during dynamic recrystallization and a decrease in UTS. Spacing between particles influence the UTS of a material, as the inter-particle distance increases with increasing rotational speed, resulting in reduction of UTS.

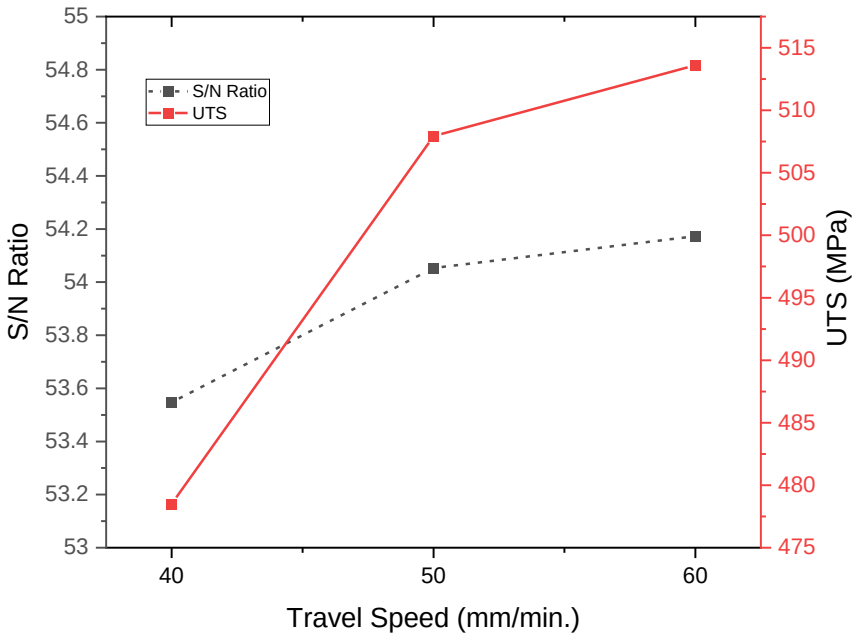

Figure 5.10S/N ratio and main effect of travel speed on UTS

5.3.5 Effects of amplitude of vibration on UTS

The Figure 5.12 indicates that the UTS first increases from 0 to 44 microns then there are decrease in UTS at 88 microns. The similar trend is observed for S/N ratio. The values first increases then drastically decrease as the amplitude of vibration varies from 44 to 88 microns. The maximum value of UTS and S/N ration is observed at 44 microns. This was due to the increased amplitude of vibration disturbance to the welded region consequently, the weld quality deteriorated leading to low values of UTS.

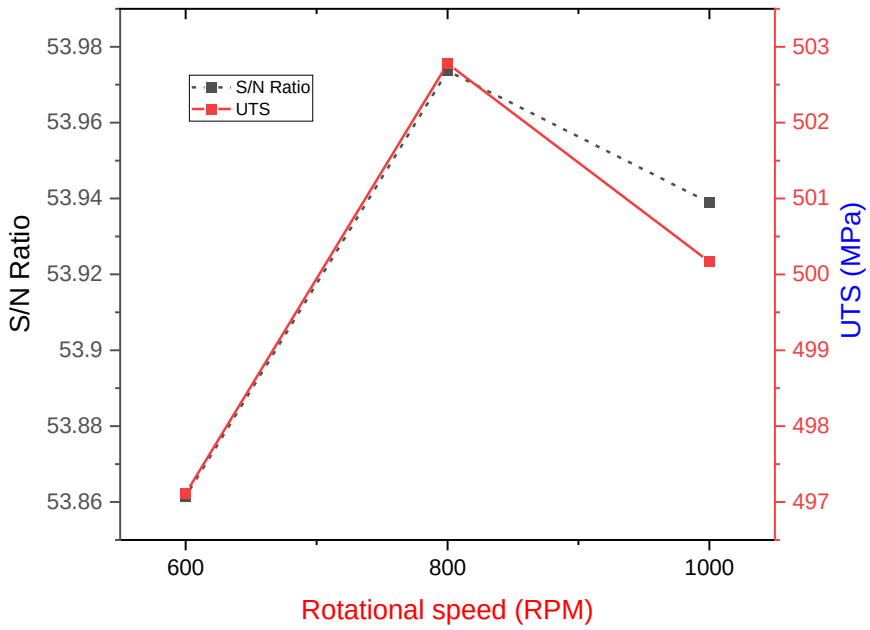

Figure 5.11 S/N ratio and main effect of rotational speed of tool on UTS

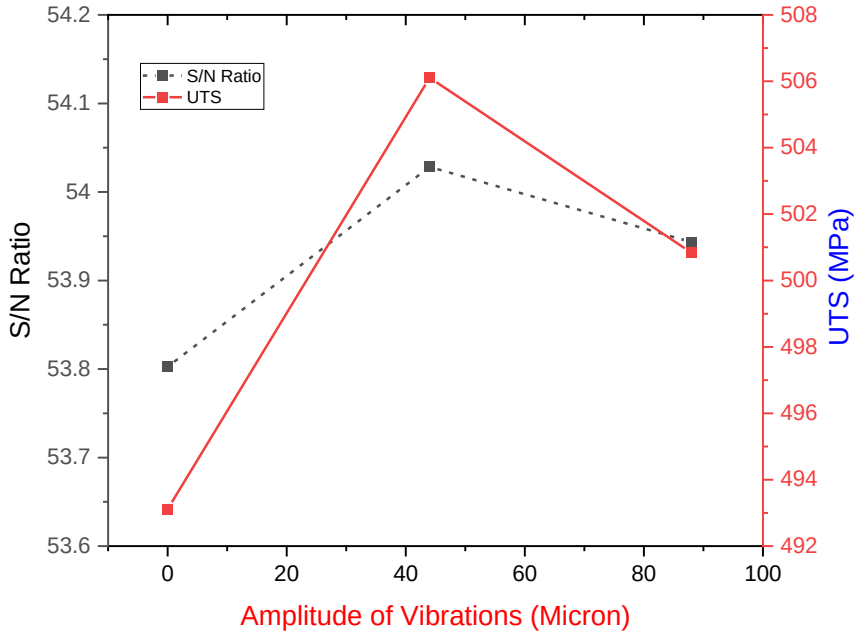

Figure 5.12 S/N ratio and main effect of amplitude of vibration on UTS

5.3.6 Selection of optimal levels for UTS

Analysis of variance (ANOVA) was performed to determine the significant influence of the process parameters on tensile strength. The ANOVA of the RAW data and the S/N ratio for UTS are displayed in Tables 5.5 and 5.6, respectively.

Table 5.5 ANOVA of the S/N Ratio for UTS

Source	**SS**	**DOF**	**V**	**P**	**F-ratio**	**Significant**
Type of vibration	10.10669	1	10.10669	58.81479	178.7651	Yes
Tilt Angle	4.193966	2	2.096983	24.40633	37.09101	Yes
Rotational speed	1.321804	2	0.660902	7.692093	11.6899	Yes
Travel Speed	1.069583	2	0.534791	6.224321	9.459283	Yes
Amplitude	0.039596	2	0.019798	0.230425	0.350183	No
E	0.452289	8	0.056536	2.632048	*	
Total (T)	17.18393	17	*	100		
Significant at 95% confidence level, F critical =5.143 (Tabulated Value) SS-Sum of Squares, DOF-Degree of Freedom, V-Variance, ‘P’- % contribution						

The ANOVA for raw data and the S/N ratio for the UTS are depicted in Tables 4.7 and 4.8, respectively. The results demonstrate that four variables significantly affected the UAFSW process's UTS for both the raw data and S/N ratio. The column “P” represents the percent contribution of the particular factor to the response characteristic. The amplitude of vibration (0.23 percent) is a least contributor and was not significantly affected. The unpooled

ANOVA table was used to identify insignificant parameters, and their effect on UTS is disregarded. The pooled ANOVA table is created, and the results are listed alongside it.

Table 5.6 ANOVA of the Raw data for UTS

Source	**SS**	**DOF**	**V**	**P**	**F-ratio**	**Significant**
Type of vibration	98560.17	1	98560.17	58.791	65.02874	Yes
Tilt Angle	41637.48	2	20818.74	24.8367	13.73594	Yes
Rotational speed	12791.26	2	6395.63	7.629968	65.02874	Yes
Travel Speed	10478.81	2	5239.407	6.250599	3.456894	Yes
Amplitude	-62510.9	2	-31255.5	-37.2877	-20.6219	No
E	66688.17	44	1515.64	39.7794	*	
Total (T)	167645	53		100		
Significant at 95% confidence level, F critical =3.223 (Tabulated Value) SS-Sum of Squares, DOF-Degree of Freedom, V-Variance, 'P'- % contribution						

Figure5.13 to 5.17 shows optimized results revealed that tensile strength increases as the translational speed increases while the rotational speed remains constant. Tensile strength tends to rise as the rotating speed is increased. After optimizing the process parameters, it was found that the maximum impact on the tensile strength contributed by the type of vibrations i.e., 58.97 %. The maximum tensile strength was achieved at 600 rpm rotational speed and 40 mm/min translational speed.

5.4 RESIDUAL STRESS

Due to the plastic deformation of metal, residual stresses are generated. These residual stresses formed on the surface of the welded sample due to metallurgical changes and the inhomogeneity of the heat flow. The experimental results of residual stress is obtained at various welded joints of UAFSW is shown in Figure 5.13.In [44], determined the pattern of residual stresses of ultrasonic vibration assisted Die-sink EDM and concluded that the stresses decreased with the amplitude; however, the impact was inverted when the increment passed a certain limit.

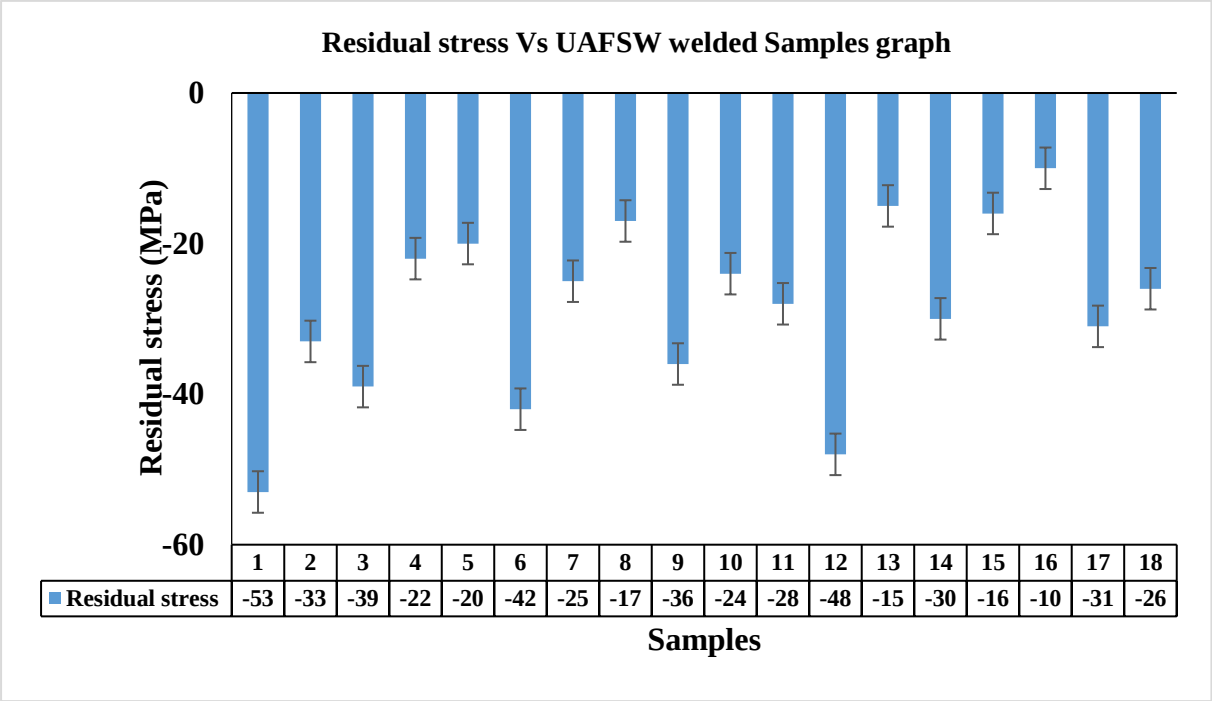

Figure 5.13Average residual stress of UAFSW joints

While performing XRD, a circular pattern known as the Debye ring was produced. Figure 5.14(a)-(c)shows the Debye ring, distortion ring, and XRD peak profile for base metal and UAFSW (for continuous and discontinuous vibrations)welded samples that were produced during the test. The concentration of residual stress is represented by various colour mixtures, with red representing the highest concentration and blue the lowest [110].

On analyzing diffraction intensity along the Debye ring, it can be seen that the intensity variation is greater for base metal compared to UAFSW samples. This is due to the fluctuating depth of X-ray penetration caused by the changing surface properties of base metal. A decrease in intensity variation indicates an improvement in surface characteristics after UAFSW[111], [112]. In Figure 5.14(a) for base metal, the blemished distribution represents coarse grains in base metals, whereas in Figures 5.14(b)-(c) for UAFSW samples, the improvement is a result of grain refinement following the UAFSW. The value of FWHM is high in base metal due to the presence of high residual stress and strain, whereas it is lower in the UAFSW samples at 800 rpm as a result of a reduction in residual stress. Due to the small grain size, FWHM increases for samples refined at higher RPM [113]. Due to the existence of coarse grains, the deviation of residual stress is greater in base metal than in welded samples [114]. The result indicates that the compressive nature of residual stress in all samples and the application of ultrasonic vibration diminished the magnitude of stresses[79].

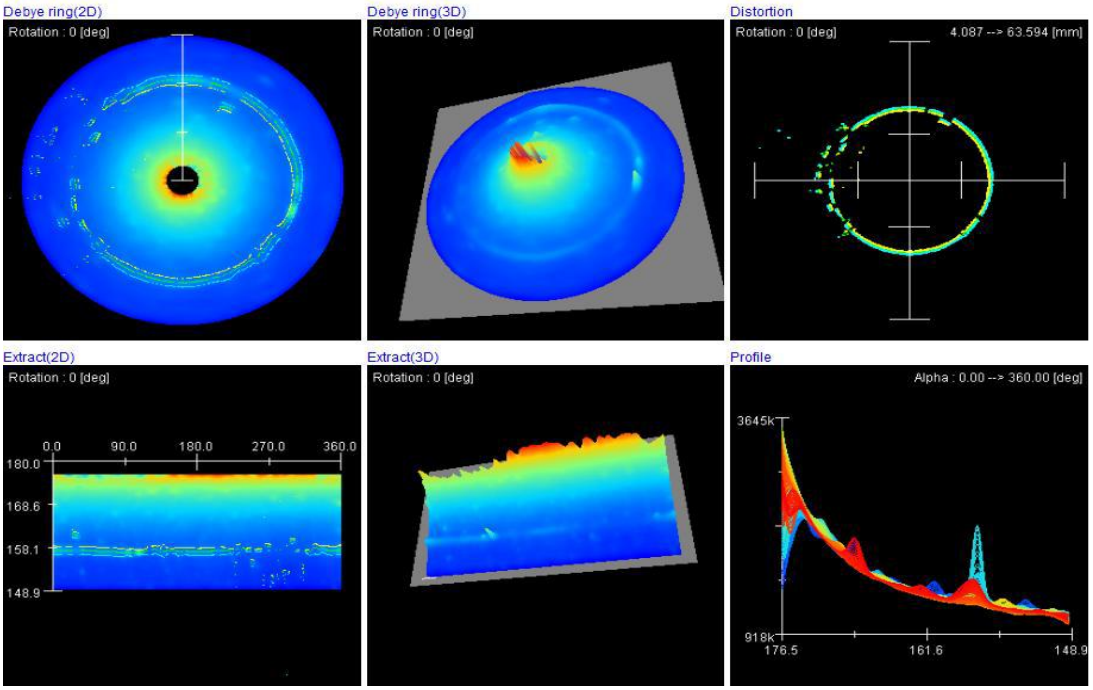

(a)

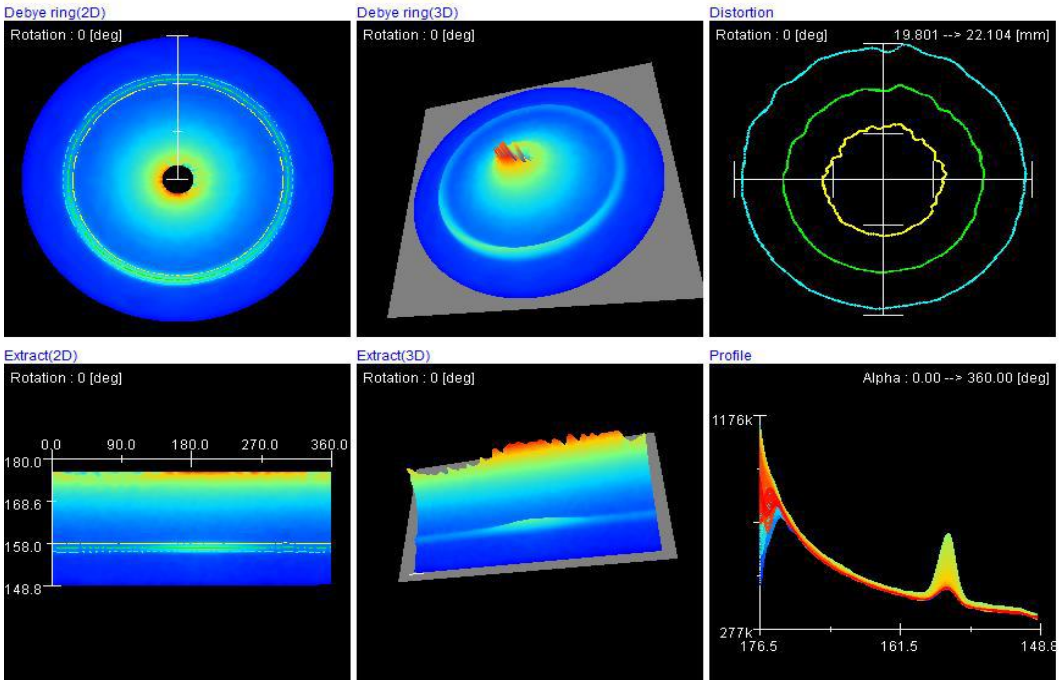

(b)

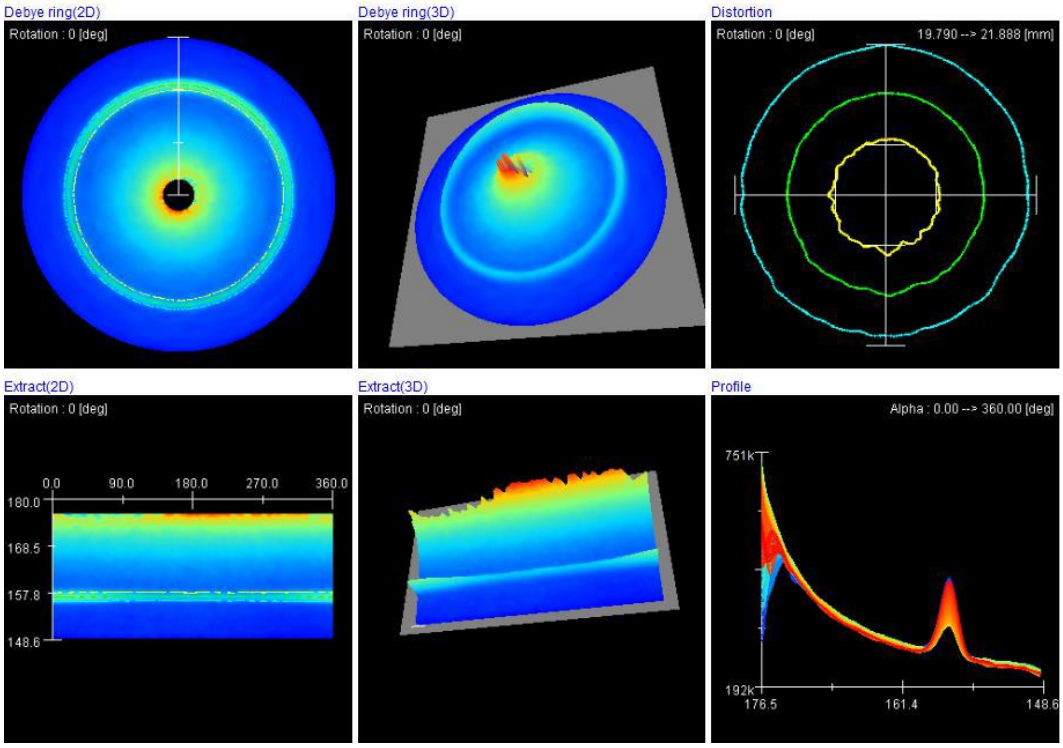

(c)

Figure 5.14Full 2D and 3D Debye ring and its distribution of residual stresses for (a) BM, (b) continuous vibration and (c) Discontinues vibrations

The distorted 3D Debye-Scherrer ring profile represented the surface damage and high compressive residual stresses on the workpiece. With ultrasonic vibration amplitude, the uniformity of the 3D Debye ring was relatively high. The uniformity of the distortion ring was indicative of a healthy surface morphology and minimal residual stresses on the machined surface.

Strong flushing impact attributable to greater amplitude of vibration in order to reduce heat concentration and re-solidification. (Khosrozadeh & Shabgard)[115] have demonstrated that stresses decrease as amplitude increases. However, when the amplitude limit exceeded a certain threshold, the impact was discovered to be inverted. Figures 5.15 depict the comparative FWHM distribution of the complete Debye-Scherrer ring at various amplitudes of vibration.

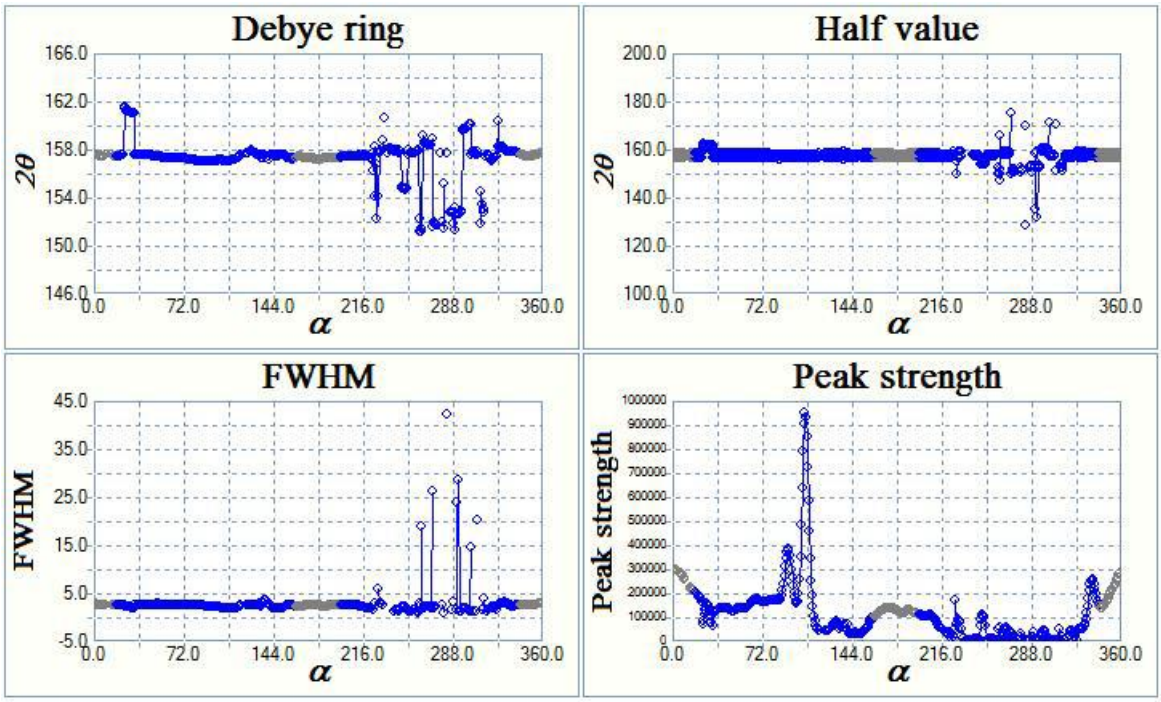

(a)

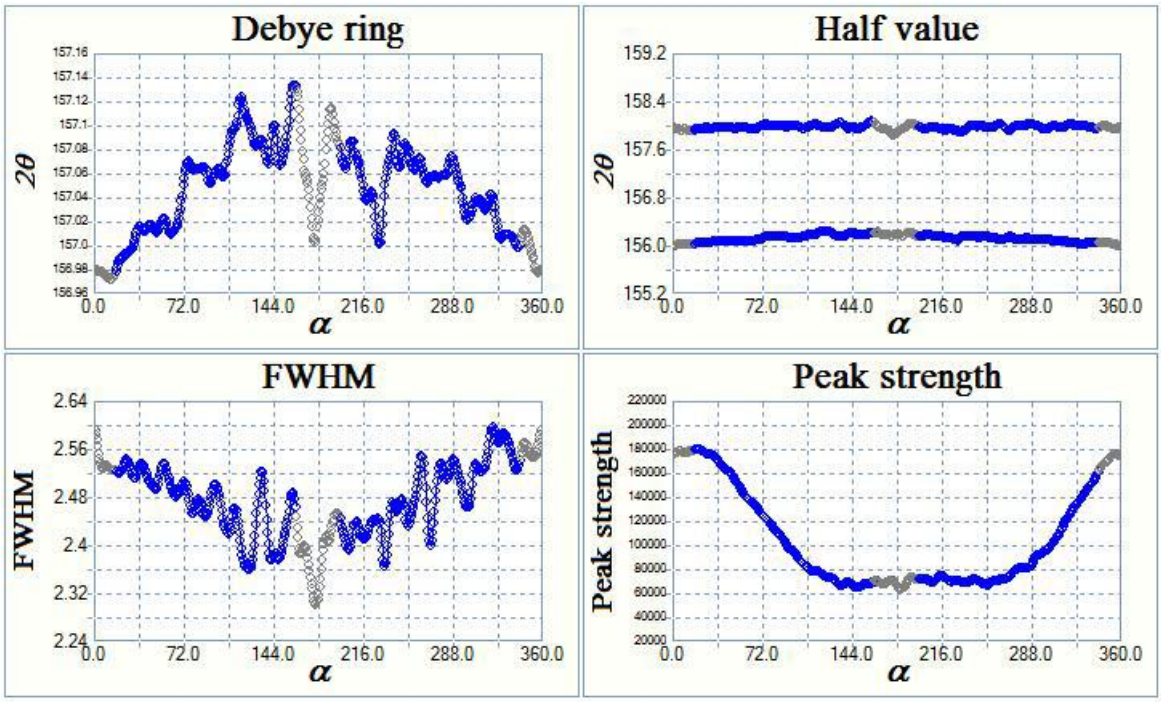

(b)

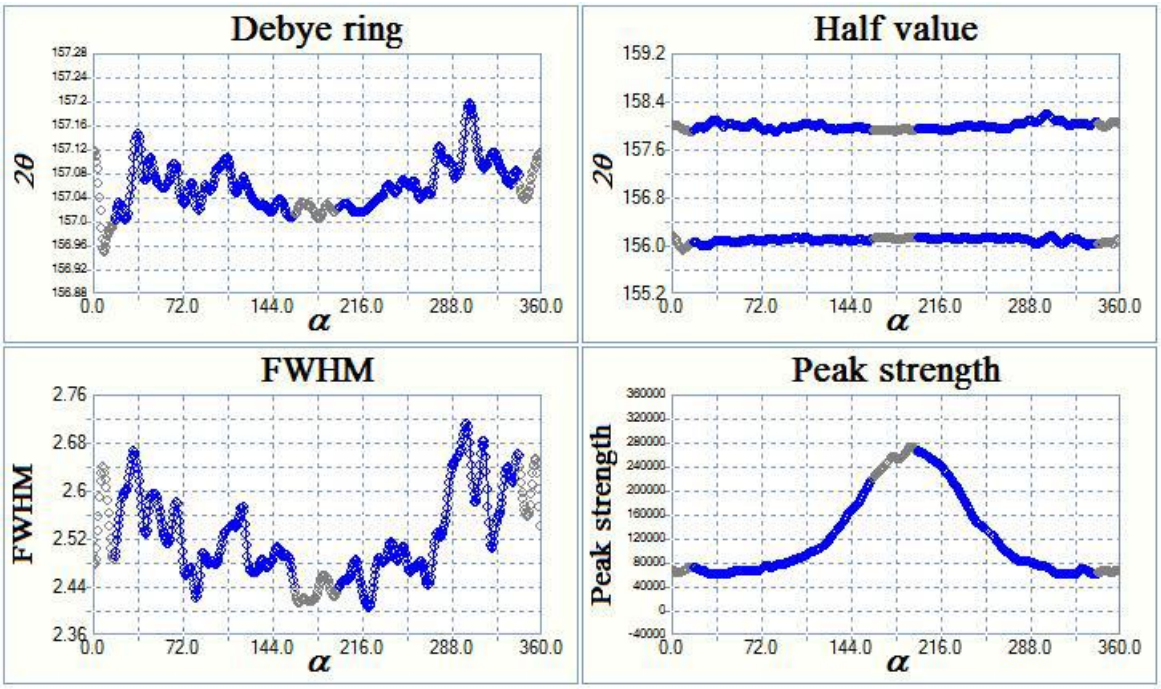

(c)

Figure 5.15 Debye ring and half value for (a) BM (b) continuous vibration and (c) Discontinues vibrations

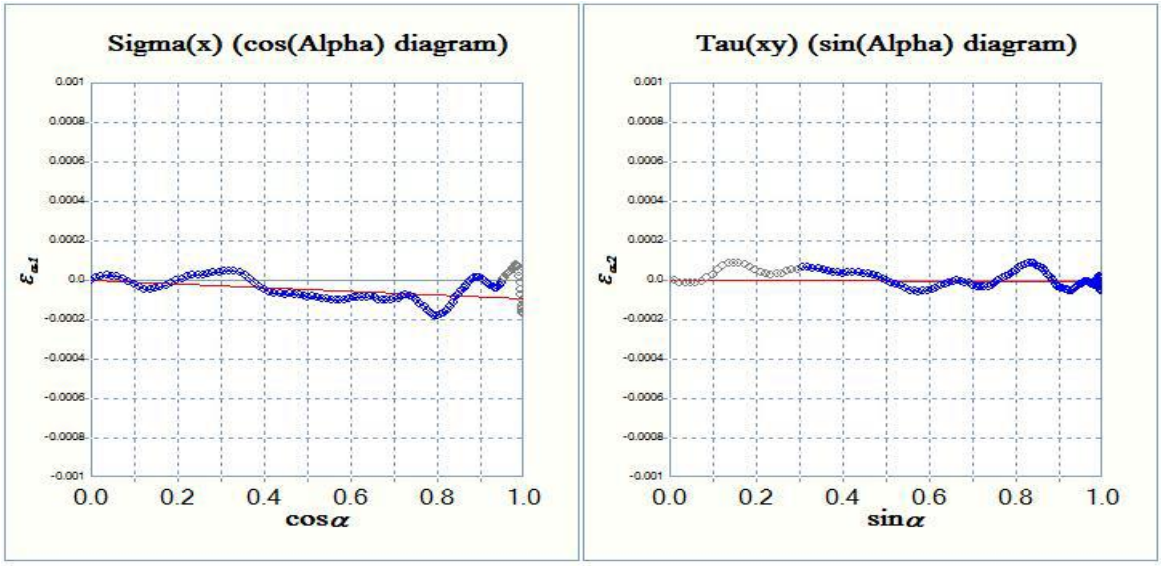

(a)

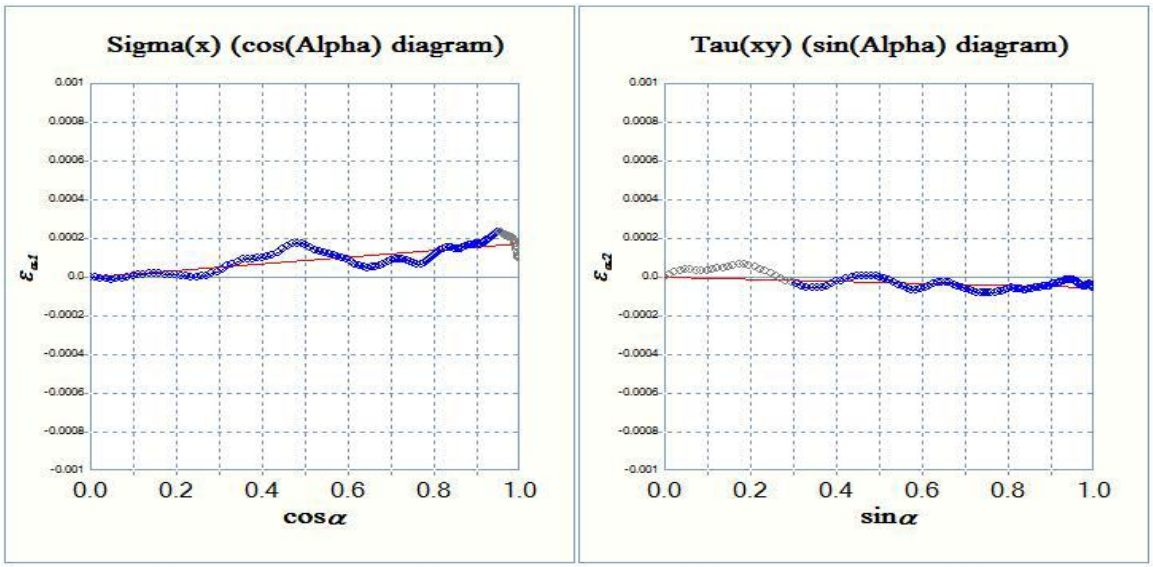

(b)

Figure 5.16 Residual stress graphs for (a) continuous vibration (b) discontinuous vibration

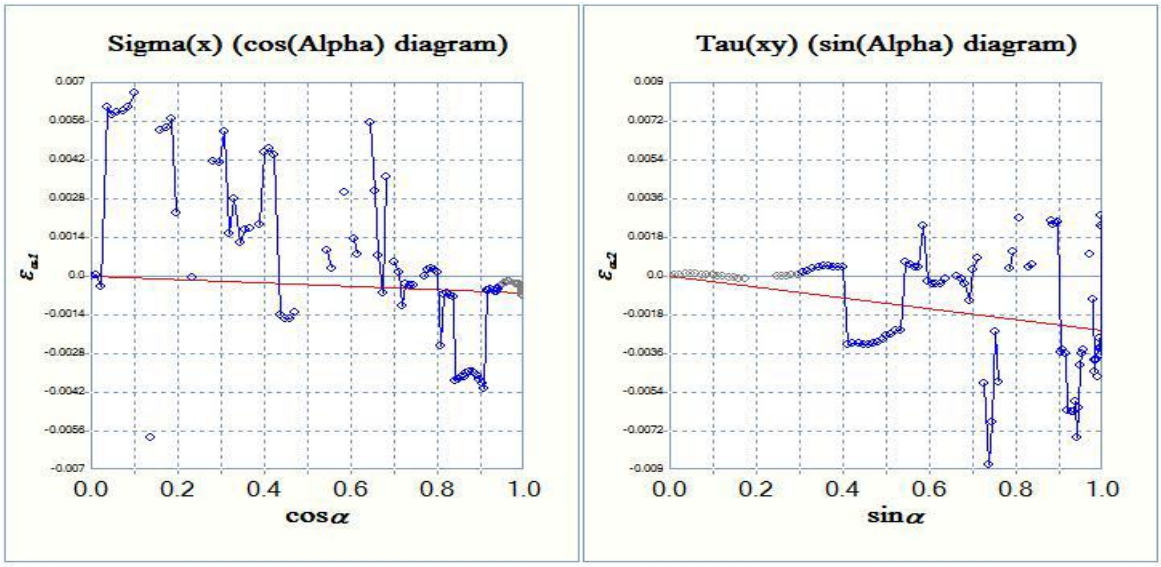

Figure 5.17 Residual stress graphs for base metal

As shown in Figures 5.16 and 5.17, the horizontal axes cos(α) are the cosine of the azimuth angle of the Debye-ring, whereas the vertical axis is a strain($\varepsilon_{\alpha 1}$). Figure 5.16 (a) for continuous vibration has a steeper slope in comparison to Figure 5.16 (b) for discontinuous vibration. In the case of base metals, however, the slope was relatively steep, as shown in Figure 5.17.

5.3.1 Optimization of parameters for residual stress

The average residual stress and S/N ratio for each UAFSW welded sample are calculated and presented in Table 5.7.

Table 5.7 Average values of UTS and S/N ratios (Lower-the-Better) for residual stress

Experiment No.	**Average value of Residual stress**	**Variance**	**Sum of Squares**	**S/N Ratio (Lower-the-Better)**
1	-54.6667	2.333333333	2990	-34.75671188
2	-33	1	1089.666667	-30.37293666

3	-41	4	1683.666667	-32.26256114
4	-35.6667	2.333333333	1273.666667	-31.05055783
5	-35.3333	6.333333333	1252.666667	-30.97835521
6	-33.3333	4.333333333	1114	-30.46885191
7	-36	4	1298.666667	-31.13497693
8	-25.6667	4.333333333	661.6666667	-28.20639256
9	-19	19	373.6666667	-25.72484358
10	-41.3333	9.333333333	1714.666667	-32.34179705
11	-35.3333	9.333333333	1254.666667	-30.9852836
12	-14.6667	2.333333333	216.6666667	-23.35792102
13	-35	16	1235.666667	-30.91901331
14	-35.6667	6.333333333	1276.333333	-31.05964112
15	-11	1	121.6666667	-20.8517161
16	-29	4	843.6666667	-29.2617089
17	-29.3333	2.333333333	862	-29.35507266
18	-14.6667	2.333333333	216.6666667	-23.35792102

5.4.1 Effects of vibrations on residual stress

Figure 5.18 shows the S/N ratio and the main effect of the vibrations. It was observed that with discontinuous vibration, residual stresses decrease. It may be because of vibration on the workpiece provided more change than continuous vibration of the workpiece. This was due to the fact that the ultrasonic energy was significantly lower during periodic vibration than during continuous vibration of the workpiece.

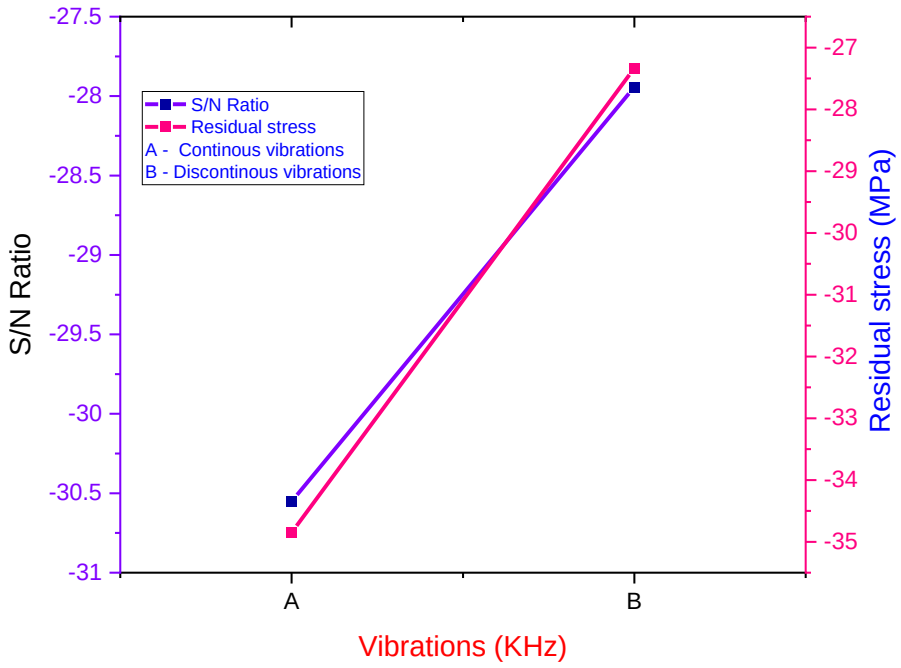

Figure 5.18S/N ratio and main effect of type of vibration on residual stress

5.4.2 Effects of tilt angle on residual stress

The effect of tilt angle on residual stress is shown in Figure 5.19. The residual stress decreases from 0 to 3° angle. The similar trend is observed for S/N ratio. The values decrease as the tilt angle varies from 0 to 3°. The maximum value of residual stress and S/N ration is observed at 3°. As the tilt angle increase, the residual stress increases in UAFSW welded joints due to non-uniform distribution of vibration and temperature variation.

5.4.3 Effects of travel speed on residual stress

The effect of travel speed on residual stress is shown in Figure 5.20. The residual stress increases as the travel speed increases from 600rpm to 800rpm. The similar trend is observed for S/N ratio. The values increase as the travel speed increases and the maximum value of residual stress and S/N ration is observed at 1000rpm.

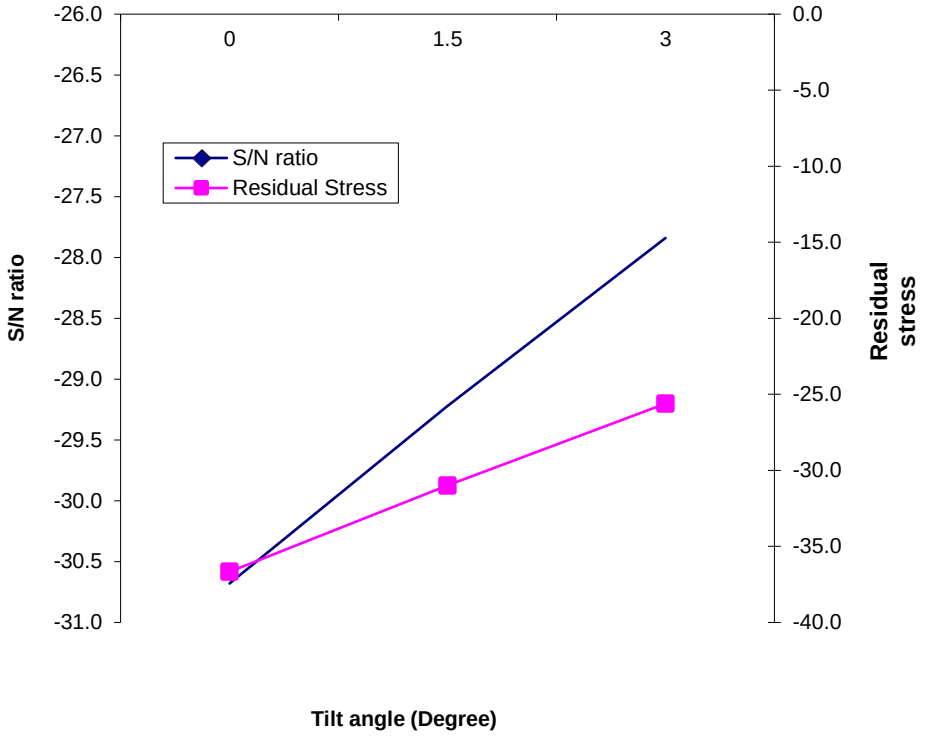

Figure 5.19S/N ratio and main effect of tilt angle on residual stress

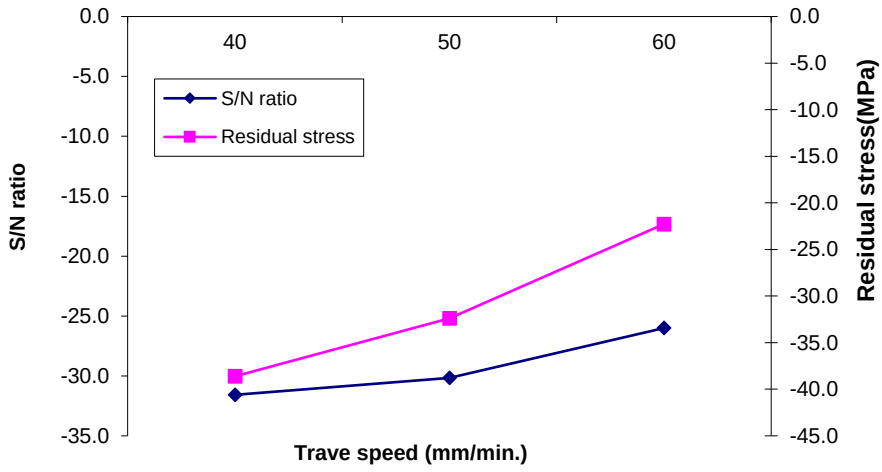

Figure 5.20 S/N ratio and main effect of travel speed on residual stress

5.4.4 Effects of rotational speed on residual stress

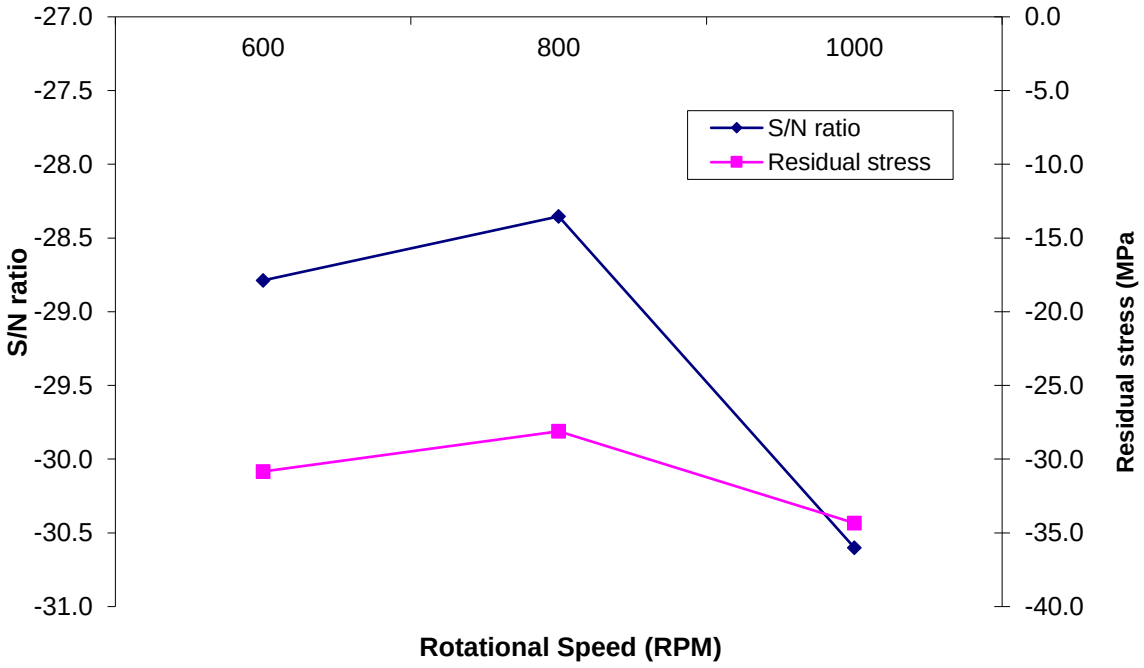

Figure 5.21S/N ratio and main effect of rotational speed on residual stress

Figure 5.21 depicts the residual stress value of UAFSW joints. During the course of the experiment, it was discovered that all residual stresses in UAFSW joints were compressive. At constant rotational speed, it can be observed that continuous vibrations result in greater residual stress than discontinuous vibrations. It has also been observed that a greater amplitude of vibration results in an increase in residual stress due to an increase in workpiece disturbances. Increasing rotational speed demonstrates an increase in residual formation[78].

5.4.5 Effects of amplitude of vibration on residual stress

The Figure 5.22 sums up that the amplitude first increases from zero to 44 microns where 44 microns is the peak point after which there is a decrease at 88 microns. The similar trend is shown in S/N ratio with lesser values than raw data of residual stress. As at the higher amplitude of vibration produces higher disturbances in the workpiece that causes more residual stress.

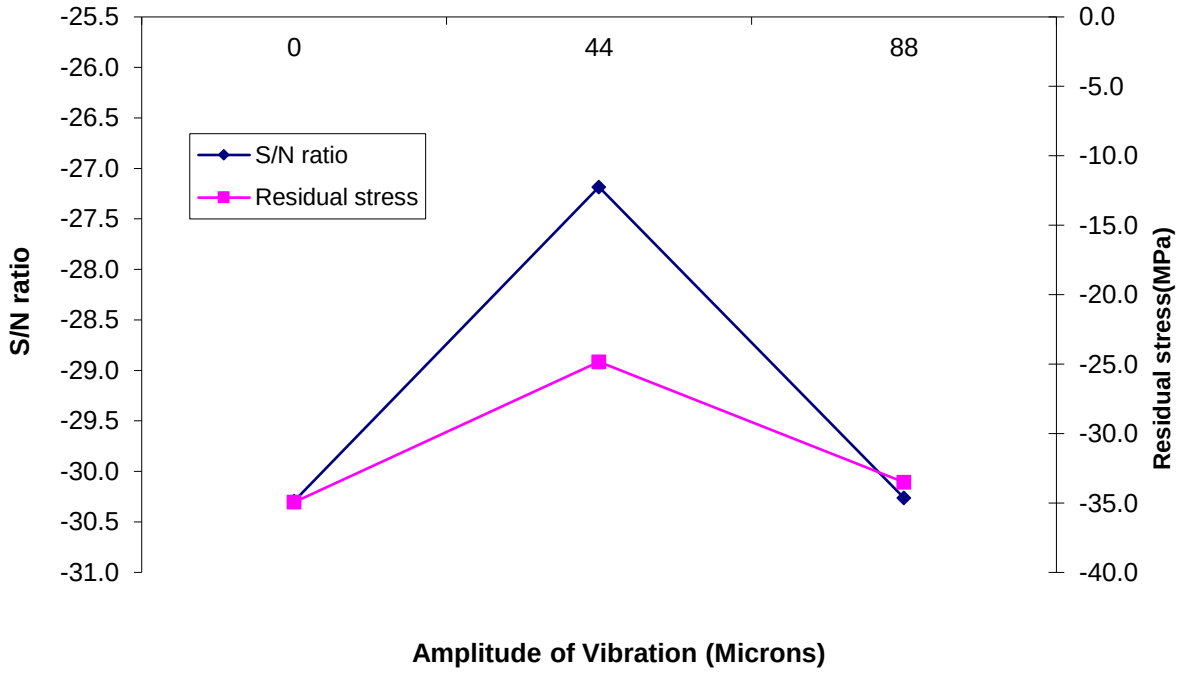

Figure 5.22 S/N ratio and main effect of amplitude of vibration on residual stress

5.4.6 Selection of optimal levels for residual stress

Analysis of variance (ANOVA) was performed to determine the significant influence of the process parameters on residual stress. The ANOVA of the RAW data and the S/N ratio for residual stress are displayed in Tables 5.8 and 5.9, respectively.

Table 5.8 ANOVA of the raw data for Residual stress

Source	**SS**	**DOF**	**V**	**P**	**F-ratio**	**Significant**
Type of vibration	30.592136	1	30.592136	13.654132	18.524848	Yes
Tilt Angle	24.192206	2	12.096103	10.79766	7.3247082	Yes
Rotational speed	100.68696	2	50.343483	44.93942	30.485134	Yes
Travel Speed	17.043653	2	8.5218268	7.607062	5.1603309	Yes

Amplitude	38.324141	2	19.162070	17.10514	11.603454	Yes
E	13.211287	8	1.6514109	5.896569	*	
Total (T)	224.0504	17	*	100		
Significant at 95% confidence level, F critical =5.236 (Tabulated Value) SS-Sum of Squares, DOF-Degree of Freedom, V-Variance, SS'- the Pure sum of Squares						

Table 5.9 ANOVA of the S/N Ratio for Residual stress

Source	**SS**	**DOF**	**V**	**P**	**F-ratio**	**Significant**
Type of vibration	763.1296296	1	763.1296296	12.2403576	59.44320231	Yes
Tilt Angle	1100.259259	2	550.1296296	17.6478101	42.85178507	Yes
Rotational speed	2446.37037	2	1223.185185	39.2390061	95.27875947	Yes
Travel Speed	350.2592593	2	175.1296296	5.61804761	13.64154345	Yes
Amplitude	1009.648148	2	504.8240741	16.1944366	39.32275514	Yes
E	564.8703704	44	12.83796296	9.06034188	*	
Total (T)	6234.537037	53		100		
Significant at 95% confidence level, F critical =3.22 (Tabulated Value) SS-Sum of Squares, DOF-Degree of Freedom, V-Variance, SS'- the Pure sum of Squares						

The results demonstrate that all variables significantly affected the UAFSW process's residual stress for both the raw data and S/N ratio. The column “P” represents the percent contribution of the particular factor to the response characteristic.

5.5 ESTIMATION OF OPTIMUM RESPONSES

To obtain validated results, three confirmation experiments were conducted for each response characteristic, MH, UTS, and Residual stress. Three confirmation experiments for each response were conducted with the process parameters optimized for optimal performance. The optimal process parameters for these responses are vibration type, tilt angle, tool travel speed, tool rotation speed, and vibration amplitude. The results as shown in Table 5.10.

Table 5.10Predicted optimal value, confidence intervals and results of confirmation

Response characteristics	**Average experimental value**	**Predicted optimal value**	**Confidence Intervals 95%**
MH	170.18	159.83	CI_{CE}: 152.77<159.83<165.23 CI_{POP}: 154.97<159.83<164.69
UTS	500.01	517.41	CI_{CE}: 495.75<517.41<539.07 CI_{POP}:490.96<517.41<543.86
Residual stress	-31.09	-25.56	CI_{CE}: -26.62<-25.56<-24.5 CI_{POP}: 26.5<-25.56<-24.62
CICE = Confidence interval for the mean of the confirmation experiments CIPOP =Confidence interval for the mean of the population			

5.6 CONFIRMATION TEST

The confirmation experiment was preformed to verify the above analysis phases.It must be determined that the optimal values fall within the parameters' predetermined range. The experimentally determined values of MH, UTS, and residual stress are within 95% of CI_{CE} for each response. Table 4.12 demonstrates that for all responses the error percentage is less than the acceptable value of 5% (confidence level = 95%); therefore, suggested regression model is valid.

5.7 THERMAL ANALYSIS AND SOLUTION CONTROLS

In three load steps, a nonlinear transient analysis is performed using the structural-thermal options of SOLID226 and CONTA174. FSW simulation incorporates nonlinearity, contact, friction, large plastic deformation, structural-thermal coupling, and varying loads for every load step. The applied solution settings account for each of these factors[93].

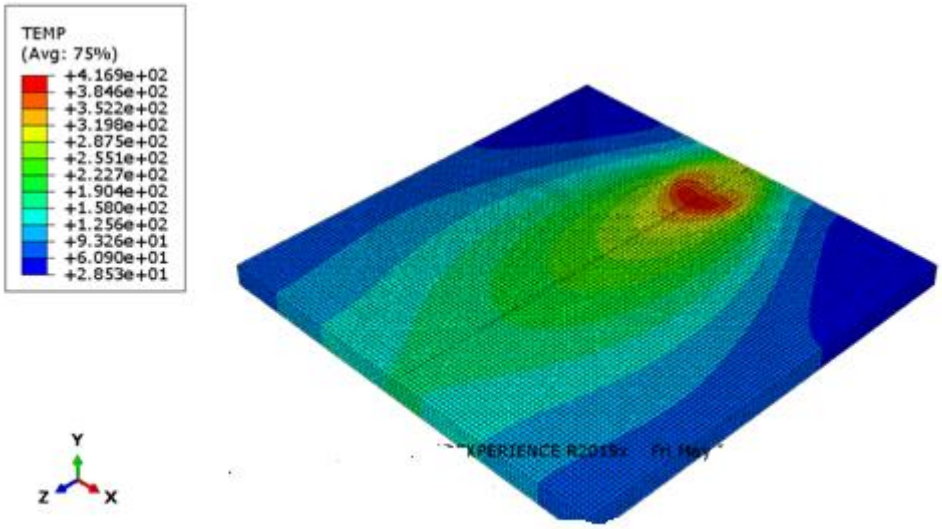

Figure 5.23Distribution of heat during welding

NLGEOM is activated to include large-deflection or large strain effects based on the element type. To enable a quicker solution, automatic time-stepping is enabled. Initial time step size is 0.1 and minimum time step is 0.001. The maximum time step in load steps 2 and 3 is set to

0.2. Multiple runs have been selected that must be conducted to determine the effects of various process parameters on the analysis results. The tool plunge depth is fixed at 1.85 mm, and the tilt angle is fixed at 0 degrees.

5.7.1 Heat distribution of UAFSW

The material's temperature rises as the tool descends into the workpiece and penetrates it. Identical pattern was observed during the experimental procedure. There is a significant increase in temperature as the pin penetrates up to its full length and during the dwell phase due to friction between the tool shoulder and the workpieces. The increasing temperature causes the areas of the workpiece in contact with the tool to soften. As seen in in Figure 5.23 and Figure 5.24.the majority of heat is confined to the area where the tool and workpiece come into contact, while the remainder of the workpiece is only minimally affected. Additionally, the advancing side has a higher temperature than the retreating side.

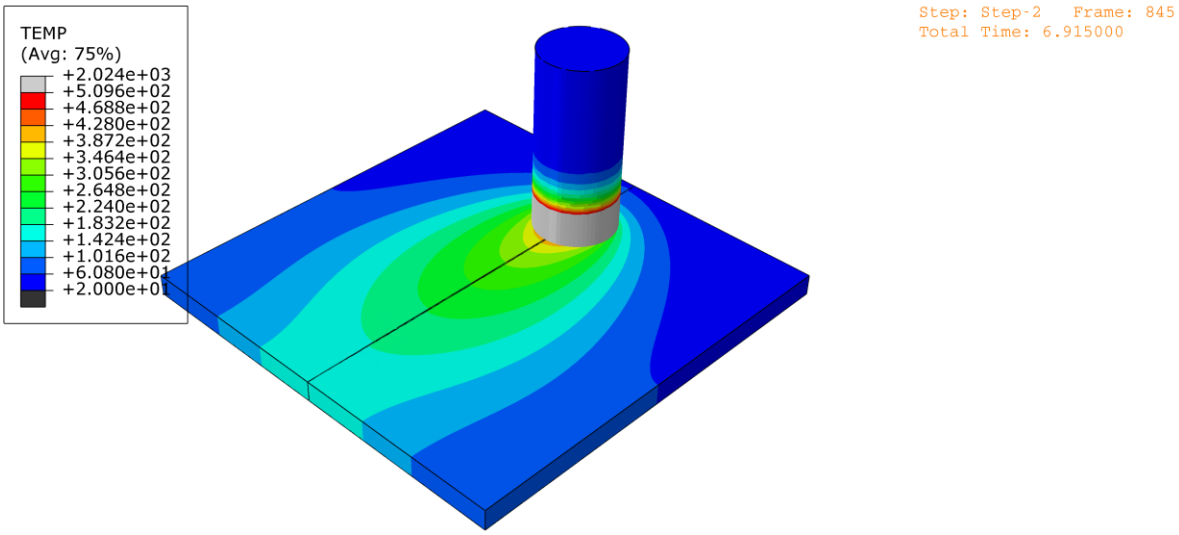

Figure 5.24Heat distribution of UAFSW in the weld zone

The dwell time has a significant effect on the maximum temperature attained in the initial contact area but has no effect on the welding or temperature of the remainder of the workpiece. Increasing the tool's rotational speed causes an increase in welding temperatures

at the same traverse speed due to an increase in frictional contact between the tool and the workpiece, which generates more frictional heat.

To validate the values obtained from soft computing analysis, the temperature of the stir zone was measured by using a thermal imaging camera and the temperature of the zone was recorded for various parameters and some images are shown in Figure 5.25.

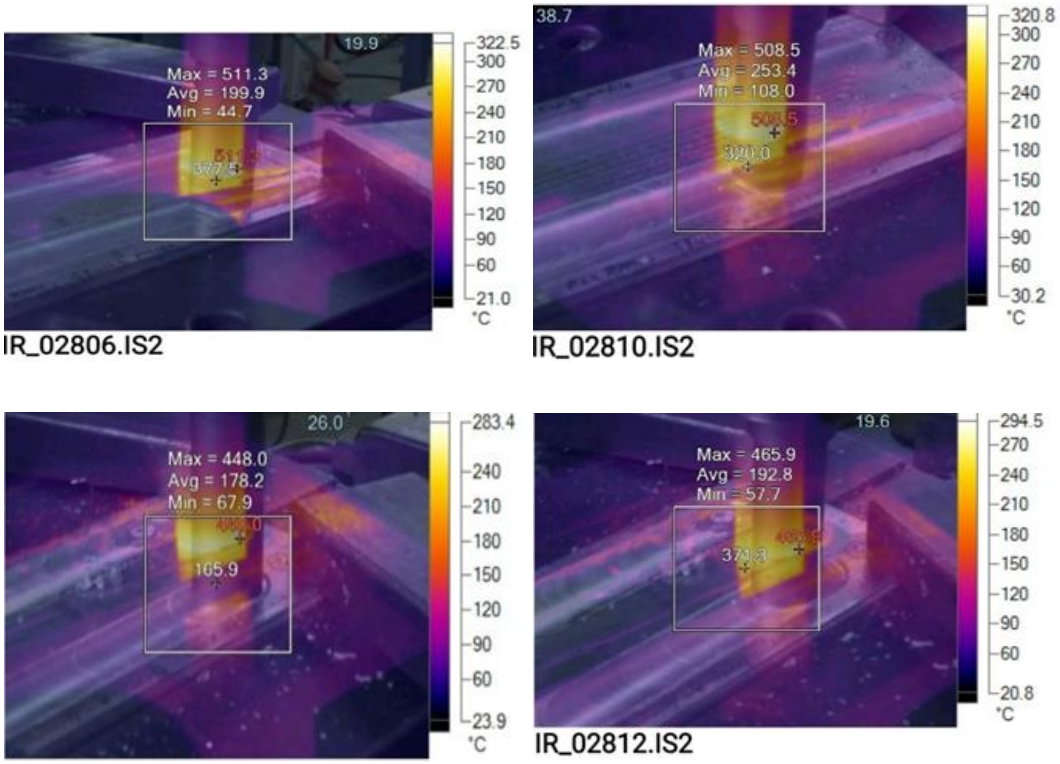

Figure 5.25UAFSW stir zone temperature (a) at 1000 RPM continuous vibrations (b) at 800 RPM with continuous vibrations (c) at 1000 RPM with discontinues vibrations d) 800 RPM with discontinuous vibrations

5.8 METALLURGICAL CHARACTERIZATION OF UAFSW

5.8.1 Microstructural characterization

Viewing the microstructure is important because one of the most significant effects of UAFSW is the resultant grain structure refinement. These are translated into superior mechanical properties imparted to the composite material. However, to be able to view the

microstructure, three more steps had to be performed to prepare the samples for viewing. The samples were ground and mounted with Bakelite powder in a mounting press. Then the samples were polished using different grades of emery papers followed by velvet cloth polishing using alumina suspension. For microstructure observations, an inverted Olympus GX41 metallurgical optical microscope was used. Images of microstructure were captured at 200X and 500X magnification. The width of the micrograph is determined using a pixel-to-scale conversion of 2 pixels per micron. Viewing the microstructure was deemed essential due to the significant effects of the UAFSW technique; this was the result of the grain structure being refined.

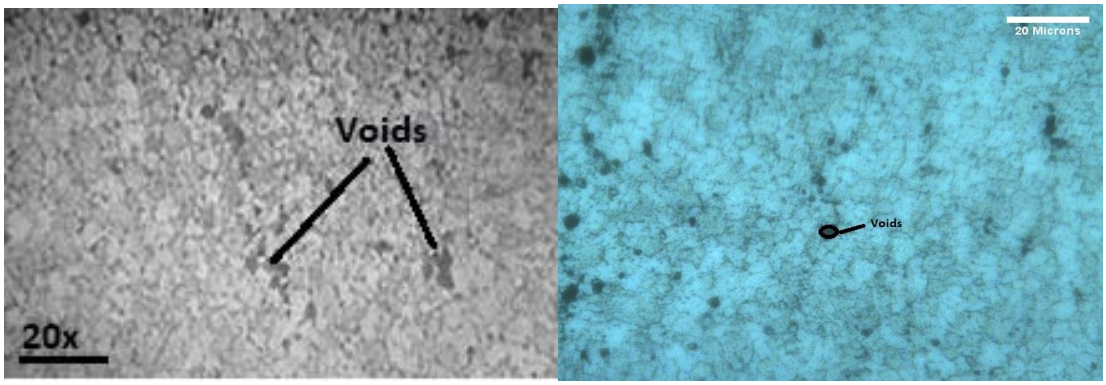

Figure 5.26 Microstructure image of BM at 20X

As depicted in Figure 5.26, it is observed that elongated and pancake-shaped grains made up the microstructure of the base metal, with second-stage particles arranged similarly to second-stage particles along introductory grain boundaries.

Figure 5.27 (a)-(b) depicts surface morphology images of UAFSW. It is evident from the image that particles were distributed uniformly across the entire surface. In the weld nugget zone, ultrasonic energy and intense plastic deformation occur, the high temperature allowed exceptionally fine and equiaxed grains to form, which was a typical characteristic of grain structures in particular, the fundamental system, such as the grain boundary stage, was

divided with ultrasonic-assisted FSW, resulting in particles that are fine and uniform. The microstructure of the welded samples of AA7075-T6 alongside the sheets thickness by SEM image microscopy image as depleted in Figure 5.28.

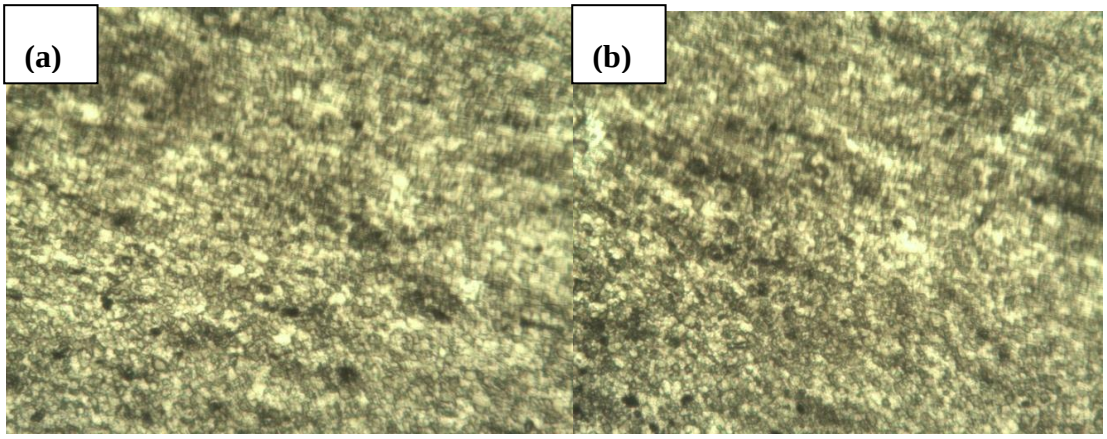

Figure 5.27 Microstructure at 20X (a) with continuous vibrations (b) Discontinuous vibrations at 800rpm

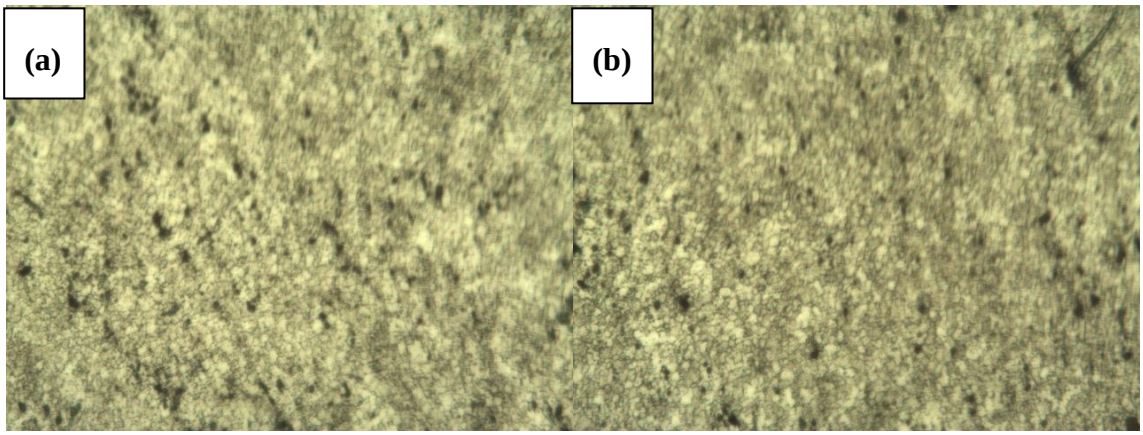

Figure 5.28Microstructures at 20X a) with continuous vibrations b) Discontinuous vibrations at 1000rpm

Figure 5.29(d) displays the EDS result of ultrasonic-assisted FSW and confirms the deposition of weight percentages in the developed welded zone, such as 88% Al, 6.1% Zn, 2.5% Cu, and the rest as other elements.

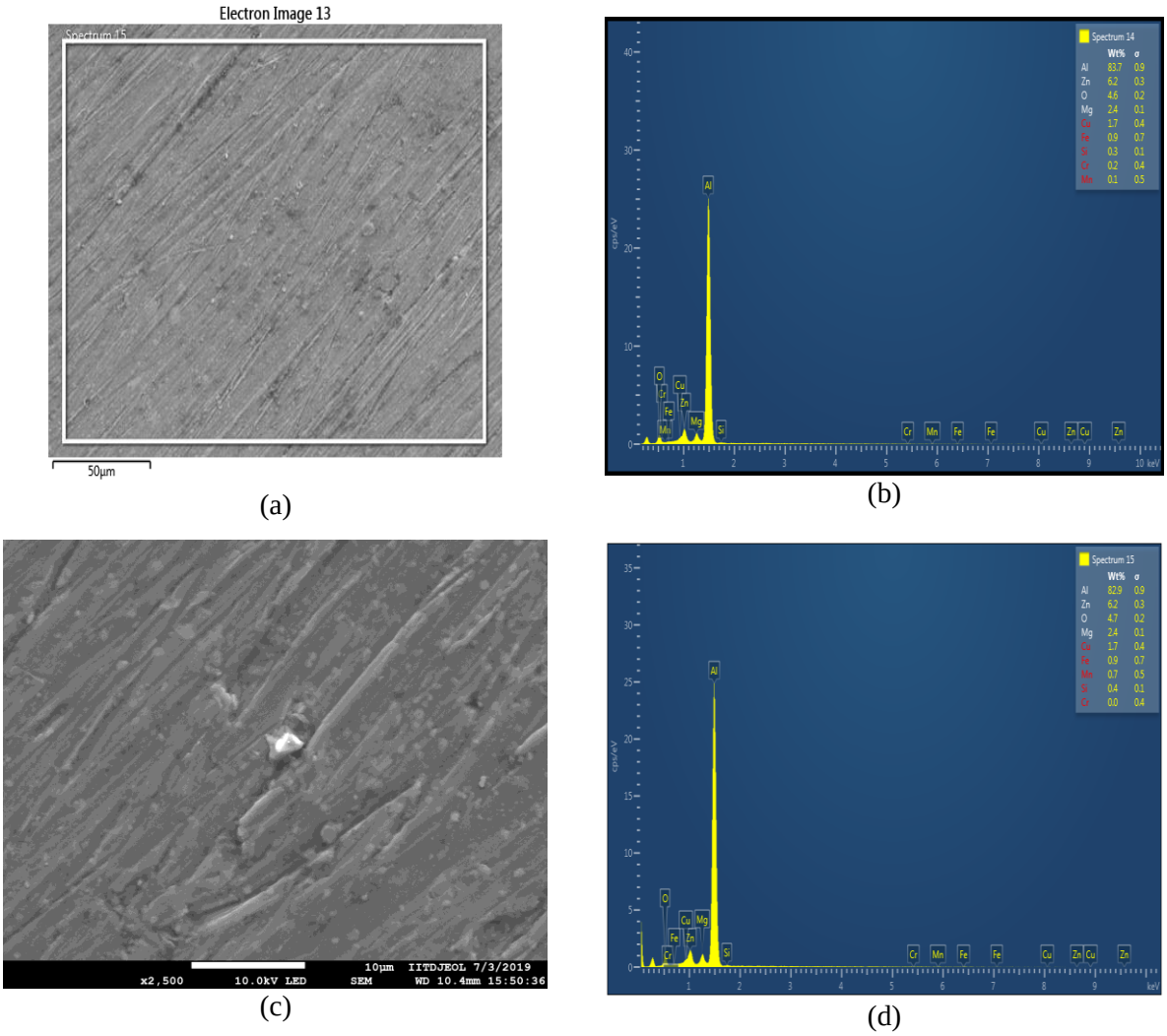

Figure 5.29 (a) SEM image of base metal (b) EDS of Base metal(c) SEM image of with vibrations welded joint (d) EDS of welded Joint

5.8.2 XRD analysis

XRD spectra were obtained in the parent metals and weld samples shown in Figure 5.30 – 5.32. The analysis confirmed the presence of binary phases like 88% Al, 6.1% Zn, 2.5% Cu, in the parent metal region of AA 7075-T6 alloy and the formation of ternary phases like AlCuZn and Cu.61Zn.39. In the base metal region, the peaks of bcc Al and Zn phases were observed. The analysis also confirmed the presence of Al-O_2 binary intermetallic phases like

Al_2O_3, and ternary phases like (Al,Zn,Si) while UAFSW welded samples shows the % of Aluminium is decreased to 83%. The XRD analysis of the welded samples confirmed the presence of $AlAl_2MgO4$ in the welded region of AA7075-T6 with UAFSW.

The experimental result shows that the prominent peak is obtained at 2θ angle at 38.78degree and at 46.34 degree. The similar trend is obtained for welded samples.

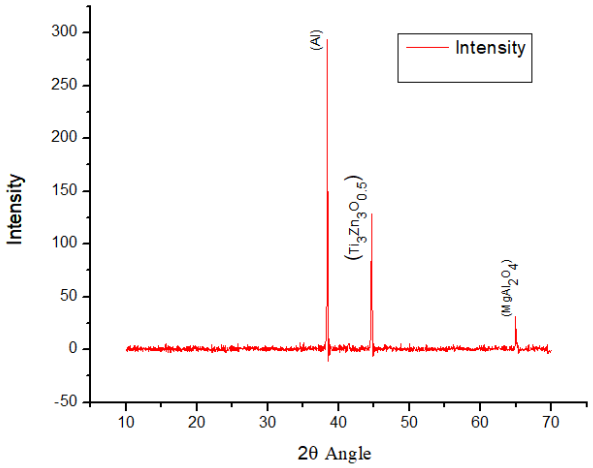

Figure 5.30 XRD analysis of base metal AA 7075-T6

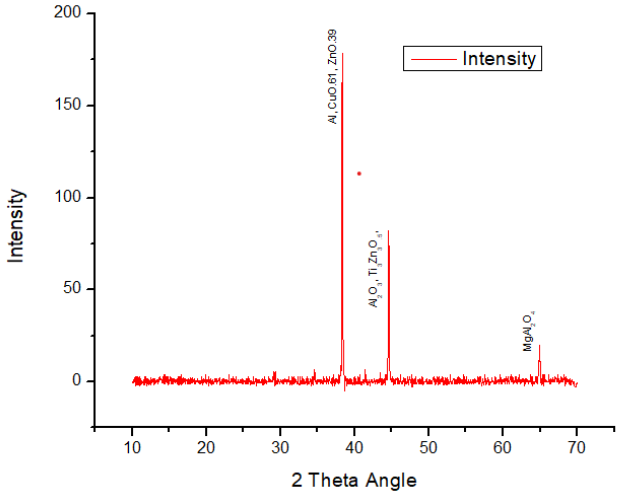

Figure 5.31 XRD analysis of UAFSW joint with continuous vibrations

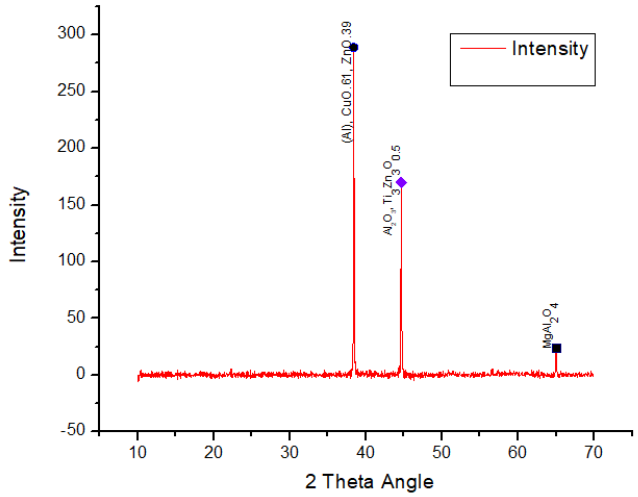

Figure 5.32 XRD analysis of UAFSW joint with discontinuous vibrations

5.9 WEAR BEHAVIOR OF UAFSW JOINTS

As shown in Figure 5.33, the tribological performance was evaluated using a pin-on-disk tribometer, which revealed a coefficient of friction (COF) range of 0.16 to 0.59, and wear in the range of 37-130 m as depicted in Figure 5.34 at temperatures ranging from 100 to 350oC, load 50 N, and sliding velocity 1m/s, respectively. A tribological examination of a UAFSW-welded workpiece was conducted to examine the wear characteristics of the welded sample. The tribological test revealed a 72.88 percent decrease in COF and a 71 percent decrease in wear at 1 m/s sliding speeds, 350^{o}C temperatures, and 50N loads.

The variation of COF with sliding distance is depicted in Figure 5.34 Point A on the graph represents the base metal, while point B represents the absence of vibration. Point C represents continuous vibrations, and point D represents discontinuous vibrations.

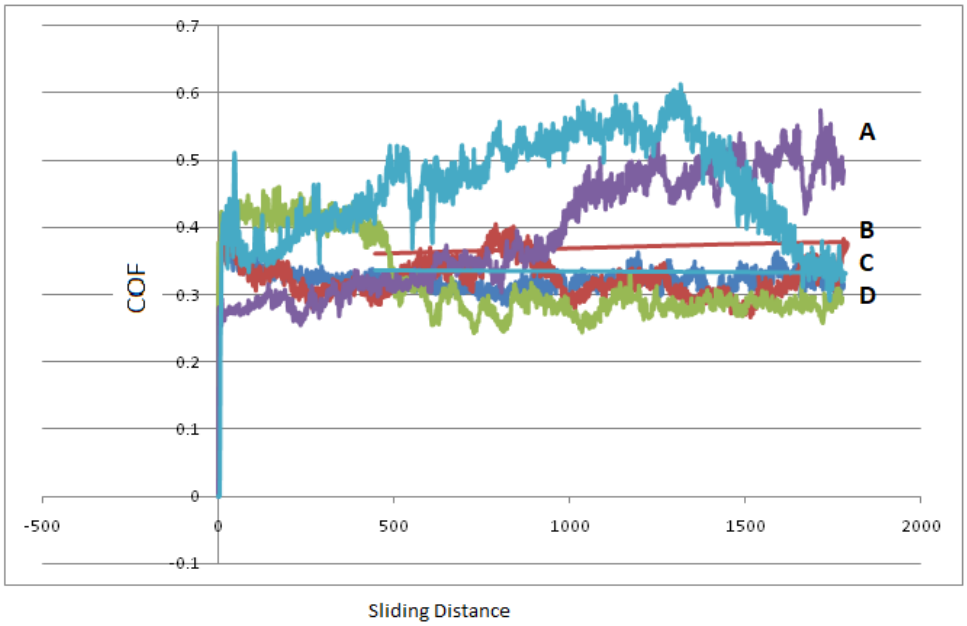

Figure 5.33 COF Vs Sliding distance graph

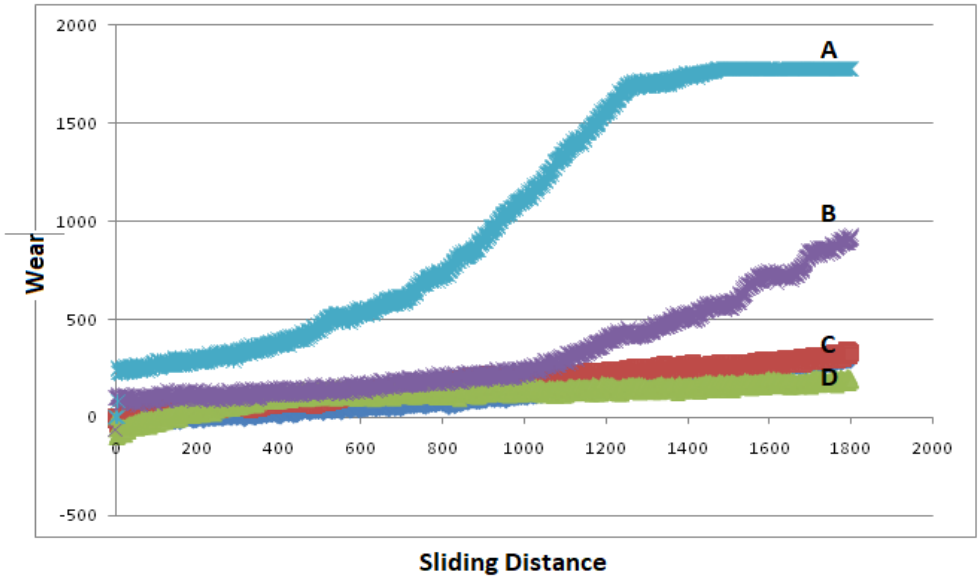

Figure 5.34 Wear Vs Sliding distance graph

COF is found to be greater in base metals compared to other experimental conditions. The COF is lowest for UAFSW with discontinuous vibrations. The similar trend is obtained for sliding distance versus wear graph as shown in Figure 5.35.

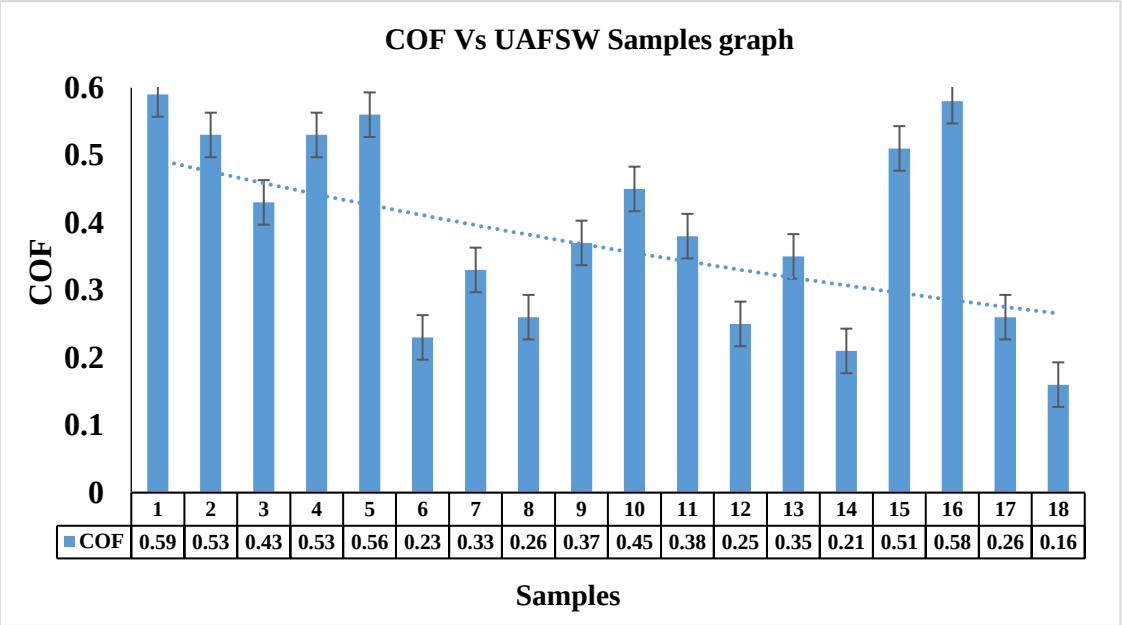

	1	2	3	4	5	6	7	8	9	10	11	12	13	14	15	16	17	18
COF	0.59	0.53	0.43	0.53	0.56	0.23	0.33	0.26	0.37	0.45	0.38	0.25	0.35	0.21	0.51	0.58	0.26	0.16

(a)

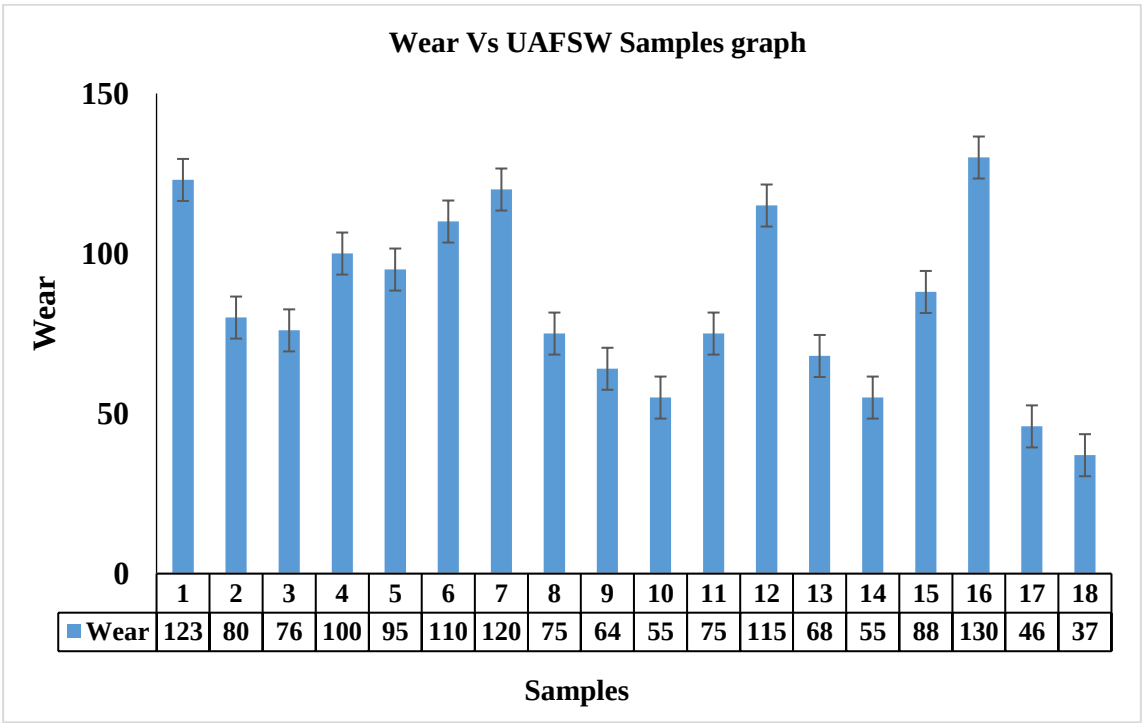

	1	2	3	4	5	6	7	8	9	10	11	12	13	14	15	16	17	18
Wear	123	80	76	100	95	110	120	75	64	55	75	115	68	55	88	130	46	37

(b)

Figure 5.35(a) COF (b) Wear Vs Sliding distance graph of UAFSW joints

The results of the experiments indicate that as the travel speed increases, the coefficient of friction (COF) and wear behaviour of welded samples increase significantly also observed a decrease in COF and wear as the load increases. Changes in phase structure, stoichiometry composition, and the behaviour of developed ultrasonic assisted FSW were crucial in reducing friction and wear.

In Figure 5.36(a)-(b), the FESEM images depict the wear characteristics of developed UAFSW with worn-out surfaces.

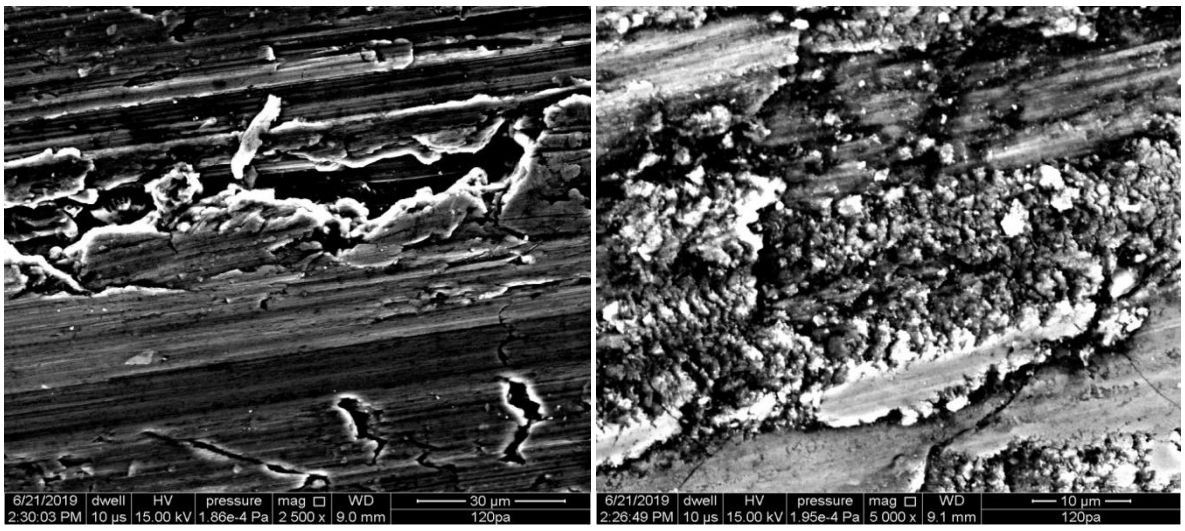

Figure 5.36 FESEM image of worm out surface of UAFSW

The FESEM obtained after a wear test reveals a brittle structure with a grain-like appearance, as well as the transformation of UAFSW from amorphous to polycrystalline. Metallic abrasive particles are evidently embedded in the developed UAFSW or adhesive wear. During the wear test, the UAFSW exhibited both ploughing action with the presence of chipped-off particles and rubbing action with worn-out particles[116], [117].

There are various stages of wear on the UAFSW joint that are depicted as:

In the first stage, when variable load, sliding velocity, and temperature are applied, asperities of the developed joint shot penetrate into the disc, resulting in plastic deformation. After that,

the second stage of disc ploughing by Al asperities results in tribofilm formation (due to Al diffusion and oxide layer formation), which weakens the asperities. At the final stage of an increase in oxides, Alumina layer formation results in the smoothing of the welded surface and a reduction in COF and wear.

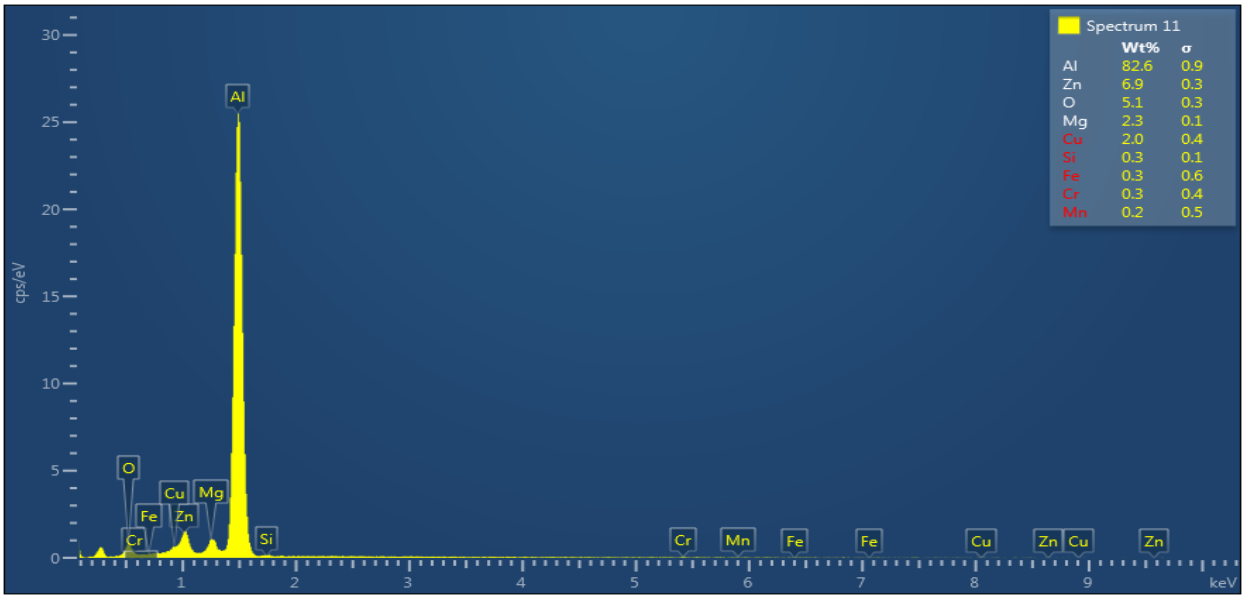

Figure 5.37 EDS analysis of worn-out surfaces of UAFSW

An abrasive wear mechanism is the most likely cause of wear on developed UAFSW based on the formation of oxides, micron-sized particles, and delamination layers. The EDS analysis of worn surfaces confirms the formation of tribofilms and oxides due to the presence of Al and oxygen. Under variable test conditions, most wear is caused by ploughing (plastic deformation). On the UAFSW joints, micron-sized Al crystallites may cause the formation of deep grooves and scratches during ploughing action. The micron-sized Al particles of UAFSW serve as a barrier against plastic deformation, resulting in abrasion resistance[118].

CHAPTER - 6

CONCLUSIONS AND FUTURE SCOPE

This experimental investigation focuses into the UAFSW process to explore the possibility of enhancing the usefulness of the conventional FSW process by applying continuous and discontinuous vibrations. This research suggests that developed UAFSW process is one of the most significant processes in the field of joining processes with enhanced mechanical properties. The experimental results indicate that mechanical properties such as MH, UTS, residual stress, and wear are most affected and improved.

6.1 CONCLUSIONS

The above experimental investigation yields the following significant findings:

a) FSW aided by ultrasonic energy produces the maximum microhardness of 201.32 HV in the welded region at rotational speed of 1000 rpm, traverse speed of 60 mm/min, amplitude of vibration of zero microns, tilt angle of 1.5 degree, and continuous vibrations, respectively. In this investigation, it was discovered that the maximum microhardness value of a UAFSW-welded joint is more than double that of its base metal at optimal parameters. It is also determined that the microhardness value in the centre of the welded region is greater than that of the HAZ. The experimental results show the minimum value of microhardness is 106.13 HV for continuous vibrations. It was also observed that the amplitude of vibration is having least effect on MH.

   The percentage contribution of L18 OA, the optimal level contribution, has been determined to be 24.73 percent for maximum travel speed. The percentage contribution for other parameters is 24.14 percent for vibration type, 4.66 percent for tilt angle, 9.7 percent for rotational speed, and 3.27 percent for amplitude type.

b) It was revealed that the type of vibrations had the greatest impact on tensile strength, 58.97 percent. Maximum tensile strength was achieved at a rotational speed of 600 rpm and a translational speed of 40 mm/min. Ultrasonic vibration has also been shown to increase heat input, allowing more material to flow around the tool and increasing the strength of the joint as a result. Additionally, it was determined that the amplitude of vibration (0.23 percent) is the least significant contributor and was not significantly affected.

c) The experimental results show that the residual stress of welded region varies from -54.66 MPa to – 11 MPa as compared to base metal's residual stress of -176 MPa. The negative sign shows residual stresses are compressive in nature.

   The optimal level contribution for maximum rotational speed has been determined to be 39.23 percent. Other parameters have a 12.24 percent contribution for vibration type, 17.64 percent for tilt angle, 5.6 percent for travel speed, and 16.19 percent for amplitude type.

d) With the structural-thermal options of SOLID226 and CONTA174, a nonlinear transient analysis is performed. FSW simulation incorporates nonlinearity, contact, friction, large plastic deformation, structural-thermal coupling, and varying loads for every load step and validated using thermal imaging.

e) With continuous and discontinuous vibrations, the UAFSW exhibits a uniform distribution of grains devoid of voids. Because of this, mechanical properties are improved.

f) Coefficient of friction and wear are found lower at 150N load and have significant effects with the rotational speed, traverse speed, tilt angle, minimum amplitude, and the type of vibrations. The tribological test showed a 72.88% decrease in COF and 71% reduction in the wear at test conditions of 1 m/s sliding velocities, 350^{o}C

temperature, and 150N load with UAFSW. The variation of COF with sliding distance shows the maximum values for base metal whereas it decreases with the applications of vibration in FSW. The COF is lowest for UAFSW with discontinuous vibrations. The variation of wear with sliding distance is greatest for base metal, whereas it decreases when vibration is applied to FSW. UAFSW has the lowest COF with discontinuous vibrations.

6.2 FUTURE SCOPE

a) In this investigation, workpiece thickness is taken as 3 mm. Greater thicknesses Al-alloy sheets can be worked with a variety of tool pin profiles and a multi-pass process with varying shoulder diameters.

b) The viability of UAFSW of high melting temperature materials, characterization of the process, microstructure, and mechanical properties of UAFSW on high melting temperature materials can be done by using a variety of tool materials.

c) Creep, fatigue strength, and bending strength tests can be performed for UAFSW.

d) In UAFSW, FEA modeling can be used to determine residual stress, surface finish, MH, and tool wear rate.

REFERENCES

[1] A. Costa, E. Botelho, M. Costa, … N. N.-J. of A., and undefined 2012, "A review of welding technologies for thermoplastic composites in aerospace applications," *SciELO Bras.*

[2] T. Ahmed, D. Stavrov, … H. B.-C. P. A. A., and undefined 2006, "Induction welding of thermoplastic composites—an overview," *Elsevier*.

[3] O. Salih, H. Ou, W. Sun, D. M.-M. & Design, and undefined 2015, "A review of friction stir welding of aluminium matrix composites," *Elsevier*.

[4] C. J. Thomas, M., Nicholas, E.D., Needham, J.C., Murch, M.G., Temple Smith, P. and Dawes, "The Welding Institute, TWI, International Patent Application No. PCT/GB92/02203 and GB Patent Application No. 9125978.8. - References - Scientific, 1991 Research Publishing."

[5] C. G. Rhodes, M. W. Mahoney, W. H. Bingel, R. A. Spurling, and C. C. Bampton, "Effects of friction stir welding on microstructure of 7075 aluminum," *Scr. Mater.*, vol. 36, no. 1, pp. 69–75, Jan. 1997.

[6] L. E. Murr, "A review of FSW research on dissimilar metal and alloy systems," *J. Mater. Eng. Perform.*, vol. 19, no. 8, pp. 1071–1089, Nov. 2010.

[7] B. Meyghani, M. B. Awang, S. S. Emamian, M. Khalid, B. Mohd Nor, and S. R. Pedapati, "A comparison of different finite element methods in the thermal analysis of friction stir welding (FSW)," *mdpi.com*.

[8] A. Squillace, A. De Fenzo, … G. G.-J. of M., and undefined 2004, "A comparison between FSW and TIG welding techniques: modifications of microstructure and pitting corrosion resistance in AA 2024-T3 butt joints," *Elsevier*.

[9] M. C. and D. W. B. London, M. Mahoney, B. Bingel, "High Strain Rate Superplasticity in Thick Section 7050 Aluminum Created by Friction Stir Process-ing" Kobe, Japan, 2001," *Proc. Third Int. Symp. Fract. Stir Weld.*

[10] A. R.-S. materialia and undefined 2008, "Flow visualization and simulation in FSW,"

Elsevier.

[11] G. Padmanaban, V. B.-M. & Design, and undefined 2009, "Selection of FSW tool pin profile, shoulder diameter and material for joining AZ31B magnesium alloy–an experimental approach," *Elsevier*.

[12] T. Chen, "Process parameters study on FSW joint of dissimilar metals for aluminum-steel," *J. Mater. Sci.*, vol. 44, no. 10, pp. 2573–2580, May 2009.

[13] S. Benavides, Y. Li, L. E. Murr, D. Brown, and J. C. McClure, "Low-temperature friction-stir welding of 2024 aluminum," *Scr. Mater.*, vol. 41, no. 8, pp. 809–815, Sep. 1999.

[14] J. Su, T. Nelson, C. S.-M. S. and E. A, and undefined 2005, "Microstructure evolution during FSW/FSP of high strength aluminum alloys," *Elsevier*.

[15] P. Liu, Q. Shi, W. Wang, X. Wang, Z. Z.-M. letters, and undefined 2008, "Microstructure and XRD analysis of FSW joints for copper T2/aluminium 5A06 dissimilar materials," *Elsevier*.

[16] S. Azeez, E. A.-P. in I. Ecology, undefined an, and undefined 2018, "Sustainability of manufacturing technology: friction stir welding in focus," *inderscienceonline.com*.

[17] E. Akinlabi, S. A.- Science, E. and Technology, and undefined 2012, "Friction stir welding process: a green technology," *ujcontent.uj.ac.za*.

[18] R. Bhushan, D. S.-A. C. and H. Materials, and undefined 2019, "Green welding for various similar and dissimilar metals and alloys: present status and future possibilities," *Springer*.

[19] T. Piping, F. Mechanics, and M. Appli, "Pipe and ' Tube Welding ~ i," no. June, 2002.

[20] W. J. Arbegast, "Friction stir welding: After a decade of development," in *TMS Annual Meeting*, 2007, pp. 3–18.

[21] G. Wang, Y. Zhao, Y. H.-J. of M. S. & Technology, and undefined 2018, "Friction stir welding of high-strength aerospace aluminum alloy and application in rocket tank manufacturing," *Elsevier*.

[22] D. Burford, C. Widener, B. T.-6th A. A. Technology, and undefined 2006, “Advances in friction stir welding for aerospace applications,” *arc.aiaa.org*, vol. 1, pp. 257–270, 2006.

[23] A. G. Boitsov, D. N. Kuritsyn, M. V. Siluyanova, and V. V. Kuritsyna, “Friction Stir Welding in the Aerospace Industry,” *Russ. Eng. Res.*, vol. 38, no. 12, pp. 1029–1033, Dec. 2018.

[24] A. Tiwari, P. Pankaj, S. Suman, P. B. the I. I. of Metals, and undefined 2020, “CFD modelling of temperature distribution and material flow investigation during FSW of DH36 shipbuilding grade steel,” *Springer*.

[25] G. Gesella, M. C.-J. of KONES, and undefined 2017, “The application of friction stir welding (FSW) of aluminium alloys in shipbuilding and railway industry,” *yadda.icm.edu.pl*, vol. 24, no. 2, 2017.

[26] G. Rückert, M. Chargy, F. Cortial, F. J.-M. S. Forum, and undefined 2014, “Evaluation of FSW on high yield strength steels for shipbuilding,” *Trans Tech Publ*.

[27] Y. Kusuda, “Honda develops robotized FSW technology to weld steel and aluminum and applied it to a mass-production vehicle,” *Ind. Rob.*, vol. 40, no. 3, pp. 208–212, 2013.

[28] H. Hori, H. H.-W. international, and undefined 2003, “Application of friction stir welding to the car body,” *Taylor Fr.*, vol. 17, no. 4, pp. 287–292, 2010.

[29] T. Kawasaki, T. Makino, K. Masai, H. Ohba, Y. Ina, and M. Ezumi, “Application of friction stir welding to construction of railway vehicles,” *jstage.jst.go.jp*.

[30] A. A. Afonja and D. H. Sansome, “A theoretical analysis of the sandwich rolling process,” *Int. J. Mech. Sci.*, vol. 15, no. 1, pp. 1–14, Jan. 1973.

[31] R. Neugebauer, A. S.-J. of materials processing technology, and undefined 2004, “Ultrasonic application in drilling,” *Elsevier*.

[32] M. Adithan, V. V.- Wear, and undefined 1976, “Production accuracy of holes in ultrasonic drilling,” *Elsevier*.

[33] Q. Zhang, C. Wu, … J. S.-P. of the, and undefined 2000, “The mechanism of material removal in ultrasonic drilling of engineering ceramics,” *journals.sagepub.com*.

[34] Ş. Kasman, Z. Y.-T. I. J. of Advanced, and undefined 2014, “Analyzing dissimilar friction stir welding of AA5754/AA7075,” *Springer*, vol. 70, no. 1–4, pp. 145–156, Jan. 2014.

[35] M. Ahmed, S. Ataya, … M. S.-J. of M., and undefined 2017, “Friction stir welding of similar and dissimilar AA7075 and AA5083,” *Elsevier*.

[36] R. S. Mishra and Z. Y. Ma, “Friction stir welding and processing,” *Mater. Sci. Eng. R Reports*, vol. 50, no. 1–2, pp. 1–78, Aug. 2005.

[37] H. J. Chauhan, A. Chouhan, and S. L. Meena, “Experimental investigation and non destructive testing of friction stir welded aluminium alloy aa 6082 using tool with and without shoulder geometry,” *academia.edu*, pp. 2656–2664, 2016.

[38] B. Gibson, D. Lammlein, … T. P.-J. of M., and undefined 2014, “Friction stir welding: Process, automation, and control,” *Elsevier*.

[39] V. Ravisankar, V. Balasubramanian, C. M.-M. & design, and undefined 2006, “Selection of welding process to fabricate butt joints of high strength aluminium alloys using analytic hierarchic process,” *Elsevier*.

[40] B. Hu and I. M. Richardson, “Hybrid laser/gma welding aluminium alloy 7075,” *Weld. World*, vol. 50, no. 7–8, pp. 51–57, 2006.

[41] P. Ramakrishnan, “Welding Metallurgy,” *Indian Weld. J.*, vol. 4, no. 3, p. 89, 1972.

[42] K. Park, “Development and analysis of ultrasonic assisted friction stir welding process,” 2009.

[43] L. Ruilin, H. Diqiu, L. Luocheng, … Y. S.-T. I. J., and undefined 2014, “A study of the temperature field during ultrasonic-assisted friction-stir welding,” *Springer*, vol. 73, no. 1–4, pp. 321–327, 2014.

[44] S. D. Ji, Z. W. Li, L. Ma, Y. M. Yue, and S. S. Gao, “Investigation of Ultrasonic Assisted Friction Stir Spot Welding of Magnesium Alloy to Aluminum Alloy,”

Strength Mater., vol. 48, no. 1, pp. 2–7, Jan. 2016.

[45] P. S. Davies, B. P. Wynne, W. M. Rainforth, M. J. Thomas, and P. L. Threadgill, "Development of microstructure and crystallographic texture during stationary shoulder friction stir welding of Ti-6Al-4V," *Metall. Mater. Trans. A Phys. Metall. Mater. Sci.*, vol. 42, no. 8, pp. 2278–2289, Aug. 2011.

[46] L. Wan, Y. Huang, Z. Lv, S. Lv, and J. Feng, "Effect of self-support friction stir welding on microstructure and microhardness of 6082-T6 aluminum alloy joint," *Mater. Des.*, vol. 55, pp. 197–203, 2014.

[47] M. S. Sidhu and S. S. Chatha, "Friction Stir Welding – Process and its Variables : A Review," *Int. J. Emerg. Technol. Adv. Eng.*, vol. 2, no. 12, pp. 275–279, 2012.

[48] I. P. Almanar, M. H. Hanapi, A. A. Seman, and Z. Hussain, "Friction Stir Welding of 6061-T6 Aluminum Alloy," *Adv. Mater. Res.*, vol. 501, pp. 145–149, 2012.

[49] A. Scialpi, L. De Filippis, P. C.-M. & design, and undefined 2007, "Influence of shoulder geometry on microstructure and mechanical properties of friction stir welded 6082 aluminium alloy," *Elsevier*.

[50] D. Venkateswarlu, N. Mandal, M. M.-W. Journal, and undefined 2013, "Tool design effects for FSW of AA7039," *files.aws.org*.

[51] K. Krasnowski, C. Hamilton, and S. Dymek, "Influence of the tool shape and weld configuration on microstructure and mechanical properties of the Al 6082 alloy FSW joints," *Arch. Civ. Mech. Eng.*, vol. 15, no. 1, pp. 133–141, Jan. 2015.

[52] K. Elangovan, V. B.-J. of materials processing, and undefined 2008, "Influences of tool pin profile and welding speed on the formation of friction stir processing zone in AA2219 aluminium alloy," *Elsevier*.

[53] C. Leitão, R. Louro, and D. M. Rodrigues, "Analysis of high temperature plastic behaviour and its relation with weldability in friction stir welding for aluminium alloys AA5083-H111 and AA6082-T6," *Mater. Des.*, vol. 37, pp. 402–409, 2012.

[54] Y. Yang, P. Kalya, R. G. Landers, and K. Krishnamurthy, "Automatic gap detection in

friction stir butt welding operations," *Int. J. Mach. Tools Manuf.*, vol. 48, no. 10, pp. 1161–1169, 2008.

[55] S. Rajakumar and V. B. Design, "Establishing relationships between mechanical properties of aluminium alloys and optimised friction stir welding process parameters," *Elsevier*, 2012.

[56] S. Rajakumar, C. Muralidharan, and V. Balasubramanian, "Influence of friction stir welding process and tool parameters on strength properties of AA7075-T6 aluminium alloy joints," *Mater. Des.*, vol. 32, no. 2, pp. 535–549, 2011.

[57] M. Rao, B. Kumar, M. H.-M. T. Proceedings, and undefined 2017, "Experimental study on the effect of welding parameters and tool pin profiles on the IS: 65032 aluminum alloy FSW joints," *Elsevier*.

[58] C. Terra, J. S.-J. of M. Processes, and undefined 2021, "Models for FSW forces using a square pin profile tool," *Elsevier*.

[59] L. Karthikeyan and V. S. Senthil Kumar, "Relationship between process parameters and mechanical properties of friction stir processed AA6063-T6 aluminum alloy," *Mater. Des.*, vol. 32, no. 5, pp. 3085–3091, 2011.

[60] H. Su, C. S. Wu, A. Pittner, and M. Rethmeier, "Simultaneous measurement of tool torque, traverse force and axial force in friction stir welding," *J. Manuf. Process.*, vol. 15, no. 4, pp. 495–500, 2013.

[61] G. G. Krishna, "Experimental Investigation of Tensile Strength and Deflection Characteristics of Friction Stir Welded Aluminum AA 6351 Alloy Joint," *IOSR J. Mech. Civ. Eng.*, vol. 7, no. 5, pp. 01–06, 2013.

[62] J. Gandra, D. Pereira, R. M. Miranda, and P. Vilaça, "Influence of process parameters in the friction surfacing of AA 6082-T6 over AA 2024-T3," in *Procedia CIRP*, 2013, vol. 7, pp. 341–346.

[63] B. Gungor, E. Kaluc, E. Taban, and A. Sik, "Mechanical, fatigue and microstructural properties of friction stir welded 5083-H111 and 6082-T651 aluminum alloys," *Mater. Des.*, vol. 56, pp. 84–90, 2014.

[64] W. S. Chang, S. R. Rajesh, C. K. Chun, and H. J. Kim, “Microstructure and Mechanical Properties of Hybrid Laser-Friction Stir Welding between AA6061-T6 Al Alloy and AZ31 Mg Alloy,” *J. Mater. Sci. Technol.*, vol. 27, no. 3, pp. 199–204, 2011.

[65] C. Bagger and F. O. Olsen, “Review of laser hybrid welding,” *J. Laser Appl.*, vol. 17, no. 1, pp. 2–14, Feb. 2005.

[66] B. Ribic, T. Palmer, T. D.-I. materials reviews, and undefined 2009, “Problems and issues in laser-arc hybrid welding,” *Taylor Fr.*, vol. 54, no. 4, pp. 223–244, Jul. 2009.

[67] H. Ninomiya and A. Sasaki, “A Study on Generalization Ability of 3-Layer Recurrent Neural Networks Input layer Hidden layer,” *Neural Networks*, pp. 1063–1068, 2002.

[68] W. Piekarska, M. K.-I. J. of H. and M. Transfer, and undefined 2011, “Three-dimensional model for numerical analysis of thermal phenomena in laser–arc hybrid welding process,” *Elsevier*.

[69] T. G. Santos, R. M. Miranda, and P. Vilaça, “Friction stir welding assisted by electrical joule effect to overcome lack of penetration in aluminium alloys,” in *Key Engineering Materials*, 2014, vol. 611–612, pp. 763–772.

[70] T. G. Santos, R. M. Miranda, and P. Vilaça, “Friction Stir Welding assisted by electrical Joule effect,” *J. Mater. Process. Technol.*, vol. 214, no. 10, pp. 2127–2133, 2014.

[71] Y. Rostamiyan, A. Seidanloo, … H. S.-A. of civil and, and undefined 2015, “Experimental studies on ultrasonically assisted friction stir spot welding of AA6061,” *Springer*, vol. 15, no. 2, pp. 335–346, Feb. 2015.

[72] X. C. Liu and C. S. Wu, “Elimination of tunnel defect in ultrasonic vibration enhanced friction stir welding,” *Mater. Des.*, vol. 90, pp. 350–358, 2016.

[73] X. Fei, X. Jin, Y. Ye, T. Xiu, and H. Yang, “Effect of pre-hole offset on the property of the joint during laser-assisted friction stir welding of dissimilar metals steel and aluminum alloys,” *Mater. Sci. Eng. A*, vol. 653, pp. 43–52, 2016.

[74] Y. Zhong, C. Wu, G. P.-J. of M. P. Technology, and undefined 2017, “Effect of

ultrasonic vibration on welding load, temperature and material flow in friction stir welding," *Elsevier*.

[75] K. Mehta, V. B.-J. of M. P. Technology, and undefined 2017, "Hybrid approaches of assisted heating and cooling for friction stir welding of copper to aluminum joints," *Elsevier*.

[76] S. Kumar, C. Wu, G. Padhy, W. D.-J. of manufacturing processes, and undefined 2017, "Application of ultrasonic vibrations in welding and metal processing: A status review," *Elsevier*.

[77] S. Kumar, C. Wu, S. Zhen, W. D.-T. I. J. of Advanced, and undefined 2019, "Effect of ultrasonic vibration on welding load, macrostructure, and mechanical properties of Al/Mg alloy joints fabricated by friction stir lap welding," *Springer*, vol. 100, no. 5–8, pp. 1787–1799, Feb. 2019.

[78] S. Kumar, S. Grover, R. W.-I. J. on I. Design, and undefined 2018, "Effect of hybrid wire EDM conditions on generation of residual stresses in machining of HCHCr D2 tool steel under ultrasonic vibration," *Springer*.

[79] S. Kumar, S. Grover, and R. S. Walia, "Effect of hybrid wire EDM conditions on generation of residual stresses in machining of HCHCr D2 tool steel under ultrasonic vibration," *Int. J. Interact. Des. Manuf.*, vol. 12, no. 3, pp. 1119–1137, Aug. 2018.

[80] I. Alinaghian, S. Amini, and M. Honarpisheh, "Residual stress, tensile strength, and macrostructure investigations on ultrasonic assisted friction stir welding of AA 6061-T6," *J. Strain Anal. Eng. Des.*, vol. 53, no. 7, pp. 494–503, Oct. 2018.

[81] L. Fratini, B. Z.-I. J. of M. T. and, and undefined 2006, "An analysis of through-thickness residual stresses in aluminium FSW butt joints," *Elsevier*.

[82] N. Nasir, M. Razab, S. Mamat, M. I.- stress, and undefined 2006, "Review on welding residual stress," *academia.edu*.

[83] A. Abolhasani, A. Zarei-Hanzaki, H. Abedi, M. R.-M. & Design, and undefined 2012, "The room temperature mechanical properties of hot rolled 7075 aluminum alloy," *Elsevier*.

[84] W. Lee, W. Sue, C. Lin, C. W.-J. of M. Processing, and undefined 2000, "The strain rate and temperature dependence of the dynamic impact properties of 7075 aluminum alloy," *Elsevier*.

[85] M. Tajally, E. E.-M. & Design, and undefined 2011, "Mechanical and anisotropic behaviors of 7075 aluminum alloy sheets," *Elsevier*.

[86] X. Liu, C. W.-M. & Design, and undefined 2016, "Elimination of tunnel defect in ultrasonic vibration enhanced friction stir welding," *Elsevier*.

[87] G. Shao, H. Li, and M. Zhan, "A Review on Ultrasonic-Assisted Forming: Mechanism, Model, and Process," *Chinese J. Mech. Eng. (English Ed.,* vol. 34, no. 1, Dec. 2021.

[88] A. Golezani, R. Barenji, … A. H.-… I. J. of, and undefined 2015, "Elucidating of tool rotational speed in friction stir welding of 7020-T6 aluminum alloy," *Springer,* vol. 81, no. 5–8, pp. 1155–1164, Nov. 2015.

[89] S. Amini, M. A.-T. I. J. of A. Manufacturing, and undefined 2014, "Study of ultrasonic vibrations' effect on friction stir welding," *Springer,* vol. 73, no. 1–4, pp. 127–135, 2014.

[90] F. Lambiase, V. Grossi, and A. Paoletti, "Effect of tilt angle in FSW of polycarbonate sheets in butt configuration," *Int. J. Adv. Manuf. Technol.,* vol. 107, no. 1–2, pp. 489–501, Mar. 2020.

[91] A. Arici and S. Selale, "Effects of tool tilt angle on tensile strength and fracture locations of friction stir welding of polyethylene," *Sci. Technol. Weld. Join.,* vol. 12, no. 6, pp. 536–539, Aug. 2007.

[92] W. Pan, D. Li, A. Tartakovsky, … S. A.-I. J. of, and undefined 2013, "A new smoothed particle hydrodynamics non-Newtonian model for friction stir welding: Process modeling and simulation of microstructure evolution in a," *Elsevier*.

[93] S. Meena, Q. Murtaza, R. Walia, … M. N.-M. T., and undefined 2022, "Modelling and simulation of FSW of polycarbonate using Finite element analysis," *Elsevier*.

[94] S. Karna, R. S.-I. journal of engineering and, and undefined 2012, “An overview on Taguchi method,” *academia.edu*.

[95] A. Freddi, M. S.-D. principles and methodologies, and undefined 2019, “Introduction to the Taguchi method,” *Springer*.

[96] P. Kumar, R. Jayaraj, J. Suryawanshi, U. S.-A. Materialia, and undefined 2020, “Fatigue strength of additively manufactured 316L austenitic stainless steel,” *Elsevier*.

[97] K. T.-J. of A. Crystallography and undefined 2018, “X-ray measurement of triaxial residual stress on machined surfaces by the cosα method using a two-dimensional detector,” *scripts.iucr.org*.

[98] A. Faheem, A. Tyagi, F. Hasan, A. A. Khan, Q. Murtaza, and K. K. Saxena, “Residual stress investigation in the metallic coating approach of micro-sized particles on the substrate: cold spray additive manufacturing,” *Adv. Mater. Process. Technol.*, pp. 1–17, May 2022.

[99] R. Roy, *Design of experiments using the Taguchi approach: 16 steps to product and process improvement*. 2001.

[100] A. Lakshminarayanan, V. B.-T. of Nonferrous, and undefined 2008, “Process parameters optimization for friction stir welding of RDE-40 aluminium alloy using Taguchi technique,” *Elsevier*.

[101] T. B. Barker, “Engineering quality by design : interpreting the Taguchi approach,” p. 250, 1990.

[102] P. Ross, “Taguchi techniques for quality engineering: loss function, orthogonal experiments, parameter and tolerance design,” 1988.

[103] S. Peace, *Taguchi methods : a hands-on approach*. Reading Mass.: Addison-Wesley, 1993.

[104] M. Komarasamy, R. S. Mishra, J. A. Baumann, G. Grant, and Y. Hovanski, “Processing, microstructure and mechanical property correlation in Al-B4C surface composite produced via friction stir processing,” *Frict. Stir Weld. Process. VII*, pp. 39–

46, Jan. 2016.

[105] A. Dolatkhah, P. Golbabaei, M. Givi, F. M.-M. & Design, and undefined 2012, "Investigating effects of process parameters on microstructural and mechanical properties of Al5052/SiC metal matrix composite fabricated via friction stir," *Elsevier*.

[106] H. Izadi, R. Sandstrom, and A. P. Gerlich, "Grain Growth Behavior and Hall–Petch Strengthening in Friction Stir Processed Al 5059," *Metall. Mater. Trans. A Phys. Metall. Mater. Sci.*, vol. 45, no. 12, pp. 5635–5644, Nov. 2014.

[107] M. Azizieh, A. Kokabi, P. A.-M. & Design, and undefined 2011, "Effect of rotational speed and probe profile on microstructure and hardness of AZ31/Al2O3 nanocomposites fabricated by friction stir processing," *Elsevier*.

[108] P. Vijayavel, V. Balasubramanian, and I. Rajkumar, "Effect of Tool Traverse Speed on Strength, Hardness, and Ductility of Friction-Stir-Processed LM25AA-5% SiCp Metal Matrix Composites," *Metallogr. Microstruct. Anal.*, vol. 7, no. 3, pp. 321–333, Jun. 2018.

[109] H. Montazerolghaem, … M. B.-K. E., and undefined 2012, "Investigation of vibration assisted friction stir welding," *Trans Tech Publ*.

[110] A. Tyagi, S. Pandey, … R. W.-M. R., and undefined 2020, "Characterization and parametric optimization of% change in residual stress of Mo composite coating using Taguchi approach," *iopscience.iop.org*.

[111] H. Shen, M. Yoshino, D. Yuan, Z. Wang, B. Wang, and S. Qu, "Comparison of residual stress before and after shot peening on the surface of a Ti-6Al-4V titanium alloy by μ-X360n equipment," *iopscience.iop.org*.

[112] R. Butola, N. Choudhary, R. Kumar, … P. M.-M. T., and undefined 2021, "Measurement of residual stress on H13 tool steel during machining for fabrication of FSW/FSP tool pins," *Elsevier*.

[113] M. Vashista, S. P.-P. Magazine, and undefined 2012, "Correlation between full width at half maximum (FWHM) of XRD peak with residual stress on ground surfaces," *Taylor Fr.*, vol. 92, no. 33, pp. 4194–4204, Nov. 2012.

[114] K. Bector, M. Singh, D. Pandey, … R. B.-A. in M., and undefined 2021, "Study of residual stresses in multi-pass friction stir processed surface composites," *Taylor Fr.*, 2021.

[115] B. Khosrozadeh, M. S.-T. I. J. of Advanced, and undefined 2017, "Effects of hybrid electrical discharge machining processes on surface integrity and residual stresses of Ti-6Al-4V titanium alloy," *Springer*, vol. 93, no. 5–8, pp. 1999–2011, Nov. 2017.

[116] N. Yuvaraj, S. Aravindan, and Vipin, "Wear Characteristics of Al5083 Surface Hybrid Nano-composites by Friction Stir Processing," *Trans. Indian Inst. Met.*, vol. 70, no. 4, pp. 1111–1129, May 2017.

[117] S. L. Meena, A. Tyagi, Q. Murtaza, R. S. Walia, and M. S. Niranjan, "Effect of load on the wear behaviour of Al2O3HVOF sprayed coating," in *Journal of Physics: Conference Series*, 2021, vol. 1950, no. 1, pp. 1–11.

[118] R. Mertens, B. Vrancken, N. Holmstock, Y. Kinds, J. K.-P. Procedia, and undefined 2016, "Influence of powder bed preheating on microstructure and mechanical properties of H13 tool steel SLM parts," *Elsevier*.

LIST OF PUBLICATIONS

International Journals

1. Meena, S. L., Butola, R., Khan, M. A., Walia, R. S., & Murtaza, Q. (2022). Influence of process parameters in synergic MIG welding of 304L stainless steel using response surface methodology. *Advances in Materials and Processing Technologies*, 1-10.
2. Meena, S. L., Murtaza, Q., Walia, R. S., Niranjan, M. S., & Tyagi, A. (2022). Modelling and simulation of FSW of polycarbonate using Finite element analysis. *Materials Today: Proceedings*, *50*, 2424-2429.
3. Meena, S. L., Tyagi, A., Murtaza, Q., Walia, R. S., & Niranjan, M. S. (2021, July). Effect of load on the wear behavior of Al2O3 HVOF sprayed coating. In *Journal of Physics: Conference Series* (Vol. 1950, No. 1, p. 012011). IOP Publishing.
4. Meena, S. L., Murtaza, Q., Walia, R. S., & Niranjan, M. S.(2020 Optimization of Hybrid Friction Stir Welding Process Parameters of Aluminium AA6063, International Journal of Advanced Science and Technology, 29, 6938-6949
5. Meena, S. L., Butola, R., Murtaza, Q., Jayantilal, H., & Niranjan, M. S. (2017). Metallurgical Investigations of Microstructure and Micro hardness across the various zones in Synergic MIG Welding of Stainless steel. *Materials Today: Proceedings*, *4*(8), 8240-8249.

Details of International Conference Papers Presented

1. "Optimization of Hybrid Friction stir welding process parameters of Aluminium" in International conference on Integration of advanced Technologies for Industry 4.0 held on 12th and 13th June 2020 at KCG College of Technology, Chennai, India

2. “Optimization of Aluminium based metal matrix surface composite using Taguchi Technique via friction stir processing” in International conference on Industrial and manufacturing systems organized by Dr, B.R. Ambedkar NIT , Jalandhar during 09-11 October, 2020.
3. “Effect of load on the wear behavior of Al2O3 HVOF sprayed coating” in international conference on Mechatronics and artificial Intelligence held on February 26-27th, 2021 organized by SGT University, Gurugram, Haryana, India.